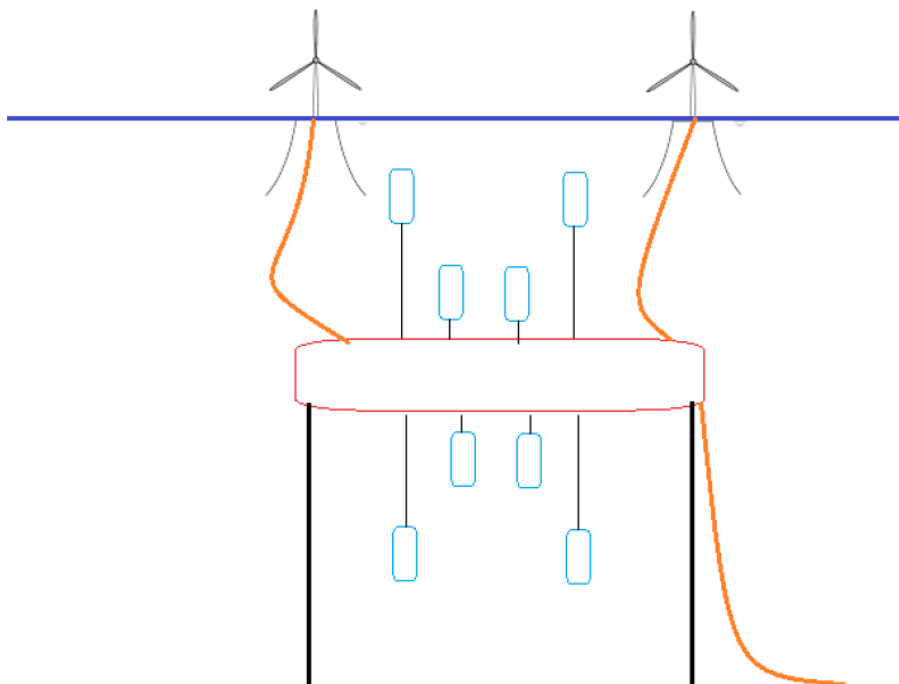


INSTALLATION OF THE SUBSEA BUOYANCY GRAVITY ENERGY STORAGE SYSTEM

DELFT UNIVERSITY OF TECHNOLOGY

Assessing the dynamic behaviour of the SBGESS during ultra-deep water installation by using non-linear vertical displacement models



Frank Mols (ID: 4458516)

Supervised by:

André R. Novgorodcev Jr.

Antonio Jarquín-Laguna

Sape A. Miedema

16 September 2021

(Page intentionally left blank)

Preface

Before you lies the thesis “Installation of the Subsea Buoyancy Gravity Energy Storage System: Assessing the dynamic behaviour of the SBGESS during ultra-deep water installation by using non-linear vertical displacement models”. It has been written to fulfill the graduation requirements of the Offshore and Dredging Engineering at the Delft University of Technology (TU Delft). This thesis was written from November 2020 to September 2021. The project was undertaken at the request of the TU Delft, as part of the overarching SBGESS project.

I would like to thank my supervisors for their excellent guidance and support during this process. Their feedback has proved to be very useful for both this thesis as well as any future projects. Furthermore, a special thanks to the Copernicus Climate Data Store for making their environmental data openly available.

I hope you enjoy your reading.

Frank Mols

Delft, September 16, 2021

Summary

The objective of this thesis was: *To assess the dynamic behaviour of the SBGESS system during installation and provide suggestions to increase workability by reducing the dynamic response.* In order to do so, the SBGESS was preliminary dimensioned based on simulations of the energy balance and the lowering operation was modelled using these dimensions.

A 10.32MWh SBGESS, with three power supply modes (including a power saving mode), is able to operate a 4.34MW water injection system with power being generated by two 12MW wind turbines. Simulations were run to assess the sensitivity of the system to the energy storage capacity and the ranges in which a certain mode was active. Based on historical wind data, this system is able to meet the empirical reliability and performance criteria for a water injection system. Using the energy storage capacity and power demand as input, the size and number of buoyancy- and gravity units were scaled to minimize overall dimensions as to reduce installation complexity.

Given the dimensions a wet tow is deemed to be the most likely transportation method. For installation the traditional methods are less appropriate as the lowering of the SBGESS classifies as a heavy lift in ultra-deep waters. An installation method with multiple AHTs and a towing configuration, likely with a form of heave compensation, to decouple the motions is suggested.

The vertical displacement of the SBGESS during the lowering phase was modelled using two non-linear mass - dashpot - spring models. It was concluded that using polyester rope for the lowering cable leads to relatively low dynamic forces during the lowering and is able to meet the DNV criteria for an offshore operation in more sea states than other alternatives. It also complies well with installing the SBGESS as a single-unit. Taking precautions such as heave compensation and a lower payout velocity are however necessary to avoid slack conditions and large dynamic forces during the beginning of the lowering operation.

A Sensitivity analysis showed that the hydrodynamic coefficients require extensive lab testing as their values have a large impact on the dynamic force. The added mass coefficient has a large value on the overall dynamic force and location of the resonance zone, while the drag coefficient mostly impacts the oscillation magnitudes in the early parts of the lowering. Further and more extensive modelling is critical to avoid stability issues during the lowering of the SBGESS.

Contents

Preface	2
Summary	3
1 Introduction	7
1.1 Subsea equipment	7
1.2 Case study in the Santos Basin, Brazil	8
1.3 Objective & Research questions	9
1.4 Content	10
2 Energy yield, Power demand and the resulting required energy storage capacity	11
2.1 Energy yield data	11
2.1.1 Wind data	11
2.1.2 Power output of the turbine	13
2.2 The need for energy storage	13
2.3 Energy demand at the seabed by subsea processing equipment	14
2.3.1 Efficiency of the system	14
2.3.2 Pump performance	15
2.4 Water injection simulation	16
2.4.1 Simulation set-up	17
2.4.2 Simulation results	18
3 Preliminary dimensioning of the SBGESS	20
3.1 Outline of the design	20
3.2 Dimensioning strategy	21
3.2.1 GES: weights	21
3.2.2 BES: floaters	22
3.2.3 Energy storage	23
3.3 SBGESS dimensions	23
4 Mooring systems and Anchors	25
4.1 Why position-keeping is important	25
4.2 Tension leg mooring system	25
4.3 Anchor types	25
4.4 Criteria to select a type of anchor	28
4.4.1 Water depth	28
4.4.2 Load capacity	28
4.4.3 Soil properties	29
4.5 Evaluation	29
5 Transportation methods	31
5.1 Categories of transportation methods	31
5.2 Dry-tow	31
5.3 Wet-tow: Floating	32
5.4 Wet-tow: Submerged	32

5.5	Considerations when selecting a transportation method	32
5.6	Summary and evaluation	34
6	Installation methods	36
6.1	The challenges of offshore installation in ultra-deep waters	36
6.2	Installation methods	36
6.2.1	Traditional installation methods: DRIM and WWIM	37
6.2.2	Wet tow methods: PBM, SDS, FID and WTIM	37
6.2.3	Other methods: SIM, PIM, HCLS and Y - method	37
6.2.4	BSR installation method	38
6.3	Equipment for lowering subsea structures in deep water	38
6.4	Summary of installation methods	40
6.5	Selection on an installation method for the SBGESS	41
7	Modelling methodology	42
7.1	Vertical displacement model of the lowering phase	42
7.1.1	Tommasini model	43
7.1.2	Gao model	45
7.2	Detailed modelling methodology	47
7.2.1	Assumptions and simplifications	47
7.2.2	Waves and vessel motions	48
7.2.3	Slack and snap forces	48
7.2.4	Hydrodynamic coefficients	48
7.2.5	Variable ballasting	49
7.2.6	Initial conditions and velocity	49
7.3	Simulation cases description	50
7.3.1	Lowering cable	51
7.3.2	Traction cables	51
7.4	Installation: single unit or modular	51
8	Results	53
8.1	Comparison between Tommasini and Gao	53
8.2	Simulations for different wave amplitudes and lowering velocities	56
8.3	Sensitivity analysis: Added mass coefficient, drag coefficient and ballasting fill percentage	60
8.3.1	Added mass coefficient	60
8.3.2	Drag coefficient	61
8.3.3	Ballasting fill percentage	61
9	Conclusion & Recommendations	63
Appendix A	Additional wind speed data analysis	72
Appendix B	Pump performance curvefit	73
Appendix C	Sensitivity analysis - Energy storage	74
Appendix D	Detailed dimensioning parameters	75
Appendix E	Detailed modelling parameters	76
Appendix F	Historical current and wave data	77
Appendix G	Detailed results and figures	79

G.1	Sensitivity analysis	79
G.1.1	Sensitivity of dynamic force to added mass coefficient	79
G.1.2	Sensitivity of dynamic force to drag coefficient	81
G.1.3	Sensitivity of dynamic force to ballasting fill percentage	82
G.2	Complete overview of results for scenarios and cases mentioned in chapter 7	84

1 | Introduction

By signing the Paris agreement in 2015 at the COP21, a near-universal commitment was made to limit the global temperature rises to ‘well below 2 degrees celsius’ and aim for no more than 1.5 degrees [1]. All countries had to deliver detailed inventories on how they plan to reduce their greenhouse gas (GHG) emissions. These inventories should include the reductions in GHG emissions from the offshore oil and gas (O&G) activities, if these occur within the exclusive economic zone (EEZ) of a country [2]. In order to accelerate the eventual decline in oil and eventually gas consumption that is projected for the coming decades, alternative energy sources such as renewables are essential [3]. Yet given the required GHG reductions the decline should be increased by the use of alternative energy sources within the oil & gas industry itself, which has a significant impact on the emissions [4]. The oil & gas production plants require energy to operate, sometimes up to tens of MWs of power [5], and the source of this energy is usually a percentage of the oil and/or gas that is produced or diesel fuel [6]. Especially offshore, where the connection to the electricity grid is often non-existent, the platforms are usually operated on fossil fuels (e.g. gas turbines) [7]. For these locations, the use of renewable ocean energy may provide a more sustainable and economical solution [8][9].

1.1 Subsea equipment

In recent years, the number of plants that are being located in deeper waters has increased [10]. Even projects in water depths of 2000m and beyond are common now. Extraction of these ultra-deep fields often requires a substantial amount of processing equipment and machinery at the seabed. Examples of these include separation, water injection, compression and power distribution systems [11][12]. All these systems require power to operate and grid connection is often impossible, as the distances to shore are large for these ultra-deep fields. The common way of supplying power to these systems is having gas turbines on board of the topside[7][13]. Many studies have suggested that substituting these gas turbines by local renewable sources is an effective way of reducing the GHG emissions of offshore O&G activities [4][14][6][13]. To avoid having to use a (back-up) gas turbine (because of the intermittency of the source), a subsea system that does not require continuous and constant power is a preferred choice when it comes to replacing the power source by a renewable source. It should also be able to shut-down and start-up relatively easy.

One such system that can operate under these conditions is a water injection system. Such a system is not dependent on continuous power (although the efficiency and production might suffer from large fluctuations) and is flexible when it comes to stopping and starting operations. Water injection is crucial to increase the oil recovery rate (ORR) after a primary pressure depletion period[15][9]. An essential aspect of the water injection system is that its variable speed drives (VSD) can handle the flexible loads and can therefore mitigate some of the challenges related to renewable power intermittency [9]. This is why multiple studies have argued that it can be feasible to have an offshore wind farm supply power to a water injection system [9][16][17]. Not only will this lead to reduced fuel costs and emissions, but it may also lead to shorter power cables. The latter meaning the cost and power losses are likely to decrease.

Even though the pump, as a result of the VSD, can handle power fluctuations and occasional shut-downs, it is best to avoid having too many stops. First of all, most pumps actually have an empirical maximum number of stops for which reliability can be guaranteed [18]. Secondly, another important reason is that pumps have efficiency curves, meaning that a lower power output than the Best Efficiency Point will lead to a lower efficiency and therefore a much lower injection rate [19][20]. If this occurs too often, it

may hurt the production and have negative economic effects. To avoid these adverse consequences of the intermittency, an energy storage system could be implemented. This will help reduce the number of shut-downs and will result in less power fluctuation. Another argument for implementing energy storage is that less energy is 'wasted' (if power supply > power demand) and it can help keeping the operating systems (such as SCADA) operational during windless periods [16].

Ideally, one would design a renewable power plant that can supply power for all of the equipment, both subsea and on the topside. However, equipment such as separation and safety systems often require a continuous supply of power [12][11], meaning that renewable energy sources are not feasible unless combined with a large energy storage unit or being grossly oversized. Given the current technological readiness level of storage and renewable generation techniques, these early projects are more likely to succeed if focussed on water injection systems (or systems that have similar flexibility in power input).

1.2 Case study in the Santos Basin, Brazil

The case that will be studied in the thesis, that will build on this literature review, is situated in Brazil. The exact location is currently unknown but is likely to be in the Libra field which is part of the Santos Basin[21]. Here, electrical power is required by a subsea water injection system to be installed at more than 2000m water depth and 160 km from shore[22]. As there is no connection to the electricity grid, its energy has to be locally generated. Novgorodcev JR. and Jarquín-Laguna [23] found by doing a multi-criteria decision analysis that floating offshore wind is the most feasible alternative to using fossil fuels for this location. Their proposal is thus to install floating offshore wind turbines that will power subsea equipment at this location.

However, the issue that is prevailing is that the supply and demand of power will often not be in equilibrium. To avoid having to use fossil fuels to bridge periods of under-supply, a sufficient amount of energy needs to be stored during periods of over-supply. A possible solution is to install a Subsea Buoyancy Gravity Energy Storage System (SBGESS) [22], with a capacity that is large enough to deliver the required power (including losses). This SBGESS consists of a main buoy element with weights and floaters connected to it. The vertical movement of these elements makes power supply and energy storage possible. A schematic overview of the SBGESS concept is shown in figure 3.1.

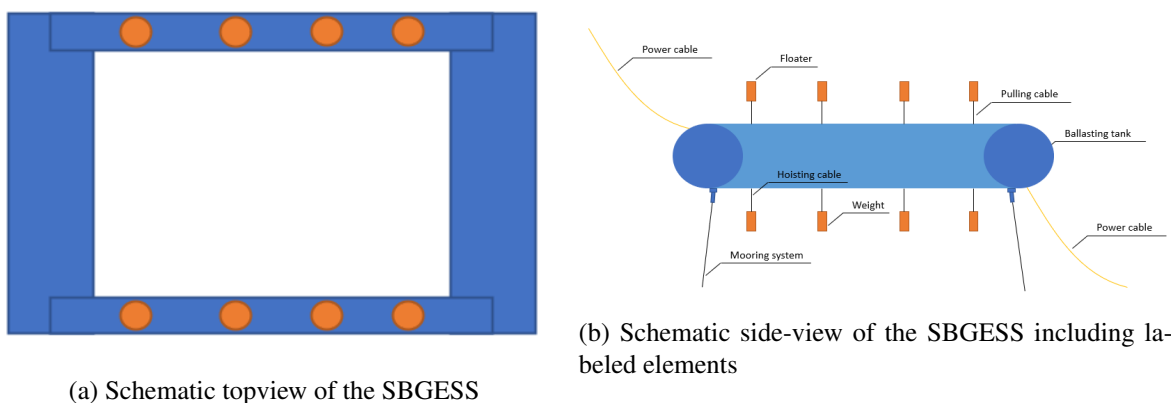


Figure 1.1: Schematic overview of the SBGESS concept, including a topview and side-view with labeled elements. Note: image is not to scale

One of the main challenges for any type of large-scale ocean energy storage is the transportation and installation of the heavy and large components [24]. This will be particularly challenging for the proposed project given the environmental conditions at the intended location. The water depth at the location is approximately 2100 meters[25]. Although large submerged structures have been installed in similar

water depths before, they tend to be installed much closer to the surface than the 1000 meters that is proposed for the SBGESS [26][27]. Another issue is the strong currents and occurrence of bi-directional swells in this region [27]. Given the challenging conditions at the location and the fact that this project is a 'first of its kind', it is critical to analyze and assess the possible installation methods and potentially improve/adjust them based on the project specific requirements.

1.3 Objective & Research questions

The objective of this thesis is formulated as: *To assess the dynamic behaviour of the SBGESS system during installation and provide suggestions to increase workability by reducing the dynamic response.* To achieve this, the following two research questions were formulated that lead up to the objective formulated above.

1. What is the dynamic response of the SBGESS during installation?
 - 1 a) What is the expected energy yield of the proposed wind turbines and how will this influence the required energy storage capacity and other SBGESS dimensions?
 - 1 b) Which installation methods for the SBGESS at the proposed location are feasible?
 - 1 c) For which wave periods and at which depths can resonance and/or slack occur for different cable properties?
 - 1 d) How do the wave conditions influence the dynamic response during resonance and slack conditions?
2. How can the selected installation method be improved for the proposed location?
 - 2 a) What are the limiting factors for the installation?
 - 2 b) Which parameters of the SBGESS project can be changed to reduce the dynamic response for the SBGESS project?

These research questions are meant to be answered in the order presented above, as each question provides input to the next one. The first sub research question (1a) is answered by running simulations of the power supply and demand to the water injection system, using historical wind data and power data from the turbine and pump manufacturer. Based on empirical pump criteria appropriate energy storage and power supply values are selected. Hereafter, the SBGESS is dimensioned. As it is a preliminary dimensioning, only the power requirements are taken into account and no structural analysis is carried out.

A literature review assists in answering the second subquestion (1b) by analyzing the current information and data on installation methods. Based on information in guidelines, project reports, (conference) papers, regulations, etc., the literature review lists possible installation methods and analyzes them. As the feasibility of a certain installation method is highly co-dependent on both the type of mooring system and transportation method, the most common types of these, including their limitations are also analyzed and presented in this thesis.

To answer the remaining research questions, the lowering phase of the installation is modelled using two different vertical displacement models. The resulting values are compared and several values are subjected to a sensitivity analysis. Finally, a comparison is made between a single-unit installation and a modular installation. plotting the natural periods of the system and comparing these to the wave periods will provide insight in the possible occurrence of resonance.

It should be noted that this thesis aims not at selecting one optimal installation method, yet rather aims at suggesting viable methods and important variables to consider and improve these methods.

1.4 Content

In chapter 2 the energy yield is computed and compared with the energy demand. This chapter concludes with a required energy storage capacity and power supply. Based on these numbers, the SBGESS main dimensions are estimated in chapter 3. In chapter 4 the types of anchors that are available for moored offshore structures will be discussed, including their usage and (dis)advantages. The viable options are listed at the end. Hereafter, the two main categories of transportation (wet- and dry tow) will be explained and analysed in chapter 5. In chapter 6 the most common ways of installing a submerged offshore structure in deep water are listed and analysed. The methodology used to model the selected installation procedure is outlined in chapter 7. A summary of the results of these simulations can be found in chapter 8, while the complete overview is presented in appendix G. Finally, in chapter 9 'Conclusions and recommendations', the main observations from the results are summarized and a suggestion are done to improve the installation method. In this chapter, it is also outlined what further research is necessary to improve the accuracy of the modelling, to increase the degrees of freedom modelled and to account for potential stability issues.

2 | Energy yield, Power demand and the resulting required energy storage capacity

How to transport and install the SBGESS is highly dependent on the dimensions of the SBGESS as a whole, yet also of the individual elements. Especially the size of the weights (gravitational energy storage) and floaters (buoyancy energy storage) that are attached to the SBGESS can only be determined based on the required energy storage capacity. This chapter describes the process of how this value was computed, also visualised in figure 2.1. First, the wind distribution and statistics for the proposed location were analysed. Combined with the powercurve from an appropriate wind turbine, this resulted in expected energy yield data. To investigate the required energy capacity, information on the energy demand is also necessary. The subsea processing system, a water injection system in this case, is described and an assumption of its energy demand is made based on an approximation of both the efficiency as well as the pump performance. With this information a simulation of the water injection was run, of which the set-up and parameters are explained. The process is iterative (see also figure 2.1) as the required result (energy storage capacity) is also an input parameter in the simulation. Only the final selected value and results are shown in this chapter.

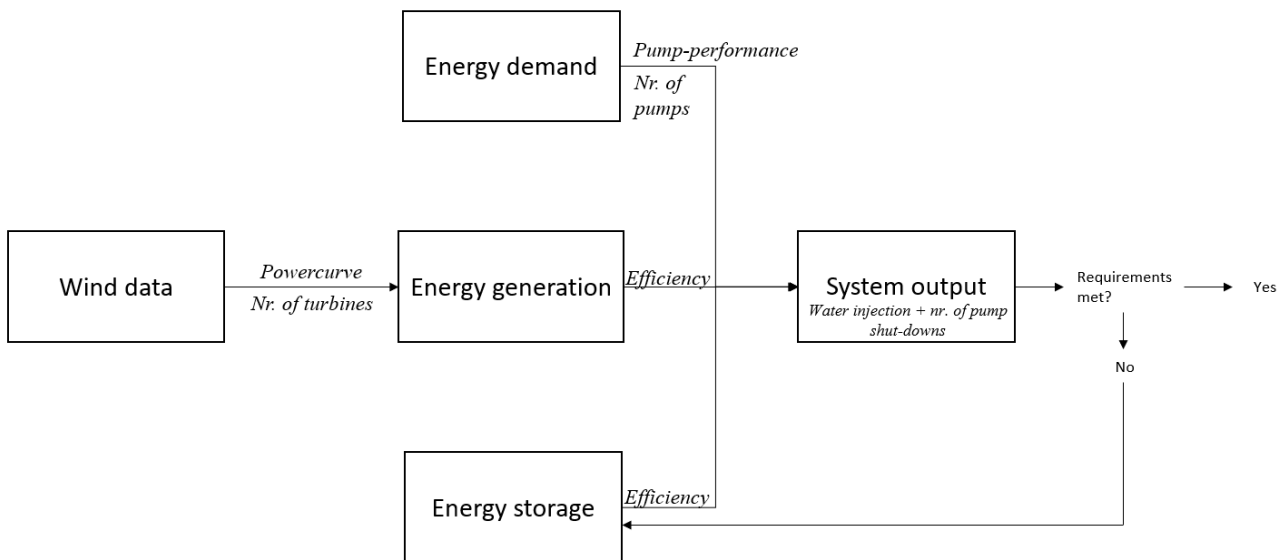


Figure 2.1: Overview of the methodology that is used to determine the required energy storage capacity and power that should be delivered by the SBGESS.

2.1 Energy yield data

2.1.1 Wind data

Historical wind measurements were interpolated (for lat = -24.5 lon = -42.2, which is located in the middle of the western part of the Libra field) and obtained from the copernicus climate data project [28]. The data consist of hourly measurements at 100m height of the wind speed in u and v direction over 41 years (1979 - 2019) [29]. These wind speeds were transformed from the measurement height of 100m to the hub height of the selected turbine at 150m (see next section) by use of the power law. Generally,

the power law provides a better approximation of the true wind speeds at larger heights compared to logarithmic scaling [30].

$$C_{150m} = C_{100m} \cdot \left(\frac{z_{150m}}{z_{100m}} \right)^{\alpha_{shear}} \quad (2.1)$$

Thus, the wind speeds were transformed using equation 2.1, where:

C_{150m} = Wind speed at hub height (150m) in m/s

C_{100m} = Wind speed at sensor height (100m) in m/s

z_{150m} = hub height = 150m

z_{100m} = sensor height = 100m

$\alpha_{shear} = 0.11$ (offshore,[30])

Hereafter, the transformed wind components were combined to compute the resultant wind speed by using equation 2.2.

$$w = \sqrt{u^2 + v^2} \quad (2.2)$$

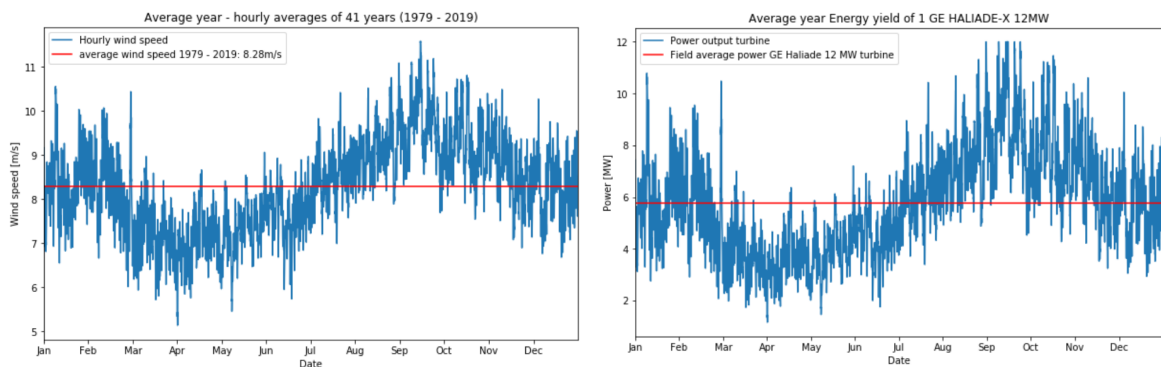
With:

u = wind component in u direction in m/s

v = wind component in v direction in m/s

w = Resultant horizontal wind component in m/s

Many statistic values could be extracted from this dataset, but to assess which size of wind turbine is economical for this location, a rough indication of wind class/occurring wind speeds is needed. To create this insight, the hourly data of 41 years was averaged to show the average year. For each hour of each day of the year, the average was taken of this specific hour's values of the 41 years. The result is shown in figure 2.2a.



(a) Hourly wind speeds for the average year, based on 41 years of data from: [28] (b) Hourly power output of one GE Haliade-X 12 MW turbine for the average year shown left

Figure 2.2: Average year wind speeds and power output

What can be extracted from the visualisation in figure 2.2a is that on average, the wind speeds in the months March to June are substantially lower than in the other months. The consequences of this will be discussed in the next section.

2.1.2 Power output of the turbine

Figure 2.2a shows that the average wind speed is around 8.5m/s, indicating low to medium wind speeds in the area. As the wind speeds are relatively low, particularly in the months March to June, a low cut-in and/or rated wind speed is deemed preferable for the selected wind turbine. A way to achieve these lower values is to have a turbine with a large rotor [31]. After considering several wind turbines with large rotors, the GE Haliade-X was selected, as it offers one of the industry’s lowest cut-in wind speeds and its recent development leads to technological advantages. Currently the turbine is being tested onshore, but it is expected that by the time the SBGESS project is realized, the turbine will be commercially available [32]. Using the average year wind speeds as input and combining these with the Haliade’s power curve [33], figure 2.2b was computed. This graph indicates that the turbine is not in an optimal location as the capacity factor is below 0.50, given that the average power output is less than half of 12MW. Especially from March to June, where the power output is low, resulting in a capacity factor of 0.33. The amplification of this difference compared to figure 2.2a can be explained by the fact that these wind speeds are on the steepest part of the power curve, meaning that a small difference in wind speed will lead to a relatively large difference in power output as shown in table 2.1.

Table 2.1: Statistical description of power output [MW] for each month for a 12MW Haliade-X GE turbine. Based on 41 years of hourly wind speeds [28]

	Jan	Feb	Mar	Apr	May	Jun	Jul	Aug	Sep	Oct	Nov	Dec
Mean	6.25	6.25	4.73	4.48	4.77	5.30	6.30	7.11	7.41	6.98	6.41	5.97
STD	4.65	4.63	4.24	4.10	4.28	4.35	4.45	4.50	4.51	4.57	4.64	4.60
Min	0.0	0.0	0.0	0.0	0.0	0.0	0.0	0.0	0.0	0.0	0.0	0.0
25%	1.58	1.59	0.86	0.88	0.88	1.21	2.06	2.73	3.01	2.53	1.78	1.46
50%	5.92	5.93	3.53	3.18	3.47	4.34	5.96	7.62	8.28	7.17	6.07	5.26
75%	12.0	12.0	8.16	7.52	8.35	9.40	11.79	12.0	12.0	12.0	12.0	12.0
Max	12.0	12.0	12.0	12.0	12.0	12.0	12.0	12.0	12.0	12.0	12.0	12.0

2.2 The need for energy storage

In the introduction it was already mentioned that because of the distance to shore (160km) no grid connection would be available at the location. Combined with the intermittency of the power output of wind energy, this could lead to the need for energy storage, depending on the power demand of the system that the power will be supplied to. Table 2.1 also shows the intermittency as the mean values differ for each month, and the standard deviation is relatively high.

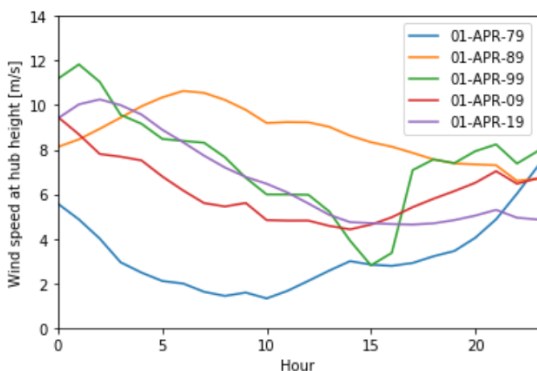


Figure 2.3: Wind speeds at hub height for the 1st of April 1979, 1989, 1999, 2009 and 2019 to illustrate the intraday variation in wind speeds.

Even if the power plant were 'overdesigned' with a large amount of turbines, it still wouldn't completely eliminate the need for energy storage as the minimum value for each month is 0.0MW as shown in table 2.1. However, increasing the amount of turbines based on the 'bad months' tends to be not economical. Only for a system which does not need continuous power supply, is allowed to have a large number of stops per year, and has a quick start-up procedure, it could be a possibility to exclude energy storage and therefore accept both the intermittency supply and a high number of shut-downs. Another reason why energy storage is required is the intraday variation in wind speeds and therefore power generation as is shown in figure 2.3. The figure shows the intraday variation for five days in April. As stated

earlier, March to June have relatively low wind speeds, yet combined with the intraday variation, it is likely that there will be a high number of hours in these months where no or minimal power is generated and energy storage will be needed to bridge these hours.

Using the 41 years of hourly wind speed measurements resulted in a capacity factor of 0.48 for one turbine. For the months March to June, a capacity of only 0.33 was computed. Since this number is relatively low [32], it is expected that multiple turbines are needed to power a larger system. Another argument for multiple turbines is to create redundancy in case of downtime of one of the turbines. The amount of turbines that is needed is looked into in the next sections.

2.3 Energy demand at the seabed by subsea processing equipment

Extraction of ultra-deep fields often require a substantial amount of processing equipment and machinery at the seabed. Examples of these include separation systems, water injection systems, compression systems and power distribution systems [11][12]. All these systems require power to operate and grid connection is virtually impossible, as was stated earlier. The common way of supplying power to these systems is having gas turbines on board of the FPSO. The goal of this study is to power a (part of a) subsea processing by the power generated by the proposed floating turbines. As was concluded earlier, the intermittency of the power source, even with energy storage, combined with the wish to not having to connect this subsea system to a (back-up) gas turbine anymore, means that a system should be chosen that does not require continuous and constant power. It should also be able to stop without breaking down and being able to start-up again in a relatively short amount of time. A water injection system is deemed the most feasible system to supply by wind power, given these challenges [9][16][17]. They are not dependent on continuous power (although the efficiency and production might suffer from large fluctuations) and are flexible when it comes to stopping and starting operations. Water injection is crucial for offshore oil production to increase the oil recovery rate (ORR) [9].

For this study, a hypothetical yet realistic water injection system was used. The size of the system was determined by using a reference project in the Merol oil field, which has a system that is able to inject 75000BPD of water [18]. To reach this value in this study, two SPRINGS systems of 42000BPD each [19] are combined. SPRINGS (Subsea PROcessing and INjection Gear for Seawater) is a qualified system for subsea processing [34][35]. It combines treatment and injection of seawater in one system at the seabed and has both communication and power tie-backs to the topside. The need for the latter will be removed by supplying power to the system by the proposed wind farm. The pumps that will be used in the SPRINGS systems are designed to be in a 1 - 3 MW range [36]. In this study, each pump will be operating in a frequency range of 25 - 74HZ and have a rated shaft power of 2170kW [18]. The pumps use a variable speed drive (VSD) and have a soft-starter function, making them highly suitable to operate under alternating power supply conditions.

2.3.1 Efficiency of the system

To assess whether the system, with the parameters as indicated in the next section, can satisfy the requirements and to find the necessary energy storage capacity, it is important to include efficiency in this assessment. It is assumed that all losses within the wind turbine are accounted for in the power-curve. The following four losses are expected to be relatively high and will therefore be included in the simulation by use of an estimated value: losses of the gravitational- and the buoyancy energy storage, transportation and transmission losses and losses in the water pumps.

The round-trip efficiency (one full cycle of charging and discharging) depends on many aspects, such as the velocity, shape and electrical equipment used. However, based on the values stated in [37][24][8][38], 0.83 is used as round-trip efficiency for both gravitational (GES) and buoyancy energy storage (BES). An accurate calculation of the power losses in the cable during power transmission can be calculated using the method proposed by Mokhi [39]. The issue is however, that no information is yet available about

the core resistance of the cables used. Another problem is the variable current, which would make the losses variable depending on the power levels being transmissioned. Although this is an accurate way of computing the losses, it is too complicated for this first approximation of the total system efficiency. Therefore, an efficiency value is used that was calculated for short-distance (1-2km) three-core MVAC cables that are being used in the offshore wind industry as inter-array cables [40]. The value that will be used is 0.975 to include all transportation losses between the turbine and the pump (excluding storage losses). Finally, the pump efficiency depends on its operating point. For different RPMs and power levels, different values of efficiency exist. A conservative approximation of the mean value results in an efficiency of 0.80 [18].

Table 2.2: Efficiencies that are used to estimate the required energy storage for the selected configuration of pumps and turbines.

Efficiencies	Value
Round-trip efficiency GES	0.75 - 0.90
Round-trip efficiency BES	0.70 - 0.90
Transmission efficiency	0.975 - 0.985
Water injection pump efficiency	0.70 - 0.82
Total estimated system efficiency ¹	0.49 - 0.73

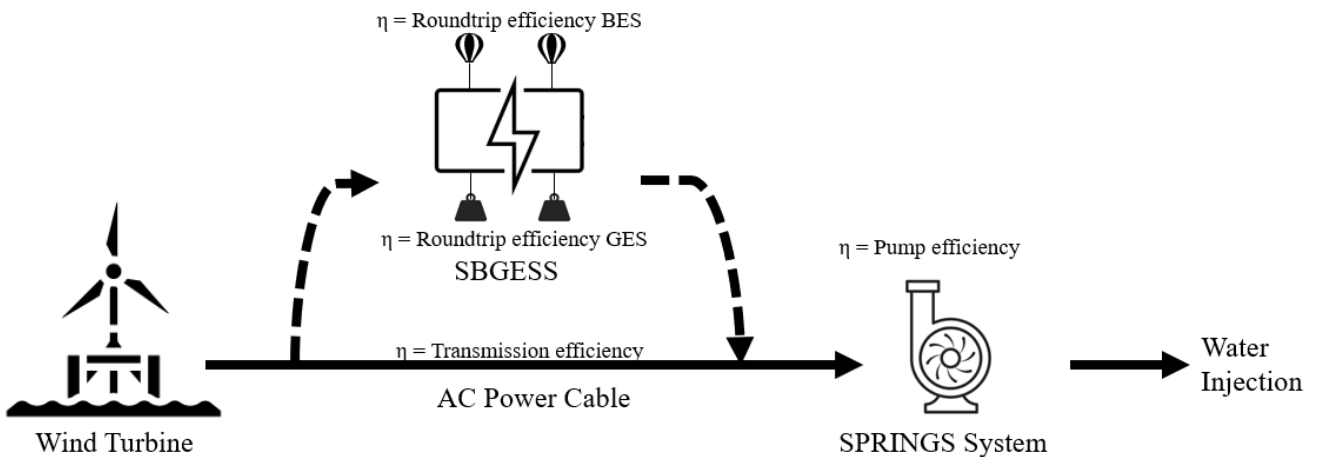


Figure 2.4: Visual outline of system components, including power conversion efficiency. Note: image is not to scale.

Two different paths for the energy should be distinguished: directly powering the SPRINGS where only the cable and pump losses should be considered (0.68 - 0.81% efficiency), and the second path that uses the SBGESS. The second path has an efficiency in the range mentioned as total estimated system efficiency in table 2.2. These two paths are visualized in figure 2.4. If the use of energy storage at a certain moment is unnecessary, the power losses are reduced as the storage losses do not have to be accounted for. The simulation will account for both paths accordingly.

2.3.2 Pump performance

Figure 2.1 shows that the flow that comes out of the pump can be computed by using a P-Q curve. This curve uses the power (P_{OUT}), corrected for the losses in the pump, to calculate the flow that is injected in the seabed. This data is needed as the production of the field depends on this rate and the study is aiming

¹computed by multiplying the average Round-trip efficiency of GES and BES, by the remaining efficiencies.

to substitute a 75000BPD injection system. The water injection can be variable, as the SPRINGS system uses a VSD, resulting in a range of frequencies that the system can operate in. As the frequency range in which the pumps operate (25 - 74Hz) is known, equations 2.3 and 2.4 can be combined to compute related P and Q values [20]. This was done for 100 values, after which a third degree polynomial was fitted to these points and hereafter used as the P-Q curve of which the function is presented as equation 2.5. A third degree was selected based on the cubic relationship between power and flow that can be derived from equations 2.3 and 2.4. It should be noted that the values at 74Hz, namely $P = 2170\text{kW}$ and $Q = 278.23 \text{ m}^3/\text{h}$ (42000 BPD), were used as Best Efficiency Point (BEP) [18].

$$\frac{Q}{Q_{BEP}} = \frac{n}{n_{BEP}} \quad (2.3)$$

$$\frac{P}{P_{BEP}} = \left(\frac{n}{n_{BEP}} \right)^3 \quad (2.4)$$

With:

Q = Water injection in m^3/h

Q_{BEP} = Water injection at the best efficiency point = $278.23 \text{ m}^3/\text{h}$

P = Power input in kW

P_{BEP} = Power input at the best efficiency point = 2170kW

n = frequency

n_{BEP} = frequency at best efficiency point = 74Hz

$$Q_{system} = \text{number of pumps} \cdot (aP^3 + bP^2 + cP + d) \quad (2.5)$$

With:

Q_{system} = Water injection by the total system in m^3/h

P = Power input per pump in kW

a, b, c, d = Polynomial fit parameters

Equation 2.5 was used in the simulation in the next subsection, resulting in an hourly output of the flow produced by the water injection system. The curvefit values and the numerical equation that was used can be found in appendix B.

2.4 Water injection simulation

To select the capacity the energy storage should have, a simulation was conducted using the parameters in table 2.3. The system should be able to fulfill two primary requirements:

1. The maximum number of stops per year is seventy. This is to ensure the reliability of the pumps [18].
2. The average water injection should be $496.85 \text{ m}^3/\text{h}$ (75.000 BPD), based on the Mero field reference project [18]. This is the average value that should be reached over the project's lifetime. Monthly or yearly deviations from this value are allowed, but may reduce the production during that period.

2.4.1 Simulation set-up

To check whether the selection of parameters and ultimately the energy storage capacity meet these two requirements, the forty-one years of wind data were used. Using the hourly data as input, the simulation has hourly power and flowrates and the yearly number of stops as output. These samples are then used to fit normal distributions to calculate the probabilities of not satisfying the requirements.

Table 2.3: Parameters that were used in the simulation.

Parameter	Value	Parameter	Value
Nr. of Wind turbines	2	Efficiency Transmission (η_T)	0.975
Nr. of water pumps	2	Efficiency Pump (η_P)	0.80 ²
Minimum power demand per pump	80.37kW	Round-trip Efficiency BES,GES (η_{ES})	0.83
Maximum power demand per pump	2.170MW	Start value ES ($ES_{t=0}$)	$0.5 \cdot ES_{cap}$

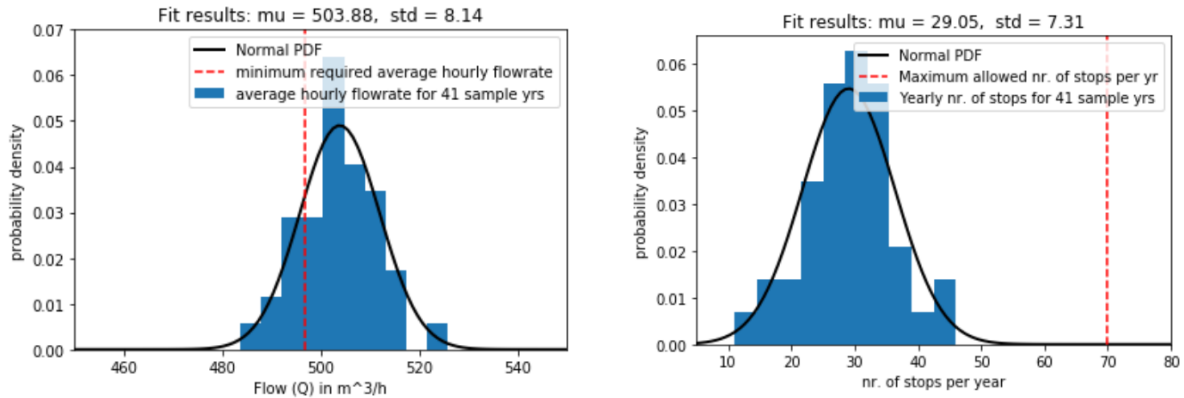
In the subsection on efficiency, it was already mentioned that the model should distinguish between two ways of delivering the power: direct and indirect (via the SBGESS). Because of the upper and lower limits of the power demand of the pump and the two values of system efficiency, three modes should be considered in the model. After several iterations did not lead to a satisfactory amount of yearly stops, a Power-saving mode was introduced as explained below. Figure C.1 in appendix C also indicates that without a power saving mode, the Energy storage capacity would need to be higher as the amount of stops is critical in that case.

- *Mode 1*: If the power generated by the wind turbines is higher than the upper limit in power demand of the pumps (including losses), the power of the turbines is supplied directly to the pumps. All remaining power will be used to charge the SBGESS until the capacity is reached.
- *Mode 2*: If the power generated by the wind turbines is between the upper and lower limits in power demand of the pumps (including losses), the power of the turbines is supplied directly to the pumps. Whether or not the SBGESS will be used to complement the power supply to the upper limit depends on which sub-mode is active:
 - *Submode 2a*: If the SBGESS is more than 12 hours of minimum power demand charged, the SBGESS will be used to supply the additional power needed for the pumps to operate at the upper power demand limit.
 - *Submode 2b*: If the SBGESS is at or less than 12 hours of minimum power demand charged, the SBGESS will be in 'Power-saving mode'. This means that the SBGESS will only be used to avoid stops (e.g. act if mode 3 is active). The Power-saving mode will automatically end once charging exceeds the 20%. The pumps will now operate at the power level that can be supplied by the wind turbines.
- *Mode 3*: If the power generated by the wind turbines is lower than the lower limit in power demand of the pumps (including losses), again two sub-modes can be identified:
 - *Submode 3a*: If the power generated by the wind turbines (if any) combined with the power that can be supplied by the SBGESS is enough to supply the lower limit, this will be done. This means that that the pump will keep running.
 - *Submode 3b*: If the power generated by the wind turbines (if any) combined with the power that can be supplied by the SBGESS is not enough to supply the lower limit, the pump will shut-off. This will count as 1 stop. The water injection rate will be zero. Any power that is generated by the wind turbine in this interval will be used to charge the SBGESS.

²The efficiency of the pump is already included in the minimum and maximum power demand. 0.80 was used as a constant efficiency for the entire pump performance curve.

2.4.2 Simulation results

Implementing these three modes in the simulation model, the results were obtained for different values of power saving mode and energy storage capacity as can be seen in figure C.1 in appendix C. The values of 12 hours of power saving mode and 8MWh of energy storage capacity were selected. These values lead to the lowest energy storage capacity requirement, while still satisfying the requirements in an acceptable way. The detailed results of this combination is shown in figure 2.5a and b and in table 2.4.



(a) Histogram of average hourly flowrate for 41 sample years, including a fitted normal distribution PDF. (b) Histogram of the number of yearly stops for 41 sample years, including a fitted normal distribution PDF.

Figure 2.5: Fitted normal distribution PDFs for parameters given in table 2.3

It can be concluded from figures 2.5 a/b and the distribution formula, that the system does meet the two primary requirements for the given parameters. The first requirement is clearly met as all 40 sample years have a total amount of stops lower than 70. The probability of exceeding 70 stops per year is $1.05 \cdot 10^{-4}\%$. This is deemed an acceptable risk. Any increase in Energy storage would be costly, yet hardly beneficial when it comes to reducing this number even more.

The second requirement is satisfied when only the average ($\mu = 503.88$) is taken into account. Yet it is clearly visible that the conditions are not met for each year in the sample. The probability of the average injection rate being below the required value for a certain year is 19.4% (table 2.4). It must be noted however, that all the sample years that are below the target value have an average injection rate that is within 3% of the target value. Questions could therefore be raised whether increasing the energy storage, given the extra production, installation and transportation costs, would be economical. Over the whole project lifetime the target value is reached. Considering all this, an energy storage capacity of 8MWh is selected as the design value that will be used to dimension the SBGESS.

Table 2.4: Results of the simulation of the water injection system, for forty-one years of data, using the parameters from table 2.3

Results	Value
Mean & STD nr. of stops per year	29.05; 7.31
Probability of exceeding 70 stops per year	$1.05 \cdot 10^{-6}$
Mean & STD water injection	503.88; 8.14
Probability of water injection being less than $496.85m^3/h$	0.194
Energy storage capacity (ES_{cap})	8MWh
Power-saving mode	12 hours \cdot <i>MinimumPowerDemand</i>

As this is a simulation to get an approximation of the required energy storage capacity, several assumptions and simplifications were implied. While running the simulation and fitting the distribution, all

fourty-one years were accounted for equally. Regional effects such as El Niño/La Niña, but also global events such as climate change could mean that recent shifts in wind patterns [41][42] are less prominent in the distribution than they would have been if recent years would be weighed heavier. Figure A.1 and table A.1 in appendix A may suggest an upward trend in mean wind speeds. However, as this is an exercise to find an approximate value and extensive research would be needed to assess these weighing factors, this simplification is deemed acceptable. Also, an upward trend in wind speeds would be favourable towards a smaller energy storage capacity, meaning that it is more conservative to not account for this trend. Furthermore, an r value of 0.37 is too low to take this trend into account. Another assumption is that a normal distribution is the correct distribution for the sample data. This is why it was also checked for each sample year, whether the fourty-one sample years did meet the requirements. Finally, availability of the pumps was not accounted for in the simulation. Yet, as the availability of the topside was also unaccounted for, it can be assumed that the small drop in water injection supply will not affect the production in a significant way.

3 | Preliminary dimensioning of the SBGESS

In the previous chapter, the system was analysed resulting in values for the required energy storage capacity and the power supply range. These values will be used as input in this chapter to assess the preliminary dimensions of the SBGESS. These dimensions are essential parameters for the selection of transportation and installation methods, and are essential input values for the model concerning the lowering of the SBGESS. This chapter will start with a general description of the proposed structure and the various segments that can be identified within the SBGESS. Secondly, the dimensioning strategy will be discussed including the relevant parameters and formulas. Hereafter, a list of dimensions is presented, with which the SBGESS is able to meet both the required energy storage capacity as well as the power supply range that will be needed to operate the water injection system.

3.1 Outline of the design

The design of the SBGESS is partially based on the design of the buoy supporting riser (BSR) developed by Petrobras and Subsea7 [26][27]. The BSR is in many ways similar to the SBGESS as it is installed in the ultra-deep waters of Brazil, has connections to both the topside as well as the seabed and is also installed at a large depth below the sea level. Although this design will be used as a base for the design of the main structure of the SBGESS, there are also significant structural differences. Most importantly, the BSR is asymmetrically shaped due to the vertical loading of the risers on one end. The SBGESS will be shaped symmetrically as the loads (neglecting power cables) are mostly symmetrical. Another essential difference is that the risers and other elements of the BSR are all connected to the main ballasting part. For the SBGESS, most elements, apart from the anchoring lines will be connected to the connecting structural elements between the two main ballasting parts. A schematic overview of the SBGESS can be found in figure 3.1.

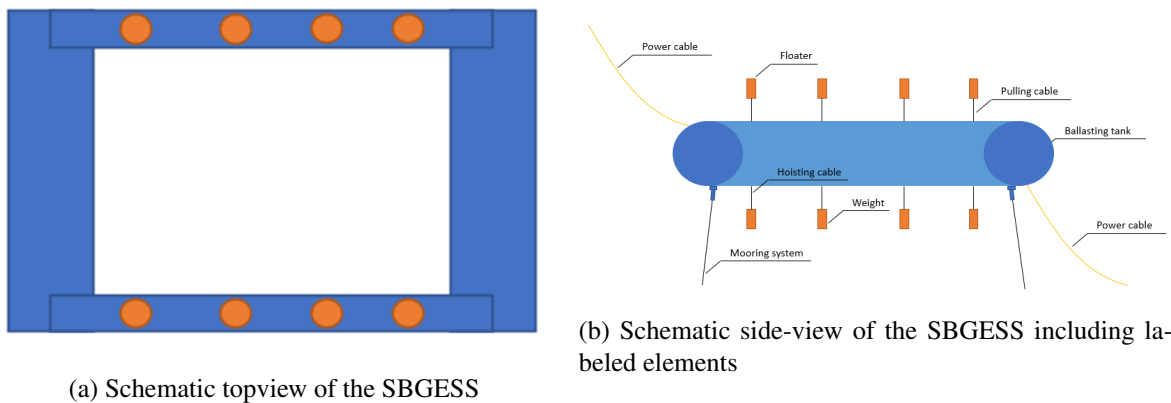


Figure 3.1: Schematic overview of the SBGESS, including a topview and side-view with labeled elements. Note: image is not to scale

As this thesis is not a detailed design exercise, the process is simplified by emulating the general dimensions of the BSR. Meaning that the length and width of the structure are assumed to be nearly the same as for the BSR. The same goes for the total ballasting tank volume that is present in the BSR. The detailed calculations of how this volume is distributed can be found in table D.2 in appendix D. The type of anchoring will be discussed in chapter 5. Materials and other structural details are not within the scope of this study, but an approximation of the total mass will be made for the modelling of the

installation phase. For now the shape as in figure 3.1 is assumed and used in the model, however this could be altered in a later design study. The weights and floaters are cylindrical in this design phase [22].

3.2 Dimensioning strategy

The previous chapter lead to requirements concerning the energy storage capacity and the power that the SBGESS should be able to deliver. The parameters of the SBGESS should be such that these two requirements are met, preferably with some redundancy. All the input parameters that are used in the following section can be found in table D.1 in appendix D. Because of the water injection simulation set-up, it is assumed that the SBGESS can fully charge in one hour or less. After dimensioning it should be checked whether this criterion is met.

The dimensioning started with the power requirement. The required power supply by the SBGESS is not equal to the maximum power demand of the pump because of two reasons. First, the efficiencies of the power cable and the storage efficiency should be included. They are both included for 50% as the cable length is half of the total length and the power supply only deals with a one-way efficiency of the storage cycle. Secondly, because of the set-up with the modes the energy storage should, in the most critical case, only deliver the power difference between the maximum and minimum power demand of the pumps. These two points are implemented in equation 3.1. Once again the pump efficiency is not included in this equation, as it was already included in the pump's power demand.

$$P = \text{NumberOfPumps} \cdot \frac{\text{MaximumPowerDemand} - \text{MinimumPowerDemand}}{\frac{1}{2}\eta_{ES} \cdot \frac{1}{2}\eta_T} = 2P_{unit} \quad (3.1)$$

Equation 3.1 leads to the necessity of the SBGESS being able to supply at least 4.65MW. It was decided that the SBGESS should be able to supply this amount of power by using only one combination of one weight unit and one floater unit. Such a combination including all electrical and mechanical equipment will from here on be called an Energy storage module (ESM). If an ESM is used instead of a single weight or floater, the net vertical force of this ESM as a result of the movement is nearly zero. In the next sections, the dimensions of both the weights and the floaters will be selected such that they can satisfy the power supply. Hereafter, the total number of ESMs can be determined based on the total energy storage capacity requirement.

3.2.1 GES: weights

Now that the required power for one ESM is known, 50% of this power should be supplied by one weight unit. With the velocity assumed to be fixed at 1m/s (Appendix D) equation 3.2 can be used to calculate the required mass for one weight. Hereafter the volume and the height of the weight (a cylinder) can be calculated by using equations 3.3 and 3.4. In these calculations, the weights are assumed to be 100% concrete and all other components of the unit are massless as a simplification. For the GES elements, high-density concrete is used to reduce the dimensions and therefore the added mass and drag.

$$m_{weight} = \frac{P_{unit}}{g \cdot v} \quad (3.2)$$

$$V_{weight} = \frac{m_{weight}}{\rho_{concrete}} \quad (3.3)$$

$$h_{weight} = \frac{V_{weight}}{\pi \cdot r^2} \quad (3.4)$$

With:

m_{weight} = Mass of 1 weight unit in kg

P_{unit} = Power by 1 weight unit in W

g = Standard gravity in m/s^2

v = (Dis)charging velocity in m/s

V_{weight} = Volume of 1 weight unit in m^3

$\rho_{concrete}$ = Density of concrete in kg/m^3

h_{weight} = Height of 1 weight unit in m

r = Radius of 1 weight unit in m

The resulting dimensions are shown in table D.1 and in figure 3.2.

3.2.2 BES: floaters

As stated in the previous section, 50% of the required power should be supplied by one floater unit. With the velocity assumed to be fixed at 1m/s (Appendix D) equation 3.5 can be used to calculate the required force for one floater. This is the net vertical force. Because the velocities of the weights and floaters and the power supplied are the same, the forces exercised by both units are equal (neglecting drag forces for now). Hereafter the volume and the height of the floater (a cylinder) can be calculated by using equations 3.6 and 3.7. In these equations the floaters were assumed to be 100% Styrofoam, which is a light-weight material with a relatively low drag coefficient [22][43].

$$F_{floater} = \frac{P_{unit}}{v} \quad (3.5)$$

$$V_{floater} = \nabla = \frac{F_{floater}}{g \cdot (\rho_{seawater} - \rho_{Styrofoam})} \quad (3.6)$$

$$h_{floater} = \frac{V_{floater}}{\pi \cdot r^2} \quad (3.7)$$

With:

$F_{floater}$ = Net vertical force of 1 floater unit in N

P_{unit} = Power by 1 floater unit in W

v = (Dis)charging velocity in m/s

$V_{floater}$ = Volume of 1 floater unit in m^3

∇ = Volume of water displacement in m^3

g = Standard gravity in m/s^2

$\rho_{seawater}$ = Density of seawater in kg/m^3

$\rho_{styrofoam}$ = Density of styrofoam in kg/m^3

$h_{floater}$ = Height of 1 floater unit in m

r = Radius of 1 floater unit in m

The resulting dimensions are shown in table D.1 and in figure 3.2.

3.2.3 Energy storage

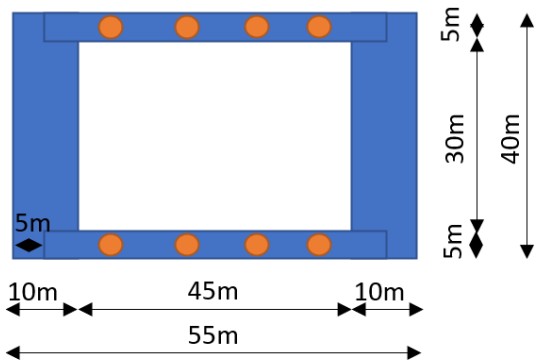
The second requirement, namely enabling sufficient energy storage capacity, can only be met if the number of floaters and weights is large enough. This should be checked by use of equation 3.8.

$$ES_{cap} = n_{units} \cdot P_{unit} \cdot t_{discharging} \geq 8MWh \quad (3.8)$$

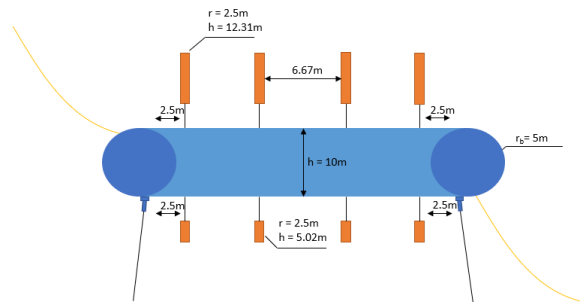
It is important to realise that the number of units is the sum of the weights and floaters on both sides of the SBGESS. Both the number of floaters and weights as well as the number of ESMs on both sides should be equal because of symmetry. The smallest value that meets all the requirements is 8 ESMs, meaning 8 floaters and 8 weights in total. This would lead to an energy storage capacity of 10.32MWh. The redundancy is also deemed acceptable as three units (or one ESM) can be non-functioning and the capacity would still be larger than 8MWh.

3.3 SBGESS dimensions

In this section, the parameters and configuration of the main structure and the weights and floaters is summarized and visualized in figure 3.2. An extensive overview of the input- and resulting values can be found in table D.1 in appendix D, but a summarised overview is given in table 3.1. The selected velocity of 1m/s allows for a minimum charging time of 16.7 minutes. This is the minimum charging time for both single systems as well as for the whole system, as multiple systems can charge in parallel. This means that the criterion of a charging time under one hour is met.



(a) Schematic topview of the SBGESS including dimensions of the main elements



(b) Schematic side-view of the SBGESS including dimensions of the main elements

Figure 3.2: Schematic overview of the SBGESS, including a topview and side-view with dimensions of the main elements. Note: image is not to scale

Table 3.1: Summarised overview of resulting parameters of the preliminary dimensioning of the SBGESS

Parameter	Value
Length of SBGESS	55m
Width of SBGESS	40m
Height of SBGESS	10m
Ballast tanks volume of SBGESS	8998m ³
radius of weights	2.5m
radius of floaters	2.5m
height of weights	5.02m
height of floaters	12.31m
nr. of weights	8
nr. of floaters	8
Total mass of weights	2681.6 tonnes
Total mass of floaters	96.65 tonnes
Energy storage capacity	10.32MWh

The model in chapter 7 will use the simplified shape of the SBGESS as shown in figure 3.2 and the values of appendix D. It is important to note that this was a preliminary dimensioning and several components were simplified with the modelling in mind. One such component is the ballasting tanks, which now consists of only four tanks. In reality, tens of ballasting tanks will be needed [26] to accommodate for adequate adjustments and to included redundancy in case of leakage/flooding.

The selected dimensions are the result of assumptions with regards to the functionality of the SBGESS. By implementing the modes described in chapter 2 it was assumed that the units can instantaneously accelerate and decelerate to the required velocity to deliver the right amount of power. In reality, because of inertia and/or system limits, this will not be the case. These system limits will also lead to a maximum and minimum allowable velocity, restricting the power range the SBGESS can supply. Also, the system should allow for both sequential as well as simultaneous movement of combinations of units as specifically charging requires parallel movements of several units.

4 | Mooring systems and Anchors

In this chapter the SBGESS' mooring system and potential anchor types will be discussed and analyzed. As the primary focus of the overarching thesis is on the installation methods, only a relatively short chapter is dedicated to mooring. A compact overview is presented with the key properties of the potential anchors. At the end of this chapter, a list of selection criteria is suggested, after which a preliminary anchor selection is made.

4.1 Why position-keeping is important

Offshore structures require position keeping, not only because of functionality, but also because of safety issues such as possible collisions [44]. Two options are available for this station-keeping, namely: Dynamic positioning (DP) and mooring systems. DP is less useful for this particular case, as it is a permanent structure at 1000m waterdepth, the latter making maintenance complicated. DP can also consume a significant part of the generated power. Therefore, a mooring system is the preferred choice here. For mooring systems, several configurations are used. The most commonly used are: catenary, semi-taut, taut and tension leg.

4.2 Tension leg mooring system

The SBGESS design is based on the Buoy supporting riser (BSR). The BSR was developed by Petrobras and Subsea7 [26][27]. Multiple BSRs have been installed in the ultra-deep waters of Brazil. These BSRs have connections to both the topside as well as the seabed and are installed at 250m below the sea surface. They support the risers, causing a decoupling of the motion of the vessel and the subsea equipment, as well as decreasing the load caused by the weight of the risers. To simplify design procedures, Novgorodcev JR. decided to select a tension-leg type mooring system, similar to that of the BSR [22]. It will contain four mooring points, with two tethers each. The tethers consist of working chains and sheathed spiral strand wires [22][26]. In the remainder of this chapter only the anchors that can cope with vertical loads (taut/tension leg) will therefore be discussed, as a tension. Anchors such as the drag embedment anchors, although being able to function in a large variety of soil types, will not be discussed because of their limited vertical holding capacity.

4.3 Anchor types

There are many available anchors to moor offshore structures. A list is presented below which shows the most common types of anchors that have significant vertical load capacity [44][45].

- Suction piles
- Deep penetration anchor
- Lowerable gravity anchor
- Torpedo anchors
- Driven piles
- Dead-weight anchors
- Vertically loaded anchors (VLA)
- Suction embedded plate anchors (SEPLA)
- OMNI-Max anchor

There are more anchors available, yet for the purpose of this study, only these types will be analyzed as the publicly available information on other anchors is not sufficient to describe their properties extensively.

An overview of the primary properties and limits of the anchors is presented in table 4.1. This table serves as a tool for a first selection based on feasibility of an anchor type for a specific case. However, the ultimate selection should be based on carefully weighing all the pros and cons as well as looking at the economic and company-specific arguments. For a detailed description of how these anchors work and should be used, the author recommends chapter 8 of the work by Ma et al. [44].

Table 4.1: Properties of different types of anchors. Data and/or insight obtained from: [18][44][45][46][47][48][49][50][51][52][53]. In case of lack of data: NA.

Anchor type	Mooring type	Resistance	Soil	Water depth	Other
Suction piles	Catenary, (semi) taut and tension leg	High, both horizontal and vertical	Sands, soft and stiff clay	Up to ultra-deep waters	Together with driven piles most commonly used deepwater anchor
Dead-weight anchor	Catenary, semi-taut	small vertical capacity (few tonnes)	Mostly hard/medium soils	Up to ultra-deep waters	Rarely used because of the limited capacity. A feasible option only in really hard soil
Driven piles	(Semi) taut and tension leg	High vertical resistance	Sand and Clay; wide range of soils possible	Up to 2400m (although less common in ultra-deep water)	Together with suction piles most commonly used deepwater anchor
VLA	Catenary, (semi) taut	Some vertical capacity, depending on orientation and embedment depth	(Layered soil with) soft clay	Up to ultra-deep waters	-
SEPLA	Taut	Medium vertical load capacity	Soft clay	Up to ultra-deep waters	-
Lowerable gravity anchor	Tension leg	Same as dead-weight anchor	Same as dead-weight anchor	Up to 350 - 500m	Still in conceptual phase
Torpedo anchor	(Semi) taut	75 - 100 tonnes	(soft) clay	Up to ultra-deep waters	More than 2000 installed
OMNI-MAX anchor	(Semi) taut	Highly dependent on embedment depth	Clay	Up to ultra-deep waters	Booster can increase embedment depth and therefore load capacity
Deep penetration anchor	(Semi) taut	NA	NA	Up to ultra-deep waters	Very little information in publicly available literature

It is important to place a footnote with this table, as in practice the possibilities and limitations may deviate from those found in literature. For example, using a booster may cause OMNI-MAX anchor to

be usable in crust-over-soft-clays [52]. Another way of increasing the potential is using counter-weights, which was used for the BSR's suction piles [26][27]. Table 4.1 thus gives an overview of what should be at least possible.

4.4 Criteria to select a type of anchor

The mooring system should be considered in an early phase of the design process as it should function with the installation and transportation methods. Some anchors such as the lowerable gravity anchor require a specific transportation method (wet tow in this case) and installation method. For other anchors the possibilities may be larger, but may influence details of the installation procedure, such as whether or not temporary hook-ons are implemented.

To select an anchor, a detailed soil survey should be conducted as this is a limiting factor for many anchors. Also the load capacity should be considered, primarily the vertical upward force should be countered as well as the horizontal force induced by the currents. Decommissioning and maintenance should also be included in the final consideration.

For the purpose of this study a selection of criteria was made. Decommissioning and maintenance for example, will not be taken into account, as this study primarily focuses on the installation phase. It also important to note that the design of the SBGESS and the location are still preliminary, therefore only a preliminary anchor selection can be made, not requiring an exhaustive list of criteria.

- Water depth
- Load capacity
- Soil properties
- Installation
- Field proven
- Fixed or temporary

The following subsections will elaborate on some of the criteria and state the project specific parameters that should be taken into account.

4.4.1 Water depth

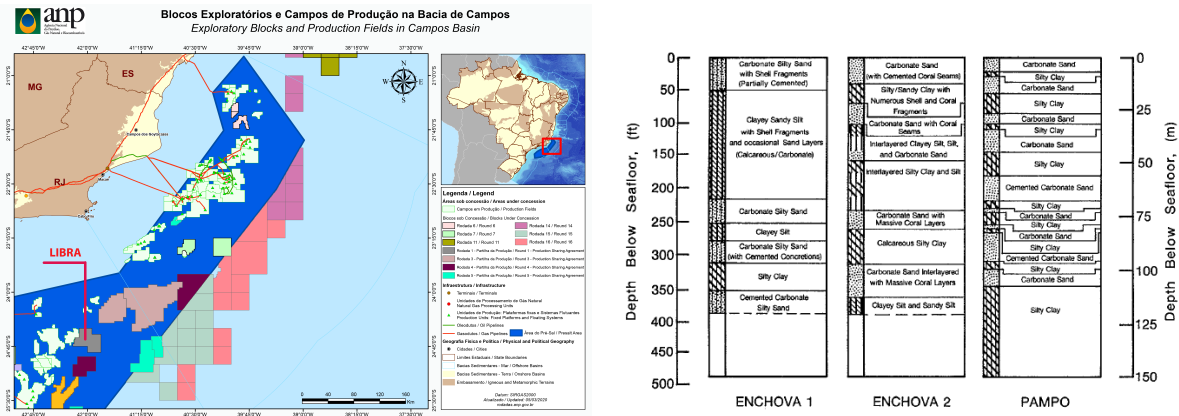
The SBGESS is likely to be installed in the western part of the Libra field (inside the Santos Basin), Figure 4.1a. Using the same coordinates as were used for interpolating the wind data (Chapter 2), Serviço Geológico do Brasil [25] indicates a water depth of approximately 2100m at the project location. Any anchor that may be used should therefore be able to meet the requirements at this depth.

4.4.2 Load capacity

Although there will be horizontal loads on the anchor, given that the mooring lines will be positioned similar to that of the BSR, the vertical loads will be more significant in this taut mooring system. The proposed anchor should therefore have a high vertical load resistance. For the SBGESS, the upward vertical load induced by just the the buoyancy minus the steel weight is approximately 7200 tonnes [26]. As the SBGESS will not have risers and the vertical forces of the weights and floaters will cancel each other out, this number could be seen as a first rough estimate of the minimum required vertical strength. If required, vertical load capacity can be increased by use of measures such as counter-weights as was done for the suction anchors of the BSR (800 tonnes counter-weights) [26].

4.4.3 Soil properties

No location-specific soil data is available within public sources. Also, no data from adjacent fields is available, other than general soil types mentioned in installation reports from platforms in the area. In order to select a type of anchor, soil data is necessary. Hence, generalized soil data from the adjacent Campos basin is used. A visualization of this data and the location are shown in figure 4.1. For this estimation of the soil conditions to be as accurate as possible, the area within the Campos basin that is closest to the Libra field was used, the so-called 'South pole area' [54].



(a) Overview of the Campos basin including an indication of the location of the Libra field in the adjacent Santos basin. Map obtained from: [21] (b) Generalized soil conditions of the Campos basin's south pole area, image from: [54]

Figure 4.1: Soil properties from the adjacent Campos Basin

As this location is relatively far from the Libra field for the soil data to be considered accurate, it can be argued that it is best to consider all soil types mentioned in the three locations within the south pole area instead of picking one of these three. As the soil data will be used to assess the feasibility of certain anchors, it is reasonable to only consider the top layers within the first 50 meters below the seafloor, particularly focussing on the top 25 meters. Although 50 meters might be more than the embedment depth of some of the anchors considered, it is important to consider larger depths as for example torpedo anchors may have a penetration depth of more than 30 meters [55].

Within those first 50 meters, the following dominant soil types can be distinguished: carbonate (silty) sand, silty/sandy clay and clayey sandy silt. For the purpose of this study, it is required of the selected anchor to be able to be deployed in these soil conditions. It was also noted that shell and coral fragments were found within the layers which, depending on the currents, could also be expected for the Libra field.

4.5 Evaluation

Based on a first analysis multiple anchors can be disregarded. Dead-weight anchors are rarely used for mooring operations because of the limited holding capacity and are therefore less appropriate for this project. The lowerable gravity anchor is not (yet) able to function at the project's waterdepth [45]. Driven piles have an uplift resistances of 5000 tons or more and are well suited for TLP support (direct uplift) [44]. Although driven piles are known to be used in water depths of up to 2400m, they are less common for ultradeep water. Therefore, they are less likely to end up as the selected anchor for this study.

VLAs can be used in layered soils with soft clay, but given the presence of (carbonate) sands in the upper layers, it is not a logic choice. The VLAs also has a lower vertical load capacity than suction piles,

while not having the benefits of a simple installation such as dynamically installed anchors. Torpedo anchors and OMNI-MAX anchors both have been installed in large numbers in ultra-deep waters [53][52]. Although their vertical load capacity is relatively small (75 - 100 tonnes), the installation procedure is trivial and boosters can increase the hold. The preferred soil conditions for these type of anchors (dynamically installed anchors) is soft clay, yet they can work with layered soils and other soil types as well, indicated by the large amount of installed anchors in the Santos and Campos basin [53][55][52]. They could therefore be a viable option.

Suction piles and SEPLAs are meeting all the criteria for this project, as their vertical load capacity is large, they are commonly-used in ultra-deep waters and they can operate in a large range of soil conditions. SEPLAs combine the precise vertical and horizontal positioning of a suction pile with the lightness and efficiency of a plate anchor. Installation time is in the order of 20% greater than for a conventional suction pile installation [44]. However their vertical load capacity is limited, therefore suction piles are deemed more appropriate for this project. Ultimately, that leaves both dynamically installed anchors and suction piles as viable options to consider for this project. However, as the choice between these options is not likely to have a significant impact on the overall transportation and installation phases, a final selection can be made once a detailed soil investigation is conducted.

5 | Transportation methods

Transportation is an important phase of the project, especially since more and more projects move further offshore [10]. As the distances increase, the importance of having an economic and efficient transportation method increases. Another aspect to consider is that as a result of the longer travel times, it is more likely to encounter a large variety in sea-states while transporting. This could not only affect the vessel's behaviour, but also that of the tow [56]. Selecting the right transportation method is therefore critical to ensure sufficient weather window and to minimize delays in this phase of the project. This chapter will discuss the most common transportation methods that are used for large offshore structures. Within the three main categories, multiple variants can be identified. These will be analysed, including their (dis)advantages, equipment needed and limitations. Hereafter, a first evaluation will result in a selection of methods that are deemed feasible for the SBGESS. The criteria based on which the final selection can be made will then be outlined.

5.1 Categories of transportation methods

When looking at ways of transporting large offshore structures, two main categories can be distinguished: dry-tow and wet-tow [57][58]. However, for the purpose of this research, there are actually three categories to be considered, as the wet-tow can be divided into two subcategories. A wet-tow can be done on the surface (floating) or fully submerged[58]. As the response to the environmental conditions is significantly different for these two options, they will be considered as separate categories. As a result, three categories will be further analysed:

1. Dry-tow
2. Wet-tow: Floating
3. Wet-tow: Submerged

5.2 Dry-tow

A dry-tow can be conducted in multiple ways. Depending on the availability of vessels and the size/number of objects, a heavy lift vessel (HLV) may be used with or without a barge. Some papers distinguish between these options and name the option without a barge 'on deck'. However, as the challenges and advantages are quite similar, these are combined here as 'dry tow'. If a barge is used this barge may be towed while floating (figure 5.1a) or be slightly submerged [57]. Compared to wet-towing it does offer advantages such as the ability to repair/assemble at sea yet it does involve more steps like sea-fastening and heavy-lifting through the splash-zone. The lift-off and subsequent immersion is a critical phase of the operation due to potential large dynamic loads and risk of collisions due to relative motions of the vessel and structure. In the splash-zone the most critical wave loading occurs. The fact that dry towing includes this phase is therefore a serious consideration during selection. Another limiting factor may be the dimensions of the structure as the vessel and/or barge will have a maximum load and size that it can handle[59]. Therefore, for large-sized structures, dry-tow is often neglected for economic reasons [59][60]. Structures with tens of meters in length will limit the number of HLVs that have sufficient deckspace. It is also important to note that the dayrates of HLVs are expensive, especially in cases where flexibility in scheduling is needed [60].

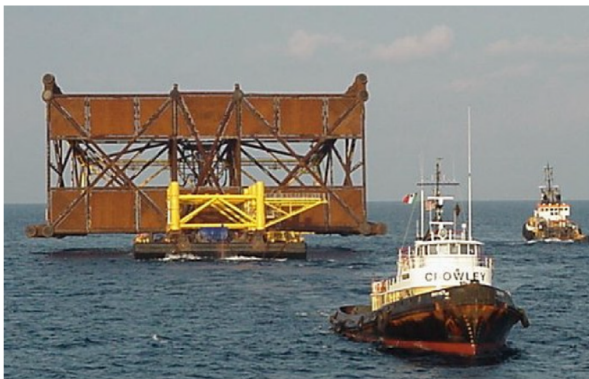
5.3 Wet-tow: Floating

A wet-tow is conducted by having the structure transported through the water. The structure is usually towed by multiple tugs or a single offshore service vessel. Possibly the biggest advantage of floating (or surface) towing compared to submerged towing is the lower amount of resistance as the structure will experience less drag. However, the structure is more prone to a large motion response induced by surface waves [58]. Like dry-towing, visual inspection is still possible. The towing configuration can be simpler but ballasting and stabilization are critical to account for the motion responses.

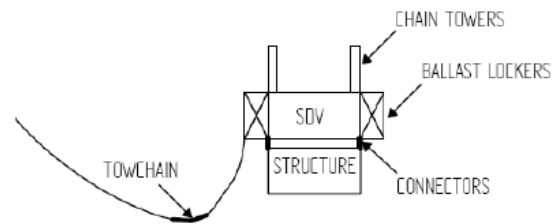
5.4 Wet-tow: Submerged

Although this is not a method that is often used, it does present some advantages as it significantly reduces the influence of the surface conditions [58][61][62]. It is important to distinguish between different methods here. One method is to use the ballasting tanks to submerge the structure and have multiple towlines to tow and stabilize the structure [58]. Another method called the subsea deployment system (SDS) involves a subsea deployment vehicle (SDV) to actively assist the structure during the tow (figure 5.1 b) [61]. SDS is applicable to structures weighing to several thousands of tonnes, in waters to 3000m deep, especially well suited to hostile environments. Subsea7 also developed a submerged wet-tow method which is called the wet tow installation method (WITM) [10]. The structure is transported by a tow through the moonpool of an offshore service vessel. Jakobsen [62] argues that this method is cost-efficient as it skips the offshore lifting phase.

As the structure is fully submerged during tow and installation phase it avoids some of the more crucial phases of the installation procedure involving heavy-lifting through the splash-zone. Also, it leads to reduced influence of surface weather during the tow phase. This combination should lead to larger weather-windows for the installation. However, there are still risks involved. The ballasting phase, in combination with the towing configuration, is absolutely critical to not only reach the required depth, but also acquire stability throughout the whole process. As was stated before, this method of transportation is not often used in the field and should be very carefully modelled and tested before use. Especially the hydrodynamic loads on the different components of the system should be carefully analysed [62].



(a) dry tow of a structure by using a barge, image obtained from [63]



(b) Visualization of a submerged wet tow by using an SDV, image obtained from: [61]

Figure 5.1: Two examples of a dry and a wet tow transportation

5.5 Considerations when selecting a transportation method

How to transport the structure is also highly co-dependent on the chosen type of anchor and the installation method. For example, when selecting the lowerable gravity anchor developed by GICON-SOF, it is implied to use a wet-tow [45][64]. The installation method can also limit the number of possible

transportation methods as it can require specific type of vessels. Once these frameworks are established, other criteria are considered. In order to select a transportation method for a project, it's vital to consider several parameters of both the structure and the location. Below, a list is presented with important considerations to take into account when evaluating transportation methods.

General considerations:

- *Dimensions and weight of structure:* These should be known as they may limit the possibilities, e.g. the size limits of the vessels involved in a dry tow or the weight limits of a wet tow.
- *Statistical METOCEAN data:* A first statistical analysis of the wind, wave and currents data may prove useful to see how feasible one of the transportation methods is. It can also provide information on which months are deemed preferable for transportation and installation. The latter can matter for the availability of certain vessels and therefore the selected method [59].
- *Economic considerations:* In order to select an appropriate method, it is critical to look at the costs involved. These costs are build up by vessel rates and wages and therefore by the duration of the project, but also expenses like fuel should not be neglected. How this can influence the method is nicely illustrated by the towing velocity. If this parameter is increased (if conditions and simulations allow it) it will reduce the project duration yet it can cause the fuel expenses to increase due to the increased drag and required thrust [58].
- *Risks:* Although all other considerations are related to risks and provide information on the permissible conditions, it is good to identify and quantify risks of potential methods. Especially once a method is selected, an effort should be made to quantify the risks, due to a lack of guidelines and data [57], while it can help to improve or adjust the method.

Dry-tow considerations:

- *Size and weight limits; equipment availability:* The vessel and/or barge that will be used will have limits to what size and loads can be carried [65]. Exceeding the load capacity of the deck or maximum dimensions may lead to usage of a barge which will have to satisfy these requirements. The crane lifting capacity of the available vessels could limit the weight of the structures they can transport and install. Depending on the dimensions of the structure to be installed, the vessels and cranes that can be used could be limited to only a few worldwide.
- *Statistical METOCEAN data:* As the lift-off and lowering through the splash zone is arguably the most critical phase of the dry-tow process [56], it is vital to assess the available wave data and forecast to find permissible sea-states and adjust the schedule accordingly [63]. Besides waves, wind should also be considered, as this may impact the relative motions of the crane, structure and vessel as described below.
- *Relative motions:* Contrary to wet-tows, one or multiple cranes are involved in the installation process following on a dry-tow. This creates a risk, as the relative motions of the vessel, crane and structure can cause collision. To avoid these, it is important to simulate and find out which conditions are acceptable and to adjust the transportation schedule accordingly [59][66].
- *Assembly:* Some structures can be assembled both on- and offshore. This choice may result in a different selection of vessels and therefore different permissible sea-states. Especially when the structure is large, offshore assembly or installation by parts can provide a solution when a dry-tow is wished for.

Wet-tow considerations:

- *Ballasting and tow configuration:* Virtually all papers on wet-towing emphasize that ballasting is critical [57][56][58][64]. This not only concerns the total ballasting volume, but also the amount of compartments, the filling (and defilling) velocity and the redundancy. The tow configurations is

also important to consider as it will be co-dependent on the amount of tugs as well as the towing velocity.

- *Motion dynamics and stability issues:* The biggest risk for a wet-tow is failure due to excessive motion dynamics and/or instability. During the tow, hydrodynamic loads will act on the structure [59]. Instabilities can occur due to these hydrodynamic loads (e.g. vortices), but also because of surface inclinations in the ballasting tanks. For a dry-tow this is less of a problem, as usually the hydrodynamic coefficients and permissible sea-states of the vessels involved are known and in a (company's) database. However, most of the structures that are transported involve new shapes or configurations that are can not always be related to known coefficients [67]. Therefore, extensive simulation and lab testing is generally required to set the maximum permissible sea-states and towing velocity for the wet-tow.
- *Statistical METOCEAN data:*
 - *Floating:* For a floating wet-tow, waves should be considered as they induce loads and may affect stability. The tow configuration and ballasting should be adjusted to cope with these loads [59].
 - *Submerged:* Besides stability, one of the main concerns while selecting the level of submergence and the towing velocity is the drag forces [58]. Current plays an important role in that perspective and should therefore be taken into account. Currents can also cause instabilities, e.g. due to vortex formations.
- *Equipment and availability:*
 - *Floating:* For a floating wet-tow equipment availability is less of a concern, as (anchor handling) tugs (which are most commonly used) are widely available [44].
 - *Submerged:* However, for the submerged wet-tow, either an offshore vessel with a moonpool or special devices like the SDV are required.

This list is not exhaustive, but acts as a guideline and tool to make a first assessment of the feasibility of different methods. Ultimately, the companies involved in the project will be influential as well, as their preferences and available vessels could make a certain method stand out.

5.6 Summary and evaluation

What should be considered when analysing and evaluating the methods that were listed above, is the fact that the SBGESS consists of multiple large objects. Assembly at sea is possible for dry-towing and the floating version of wet-towing, but might be challenging for the submerged method. Alternatively, the system as a whole (including attached weights and floaters) might be submerged and then transported, yet this will influence the hydrodynamics.

For projects of similar size and planning, dry-tow is often neglected for economic reasons [59][60]. The SBGESS will have tens of meters in length and width which will limit the number of HLVs that have sufficient deckspace. It is also important to note that the dayrates of HLVs are expensive, especially in cases where flexibility in scheduling is needed [60]. Also noteworthy is that Petrobras decided to use a wet-tow for the installation of the four BSRs in similar conditions with similar dimensions [27]. Combining these arguments with the fact that not using a dry-tow avoids having to lift the SBGESS of the deck through the splash-zone, it seems acceptable to neglect dry-towing in this early stage.

This leaves the two methods of wet-towing. Yet to decide between these two, it is critical to obtain knowledge on, among others, the motion dynamics and required power to tow the structure [57]. Modelling and testing these methods to obtain these values is outside the scope of this study. Therefore, as the transportation method should be such that it matches the selected installation method, the two

remaining options will both still be considered and a final recommendation can only be made once an installation method is defined or vessel limitations are known.

6 | Installation methods

This chapter will discuss the most common installation methods that are used for large offshore structures. For these methods, multiple variants can be identified, as companies often have their own specific equipment that allows for certain adjustments on a general method. These will be analysed, including their (dis)advantages, equipment needed and limitations. Hereafter, criteria will be suggested which can be used to evaluate the installation methods for a specific case. As the SBGESS project is located in a deep water area, only installation methods that can be classified as 'deep water installation methods' will be discussed.

6.1 The challenges of offshore installation in ultra-deep waters

Several challenges need to be overcome for ultra-deep water (such as the Brazilian large reserves in the pre-salt layer) installation procedures. These challenges are the result of the harsh marine environment (weather, geology, chemical abrasion), great distances of the platforms to shore, and other issues related to the poor visibility and accessibility of subsea operations and equipment due to the immense water depth [65].

Another problem that deep-water installation procedures can particularly be sensitive to is the so-called "resonance zone". The combination of mass and stiffness properties of the structure and installation equipment (e.g. cables) will lead to a natural vibration period of the system. The range in which this natural period overlaps with the excitation periods from the ocean waves is the resonance zone [65]. The best way to avoid excessive dynamic behaviour in this range is to move quickly through this region. However, this is only possible if the resonance zone is not near the depth at which the structure will be installed. Otherwise, more careful installation and usage of motion compensation devices may be required [68].

Another potential impediment is the duration of the installation procedure. As the water depth is large, the lowering procedure is likely to take longer than the average installation. Another reason why the duration can be expected to be longer is that Remotely Operated Underwater Vehicles (ROVs) need to be used at these water depths, which can also slow down the procedure. A longer duration itself is not a direct threat to the operation, but it does mean that larger suitable weather windows are required. Therefore, selecting an installation method that has a larger range of permissible sea-states can prove to be extra beneficial for ultra-deep water projects.

Besides the challenges mentioned above, Cao et al. [60] identified two other major hurdles: deck size/crane capacity and installation costs. The latter one links to the duration of the procedure, but also to the equipment used. Penati et al. [69] describes the goal of offshore deep water installation as: 'maximise economic gain safely using the most reliable and cost-effective solutions currently available'. As offshore vessel day rates are expensive, it is essential to select and schedule the installation wisely.

6.2 Installation methods

Ten common and two specific installation methods are discussed in this section. These do not cover all possibilities, but they do represent the state-of-the-art of offshore installation.

6.2.1 Traditional installation methods: DRIM and WWIM

Typically, there are two installation methods that are defined as 'conventional' or 'traditional' installation methods: the Drilling riser installation method (DRIM) and the lifting method [10]. DRIM (also called 'drilling method'[65]) makes use of the drilling riser system that is on board of the drilling vessels. These vessels have good positioning-keeping due to their DP and can usually withstand heavy weather conditions. Cao et al. [60] describe a method fairly similar to DRIM, namely the Drill-strings installation method (DSIM) which also uses the drill string infrastructure, but does so from a platform and not from a vessel. The main limitation for DRIM is the size of the moonpool that the structure will be lowered through.

The other traditional method, the lifting method, is also known as the winch-wire installation method (WWIM). It is normally used in combination with a dry tow on the vessel of a barge, after which a crane is used to lift the structure and lower it by paying out the winch wire. Neto et al. [65] state that for deep and ultra-deep waters the dynamic amplification effects may become severe. To avoid this, the use of slings and a spreader bar is suggested as an alternative. A major concern for both traditional methods is the limited lifting capacity of the cranes and cables. This is why the traditional methods are less frequently used these days [60][10].

6.2.2 Wet tow methods: PBM, SDS, FID and WTIM

Most authors of papers on deepwater installation agree on three methods that fall in the 'wet tow' category. With the pencil buoy method (PBM) the weight of the structure will be transferred to the pencil buoy in near-shore waters, which will then be used to transport the submerged structure to the location. Here, the load is transferred to a winch which will then be used to lower the structure to the required depth (figure 6.1a) [10]. As with all wet tow methods, it eliminates the need for deck space and heavy-lift cranes. The second wet tow method is the subsea deployment system (SDS). This system was already extensively discussed in chapter 5. It uses a subsea deployment vehicle (SDV) to carry the submerged structure to the location and then lowers the SDV with the help of anchor handling tugs (AHT). This system is able to install structures up to 3000m of water depth [61]. Cao et al [60] developed a concept called the 'floating installation device' (FID). This device, made of solid buoyant material, supports the subsea equipment in the transportation and installation phase (figure 6.1b). With the use of ballasting and chains the device and the structure are lowered. Given the configuration of the FID and the structure, the dimensions and load of the structure will need to fit the FID. No information on loads or dimensions is given, but a numerical simulation in a water depth of 1500m was presented, making the FID potentially useful for deep water installation procedures.

Wang et al. [10] actually describes a fourth method that can be classified as a 'wet tow method', the so-called wet tow installation method (WTIM). This method was developed by Subsea 7 and is similar to the traditional methods, yet it transports the submerged structure with a tow through the moonpool of the vessel (figure 6.1c). As a result, a larger weather window is available for the installation and it also avoids having to deal with the limiting dimensions of the moonpool which was the main concern for the DRIM [10]. Other methods can be combined with a wet tow as well, but doing so eliminates one of the larger advantages of a wet tow transportation, namely not having to use a heavy-lifting offshore vessel.

6.2.3 Other methods: SIM, PIM, HCLS and Y - method

Recent decades have seen many new conceptual installation methods, some of them which have been actually exploited offshore. Neto et al. [65] and Cao et al. [60] both highlight SIM, PIM and HCLS as feasible installation methods. An example of this is the sheave installation method (SIM). SIM has proven to be successful in deep waters, yet it requires a semi-submersible rig and two AHTs, which makes installation complex and expensive (figure 6.1d). Because of the complexity, Cao et al. [60] also stresses the importance of numerical simulation and field-testing. Pendular installation method (PIM)

requires less special vessels, as only a crane barge and an AHT are needed (figure 6.1e). With PIM the structure is installed by letting the structure lower in a strongly damped pendular motion. This motion is caused by disconnecting the lifting cable from a triangular plate [65]. The most severe risk of this method is the lack of operator control once the structure is in this pendular motion, which can lead to stability issues.

Heave compensated landing system (HCLS) uses a buoy in the system below the splash zone, resulting in a (partial) decoupling of structure from the heave motions of the vessel. The amount of equipment and special care with regards to controlling the ROV make this method complicated to perform [65]. Neto et al. [65] also mentions a fourth method: the y-method. The Y-method is similar to the sheave method, yet the configuration and shape of the lowering cables is different (figure 6.1f). The cables together with the triplate form an Y-shape, which minimizes the effects of wave motions on the submerged structure. For this method, two AHTs are needed.

6.2.4 BSR installation method

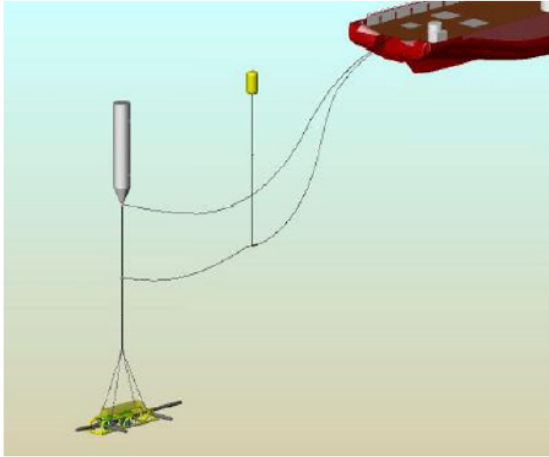
As was stated before, the design and mooring configuration of the SBGESS is partially based on that of the BSR [22]. Therefore, the installation procedure of the BSR could be extra relevant for the installation of the SBGESS which is why it is discussed here. Multiple methods were suggested for installing the BSR and the final method differed greatly from what was originally proposed. The original method proposed by Fernandes et al. [70][71] only uses one supply vessel at the surface which is connected to the BSR by a lowering line with clump weights. Furthermore, four lines with auxiliary buoys are used to position and stabilize the BSR during the process. However, the method requires a unique supply vessel and some of the adjustment procedures are very delicate. Also, not all of the tests gave satisfying results with regards to the trim and heel angles.

In the end, a method very similar to the Y - method and the FID was used. Two anchor handling tugs were used on the surface and ROVs delivered subsea support. As the BSR is a positive buoyant structure, no devices like a FID or SDV were needed [27]. The descent was conducted and controlled by using the ballasting and buoyancy tanks of the BSR and the weight of the lowering chains (connected to the AHTs). The BSR contains 48 tanks of various sizes, both ballasting and buoyancy, which creates both flexibility and redundancy for the lowering operation [26][18]. The ROVs were used to support in ballasting and pressurization but also for the hook up. Temporary tethers were used for a preliminary positioning after which the BSR was hooked up to the permanent tethers.

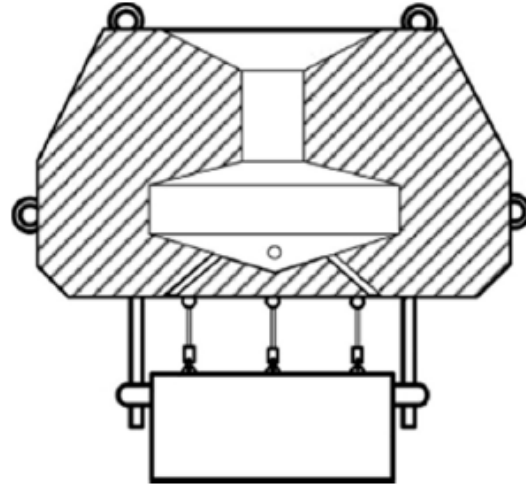
6.3 Equipment for lowering subsea structures in deep water

A variety of special equipment is used during the lowering phase. Almost all methods use one or more AHTs (also called AHV or AHTS). These vessels are ideal for installation as they can handle anchors and mooring lines, but also transport floating structures and deploy subsea equipment [44]. AHTs are widely available as they are also the commonly used vessel to support offshore platforms. Another vehicle that is often used in deep water installations is the ROV as it can operate at large depths and support with hooking, pressurization and ballasting. ROVs can also perform visual inspections to confirm the installation went right.

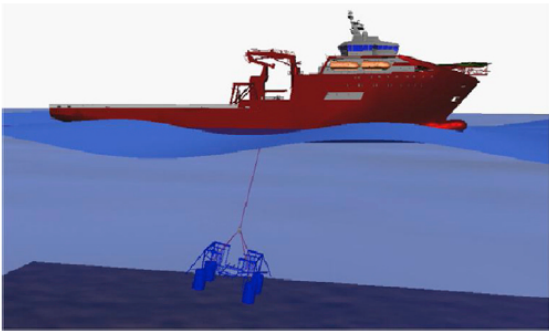
As stated above, most installation procedures need some kind of device to transfer the load to during the lowering. This can be a triplate, SDV, FID or another device specifically developed for a certain method. Often, within the lowering configuration some sort of heave compensation is included. This can be passive or active depending on the method [65]. One example of passive heave compensation is the motion compensator developed by Mahone et al. [72] as it does not require any active involvement after pressurization at the surface. Not all methods need heave compensation, as some methods already create enough stability redundancy with the cable configuration or the ballasting.



(a) Illustration of the installation set-up for PBM



(b) Illustration of the device used for FID



(c) Illustration of WTIM

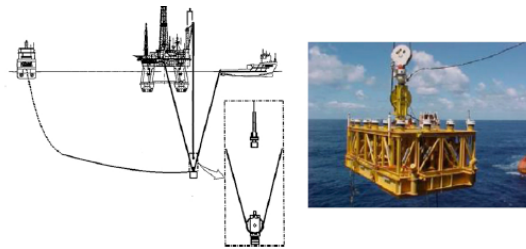
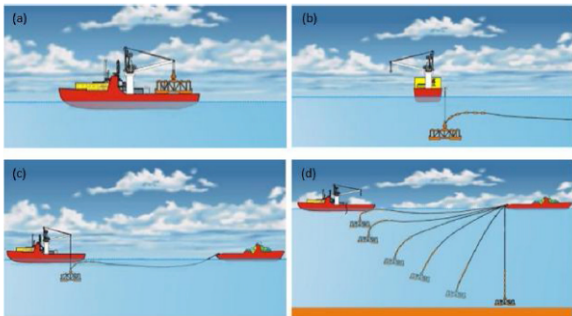


Fig. 4. Sheave method [13].

(d) Illustration of SIM



(e) Illustration of the installation procedure for PIM

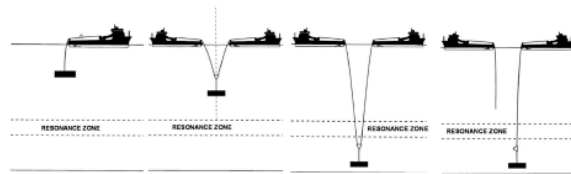


Fig. 6. Y method [17].

(f) Illustration of the y-method

Figure 6.1: Six deepwater installation methods, all figures obtained from [65]

To increase the lowering velocity or to add stiffness, clump weights are often used on the lowering cables [70]. These can be retrieved at the surface once the installation is completed. Another way to increase the lowering velocity or to create a net downward force is the use of pull-down lines [73].

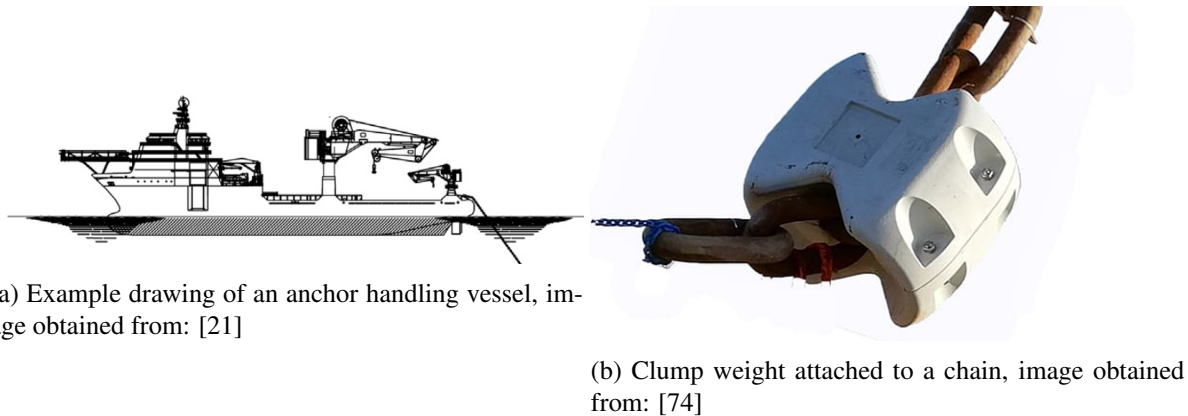


Figure 6.2: Examples of equipment and vessels used for offshore installation procedures

6.4 Summary of installation methods

The list of installation methods above is not exhaustive, but does present a variety of options to consider. To summarize these options in a clear way, the Figure below is included here. This figure represents an overview of possibilities per phase, some of which can be combined.


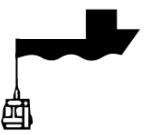

Phase	Possibilities		
Lifting 	Deck/Barge ↓ overboarding	Deck/Submerged tow ↓ lift through moonpool	Wet tow
Lowering 	Cable a. Drilling riser system b. Lifting cable c. Lowering chain i. Pendular motion ii. y - method iii. Sheave method	Support device a. Pencil buoy b. SDV c. FID	Additional lowering support a. Ballast tanks b. Clump weights c. Heave compensation i. Active ii. Passive
Positioning 	ROV	Hook-up a. Direct hook-up i. Temporary hook-up, later permanent ii. Permanent hook-up b. Submerged tow to final position i. Temporary hook-up, later permanent ii. Permanent hook-up	

Figure 6.3: Schematic overview of installation procedures per phase. Note that this table serves to show the diversity and amount of possibilities. A combination of certain options should be carefully analysed, especially if it deviates from one of the methods described earlier in the chapter.

Figure 6.3 does not represent the complete installation procedure, as some methods require additional or less phases. The installation of the mooring system is only briefly mentioned in this table. Usually, the mooring system installation consists of three phases: anchor installation, mooring prelay and hook-up [44]. Only the latter is included in this overview as it is more related to the installation of the structure itself.

6.5 Selection on an installation method for the SBGESS

As was stated earlier, to select a transportation method, extensive modelling and testing is required to test its feasibility and make adjustments. However, a first selection can be made based on limiting factors such size, weight, water depth, the occurrence of certain sea-states, equipment availability, etc. The transportation method should also function with the selected anchor type and transportation method, although those can also be selected after the installation method is checked.

In chapter 5 it was suggested that a wet tow is likely to be the most economical choice for transportation. This means that the traditional installation method are not deemed appropriate for the SBGESS project. Based on the size and dimensions of the SBGESS outlined in chapter 3 the lowering of the SBGESS is likely to classify as a heavy lift ([75], see chapter 7 for further explanation). Being a heavy-lift the motions of the vessel and the cable-subsea equipment system can not be assumed to be dynamically uncoupled. To avoid resonance conditions to cause large motions of the vessel and potential safety issues, it is wise to take precautions to decouple and/or reduce the influence of the SBGESS motions on the vessel. Precautions could include using a tow configuration similar to the BSR, SIM or Y-method or use a heave-compensator device. Installation aids such as a SDV or FID could be used, however these could be considered redundant as a unique feature of the SBGESS is that it is able to have a variable ballasting and can trim by achieving both a positive and a negative net vertical force.

The results in chapter 8 should therefore be studied carefully to determine whether these decoupling precautions are necessary, either to reduce the motions of the SBGESS or their influence on the vessel motions. Given the above considerations and the usage of a wet tow, AHTs are likely to be the vessels of choice for this project.

Independent of the selected installation method, a choice must be made whether to install the SBGESS as a single unit or do a modular installation. The latter meaning the GES and BES elements are lowered and connected after the main element is placed. This is discussed in chapter 7 and the relevant results are shown in 8.

7 | Modelling methodology

As was stated in chapter 6, to select and improve the installation method, it is vital to simulate and test the method. Since testing is outside the scope of this thesis, only the simulation is focused on for the remainder of this report. Simulations can be run by using commercial software such as 'Orcaflex', which allows for a great amount of detail and statistical analysis. However, in the current phase of the SBGESS project in which many parameters are still not fixed and only their order of magnitude is known, a more simplified model can provide useful insights in the behaviour during the installation. This insight then can be used in further optimizing the dimensions and installation parameters.

In this chapter, it is first discussed how the installation phase, specifically the lowering phase, can be modeled using a single degree of freedom mass - spring - dashpot system. Hereafter, the state-of-the-art of these type of models is presented by explaining two models currently used to do a first assessment. Finally, the methodology for doing the simulations is outlined, including a list of assumptions and variables that will be included.

7.1 Vertical displacement model of the lowering phase

In the early stages of simulating the installation procedure, single degree of freedom (SDOF) models are common. These are relatively simple to apply and give a good insight into the behaviour. For (ultra-)deep water installations, the most important degree of freedom is the vertical displacement of the structure. Although horizontal excursions are likely to occur, either because of current loads or horizontal vessel movements, they are likely to be relatively small due to the cable configuration and the usage of dynamic positioning (DP) on the vessels.

To address stability concerns, the roll and pitch angles should also be simulated and checked whether they stay within their limits. However, for this early phase, they are outside the scope of this thesis. It should also be noted that only a preliminary dimensioning was carried out, meaning that the parameters' order of magnitude is known but their lack of accuracy does not justify the usage of a more detailed model.

The earliest models that were used did not have a variable cable length, meaning it was necessary to perform several simulations with the equipment positioned at different depths [75]. One disadvantage of this way of modelling is that it does not consider the influence that the payout speed might have on the dynamics of the system and on the operational weather window. Especially for ultra-deep water installation procedures the payout velocity can be critical as a higher speed may reduce the dynamics while going through a resonance zone [68]. This thesis therefore only considers variable length models.

The two models that are described in the remainder of this chapter both assume that the motions of the SBGESS do not influence the vessel motions, being so-called: 'dynamically uncoupled'. According to DNV-RP-H103 this is the case if the lift classifies as a 'light lift', meaning that the mass of the equipment should be less than 1-2% of the displacement of the vessel(s). The vessel (type) is currently unknown, but DNV also presents a rule of thumb: more than 1000T usually classifies as a 'heavy lift'. The SBGESS, especially with the BES/GES elements attached, exceeds 4000T. Considering this, the assumption of being dynamically uncoupled would then be invalid. However, the probable lowering rigging configuration as described in chapter 6 is such that the catenary shape will reduce the effect of the motions. For this phase, the assumption is therefore deemed valid but may need to be re-assessed in a later stage.

7.1.1 Tommasini model

Tommasini et al. [76] was one of the first to develop a variable length SDOF model for ultra-deep water installations. Using a mass - damper - spring model, a Lagrangian approach led to equation 7.1.

$$\begin{aligned} \left(M_{eq} + M_{add} + \frac{1}{3}m'L \right) \ddot{w} + \left(\frac{m'\dot{L}}{3} + \frac{1}{2}\rho C_d A_p |\dot{w}| \right) \dot{w} + \frac{EA}{L}w = -\frac{(m' - \rho A)gL}{2} \\ - (M_{eq} - \rho V)g + \frac{EA}{L}w_0 - \frac{m'\dot{L}}{6}\dot{w}_0 - \frac{m'L}{6}\ddot{w}_0 \end{aligned} \quad (7.1)$$

With:

M_{eq} = Mass of SBGESS, including (if applicable) weights, floaters, ballasting in kg

M_{add} = Added mass, as calculated by $\rho V C_a$ in kg

m' = Linear mass of cable in kg/m

L = Length of the cable in m

w = Vertical displacement of the Centre of gravity (COG) of the SBGESS in m

ρ = Density of sea water in kg/m^3

C_a = Added mass coefficient of the SBGESS in [-]

C_d = Drag coefficient of the SBGESS in [-]

A_p = Acting surface of the SBGESS in m^2

EA = Cable axial stiffness in N

A = Cable intersection surface in m^2

V = Water displacement volume of the SBGESS in m^3

w_0 = Vertical displacement of the lowering point on the vessel in m

For this thesis, the model presented by Tommasini is extended. Similar to the SBGESS, the displacement of the GES elements (the concrete weight units) can be modelled using a SDOF model. Instead of using the vessel motions as input, equation 7.2 uses the SBGESS' displacement. For this equation to be valid, once again the assumption needs to be made that the GES elements are dynamically uncoupled from the SBGESS. Following the rule from DNV-RP-H103 [75], it should be checked whether this can be categorized as a 'light lift'. As a single GES element has a mass of 335.2T (appendix D and the displacement of the submerged SBGESS is $10.000m^3$, the relative mass is less than 1-2% meaning it can indeed be classified as a light lift. The assumption of the GES displacement not influencing the SBGESS movements can therefore be assumed valid.

Equation 7.2 involves less terms than equation 7.1 as the traction cable that holds the GES elements does not change in length. Several other parameters such as the drag- and added mass coefficient are also different, the used values can be found in appendix E. A schematic overview of the resulting model is shown in figure 7.1.

$$\begin{aligned} \left(m_w + m_{add} + \frac{1}{3}m'l \right) \ddot{z} + \frac{1}{2}\rho C_{dw} A_{pw} |\dot{z}| \dot{z} + \frac{EA_l}{l}z = -\frac{(m'_l - \rho A_l)gl}{2} \\ - (m_w - \rho V_w)g + \frac{EA_l}{l}w - \frac{m'_l l}{6}\ddot{w} \end{aligned} \quad (7.2)$$

were:

m_w = Mass of 1 GES element in kg

m_{add} = Added mass, as calculated by ρVC_a in kg

m'_l = Linear mass of cable in kg/m

l = Length of the cable in m

z = Vertical displacement of the COG of the GES element in m

ρ = Density of sea water in kg/m^3

C_{dw} = Drag coefficient of the GES element in [-]

A_{pw} = Acting surface of the GES element in m^2

EA_l = Cable axial stiffness in N

A_l = Cable intersection surface in m^2

V_w = Water displacement volume of the SBGESS in m^3

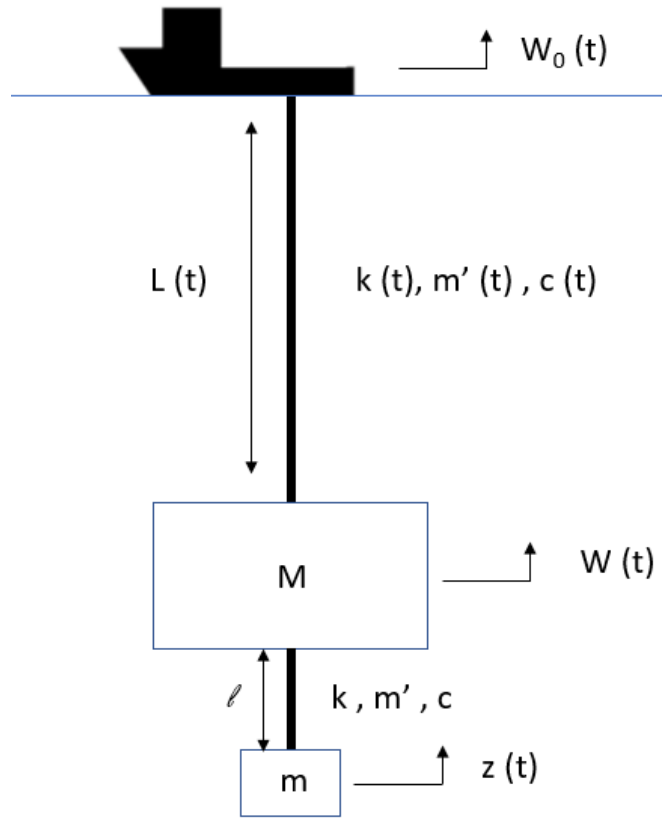


Figure 7.1: Schematic overview of the extended model for the SBGESS and GES displacements during the lowering operation.

Tommasini also provides equations for the forces in the cable, at the top and at connection to the equipment. Assessing these forces provides insight in the dynamic forces yet it is also important to check whether the forces do not exceed the safe working load (SWL) of the cable.

$$F_{top} = \frac{EA}{L}(w_0 - w) + \frac{(m' - \rho A)gL}{2} \quad (7.3)$$

$$F_{eq} = \frac{EA}{L}(w_0 - w) - \frac{(m' - \rho A)gL}{2} \quad (7.4)$$

The forces that are calculated by these equations consist of a static and a dynamic part. As the static force is a known function of the given parameters, the dynamic contribution to the force can be calculated. The equations for the static forces are [68]:

$$S(L)_{\text{top}} = [M - \rho V]g + (m' - \rho A)gL + \frac{1}{2}\rho C_d A_p |V_c| V_c \quad (7.5)$$

$$S(L)_{\text{eq}} = [M - \rho V]g + \frac{1}{2}\rho C_d A_p |V_c| V_c \quad (7.6)$$

As can be deduced from the above equations and the equations for the total forces, the differences between the force on the top and the equipment equals the submerged mass contribution, both for the total force and the static force. Therefore, the dynamic force on the top of the cable and at the equipment connection will be equal at each point in time. Only the dynamic force on the top of the cable will thus be shown in the results.

7.1.2 Gao model

Gao et al. [77] developed another vertical displacement model to simulate the displacement and forces during a deep-water lowering operation. The main difference between Tommasini and Gao is that Gao uses the 'lumped-mass' method and divides the cable into N discrete elements as shown in figure 7.2. Tommasini linearized the displacement through the entire rope as it considers the cable as one element. Gao states that using the discrete elements allows for simulating forces in the rope that reflect the real forces more accurately. It can also easily cope with slack and snap loads in the cable. Rather than letting the number of discrete elements grow, the discrete elements grow in size for each time-step, simulating the increase in cable length.

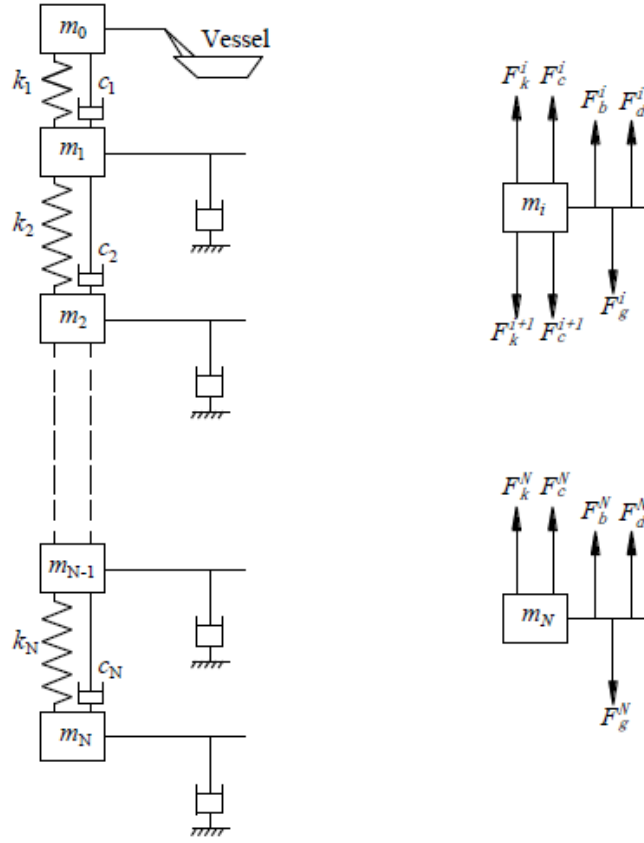


Figure 7.2: Schematic overview of the lumped-mass model for the subsea equipment lowering operation. Figure obtained from [77]

The displacement direction that is computed with Gao is u , which is similar to w in Tommasini. However, in Gao the positive direction is downwards, contrary to the upward definition in Tommasini. Gao also assumes the vessel motions and the SBGESS motions to be dynamically uncoupled. One difference between both models that can be extracted from the equations is that Gao does include the drag force of the cable whereas Tommasini does not. However, for the simulated set of parameters the drag of the cables was found to be insignificant and thus should not lead to any significant difference between the models.

$$[M][\ddot{u}] = [D][u] + [B_c][\dot{u}] - [B][\ddot{u}] * [|\ddot{u}|] + [f] \quad (7.7)$$

where $[M]$ is the Mass matrix, $[D]$ is the Rigidity matrix, $[B_c]$ is the damping matrix and $[B]$ is the viscous matrix. $[f]$ is the load vector which includes gravity and buoyancy loads. Tommasini provided equations to compute the forces in the cable at two points of interest, as did Gao. Equations 7.8 and 7.9 are used to calculate the cable forces at the top and equipment connection of the lowering cable ¹².

$$F_{\text{top}} = k_1 (u_1 - u_0) + \frac{1}{2} (\rho_l - \rho_w A_c) \Delta L g + \frac{1}{16} C_{d,r} \rho_w \pi D_r \Delta L (\dot{u}_1 + \dot{u}_0) |\dot{u}_1 + \dot{u}_0| \quad (7.8)$$

$$F_{\text{eq}} = k_N (u_N - u_{N-1}) - \frac{1}{2} (\rho_l - \rho_w A_c) \Delta L g - \frac{1}{16} C_{d,r} \rho_w \pi D_r \Delta L (\dot{u}_N + \dot{u}_{N-1}) |\dot{u}_N + \dot{u}_{N-1}| \quad (7.9)$$

¹In the second term of both equations, the standard gravity (g) was missing in the original paper by Gao et al. This was confirmed after correspondation between the author of this thesis and P. Gao.

²The second term was adjusted to account for the submerged linear mass instead of the linear mass of the cable. This to comply with the Tommasini model.

where:

k_1 = stiffness coefficient for element 1 in kg/s^2

k_N = stiffness coefficient for element N in kg/s^2

u = Vertical displacement in m

ρ_l = linear mass of cable in kg/m

ΔL = Length of one element in m

$C_{d,r}$ = Drag coefficient of cable in [-]

D_r = Diameter of cable in [m]

In order to effectively compare the two models for the thesis' set of parameters, it's important to select the right number of discrete elements for the Gao model. A convergence study was done for case 1 and 2 (see below) which concluded that having more than 20 elements gave no significant improvement to the results (less than 0.1% change). Therefore, $N = 20$ was selected as number of elements for this thesis. As Gao, due to the N elements, takes more time to compute than Tommasini and gives similar results (see chapter 8), the GES elements' displacement is not included in Gao.

7.2 Detailed modelling methodology

7.2.1 Assumptions and simplifications

For both models:

- SBGESS simplified as one pointmass in which all forces on SBGESS act. No compartments or internal inclined ballasting surfaces.
- Motions of vessel and cable/SBGESS are dynamically uncoupled.
- prismatic cable (properties same over whole length). Gao allows for different properties for different elements, but not considered in this thesis.
- No current (lift) forces considered, as inclinations/angles and horizontal displacements are not modelled.
- Small numerical errors may be introduced by solving the differential equations. Small timesteps (0.001s or less) are used to reduce the impact.
- Only vertical displacement modelled, as horizontal excursion will be relatively small and vertical displacement is of interest.
- potential lowering rigging configuration is reduced to one cable, under a 90 degree angle.
- added mass of cable is neglected

Tommasini:

- Linearizes the displacement through the entire rope
- Drag induced by the cable is neglected

Gao:

- Linearizes the displacement through an element of $1/N$ of the total length of the rope
- Does not take into account the acceleration term of the vessel movements

7.2.2 Waves and vessel motions

As was stated above, currents are not considered as the horizontal displacement is not simulated in this work. Waves will be included in the model, as the resulting horizontal displacement of the vessel may lead to insight in the behaviour of the structure in and/or near resonance zones [67]. Similar to Tommasini and Gao, a sinusoidal function is implemented to simulate the waves as shown in equation 7.10.

$$H_t = h_s \sin(\omega_s t) \quad (7.10)$$

The amplitude and frequency that are used can be found in appendix E. These are determined by the wave scatter in figure F.2. Of the most occurring conditions the lower values are taken, as the installation procedure is likely to take place in calm weather conditions and restricted to certain months. As the vessels that will be used are unknown at this point in time, the response amplitude operators (RAOs) to translate the wave motions into vessel motions are currently unavailable. Therefore, it is assumed that the vessel displaces simultaneously with the waves. Since it is likely that multiple vessel will be used for the lowering operation, these may displace with a phase angle. However, as the model only consist of one vessel, this can not be simulated.

7.2.3 Slack and snap forces

Although during most of the lowering procedure the cable is expected to be under tension due to the net downward force of the equipment, in resonance zones or for cables with a very high elasticity slack in the cable may occur. It is critical that the models take slack into account, as failing to do so may lead to underestimating the displacements and dynamics. As soon as slack occurs the axial stiffness of the cable should drop to zero as it will otherwise act as a spring and therefore a restoring force. For both models, it is assessed whether or not there is slack in the cable for every timestep. For Tommasini either the whole cable experiences slack or not at all, while for Gao this is determined for each element individually.

Once slack is introduced in the cable it is expected to return to an elongated position due to the restoring effect of gravity. As this happens it will introduces a snap load.

7.2.4 Hydrodynamic coefficients

Both the added mass and drag coefficient of the SBGESS are expected to have significant impact on the dynamics. The added mass will alter the natural frequency of the system, meaning that the resonance peak will shift to another depth. The drag of the SBGESS will introduce another damping term to the equation which is important to reduce oscillations, especially during resonance. The values for these coefficients are usually found by conducting (forced oscillation) tests, as the coefficients depend on the Keulegan Carpenter (KC) number [67][68]. With $KC = \frac{u_0 T}{L_{obj}}$, it can be seen that the coefficients will vary with the motion amplitude and period.

As the SBGESS is still in its concept phase at the time of writing this thesis, no model tests have been conducted. This means that only an estimation of the coefficients based on precedent projects and/or literature can be given. Obtaining the values from these sources gives a range of 1.2 to 2.4 for the added mass coefficient [67][18][65][75] and 1.0 to 1.5 for the drag coefficient [78][75]. In the simulations $C_D = 1.3$ and $C_A = 2.0$ are used. As the uncertainty for these values is high, both values are subjected to a sensitivity analysis of which the results are presented in chapter 8.

Finding a value for the hydrodynamic coefficients of the GES elements is more trivial as they are dimensioned as cylinders. This means that the theoretical coefficients can be found in DNV-RP-H103 [75]. For the added mass coefficient a value of 1.0 is common for cylinders. The drag coefficient for

a cylinder in parallel flow can be found by the ratio between length and diameter: $L/D = 1.004$ which leads to $C_D = 0.91$.

For the cable, the added mass is not included in the model as the contribution, even at large cable lengths, was found negligible. This is in accordance with what Tommasini and Gao found for their parameters [77][76]. Contrary to the SBGESS and GES, the drag type that is expected to be dominant for the cable is not form drag, but viscous drag. Especially in this model, where no current or horizontal excursions are accounted for, form drag can be neglected. The Tommasini model does not account for viscous drag, yet Gao does. For this viscous drag a coefficient value of 0.02 is used [79].

7.2.5 Variable ballasting

A unique feature of the SBGESS is that it is able to (de)ballast during the installation. Most subsea equipment where ballasting is required, either to reduce dynamics or to have a net downward force, need external weights or an installation device (chapter 3) to do so. Like the BSR, the SBGESS will have tens of ballasting tanks, partially for operation, partially for installation. For the simulations a constant ballasting fill is assumed during the whole lowering operation. However, this constant value of fill percentage has a range from which can be selected. This range was determined based on the static force described in section 7.1.1. It was found that the ballasting tanks need to have a minimum fill percentage of 75% to have a net downward static force and thus be able to recover from slack conditions.

The selected value for the installation phase is unlikely to correspond to the value selected for the operational phase. During installation a net downward force is required, whereas during operation a net upward force is essential to keep tension on the mooring system. The fill percentage during operation will therefore have a value which is lower than the minimum value for installation. To assess the influence of this variable ballasting during installation, the fill percentage is also subjected to the sensitivity analysis in chapter 8.

7.2.6 Initial conditions and velocity

The selection of initial conditions should be such that it simulates the eventual installation in a realistic way. It should be noted that the initial location is already some tens of meters below the surface, which is the location where final checks and pre-ballasting will be conducted, similar to the BSR installation procedure [27]. If $w_{t=0}$ would be zero, the SBGESS would be located at the depth similar to the initial cable length. However, this would induce a sudden increase in forces as the cable would then experience a quick elongation due to the net vertical force of the SBGESS. This would not be realistic as during the final check and pre-ballasting the SBGESS would automatically place itself around its static equilibrium. Therefore $w_{t=0}$ will have a value where the static equilibrium is met, meaning that the elastic force in the cable equals the net vertical force of the buoyancy and gravity forces. The same is done for the GES element's initial displacement.

During the simulations a constant payout velocity will be used throughout most of the lowering phase. Initially the velocity is increased until the target payout velocity is reached. Once the SBGESS is near the final depth of 1000 meters the velocity is decreased. To avoid a sudden increase of forces in the cable, large steps in the velocity function should be avoided. To make the acceleration and deceleration phase and the transition to the constant velocity phase smooth, a function should be used that is semi-continuous meaning the steps in velocity and acceleration should be negligible. A low-pass filter, an ordinary differential equation of the first order, was selected for this purpose as its timesteps can be set manually and the 'smoothness' of the transition can be regulated [80].

$$\begin{aligned}
\text{for } t \leq 8T : \quad \dot{V}_c(t) &= -\frac{1}{T}V_c(t) + \frac{1}{T}V_{c,ref,start} \\
\text{for } 8T < t < t_{end} - 8T : \quad V_c(t) &= V_{c,target} \\
\text{for } t \geq t_{end} - 8T : \quad \dot{V}_c(t) &= -\frac{1}{T}V_c(t) + \frac{1}{T}V_{c,ref,end}
\end{aligned} \tag{7.11}$$

where:

$V_c(t)$ = payout velocity of the lowering cable in [m/s]

$\dot{V}_c(t)$ = payout acceleration of the lowering cable in [m/s^2]

t = time in [s]

T = time constant in [s]

t_{end} = time at which target depth is reached in [s]

$V_{c,ref,start}$ = payout velocity which is targetted by the low pass filter, equal to $V_{c,target}$ in [m/s]

$V_{c,target}$ = payout velocity which is targetted during the lowering operation in [m/s]

$V_{c,ref,end}$ = payout velocity which is targetted by the low pass filter at the end of installation, equal to zero [m/s]

The used values for the parameters can also be found in appendix E.

7.3 Simulation cases description

In this thesis, four cases will be simulated using typical values for different types of cables. It is then checked whether a case does not exceed the limitations. The parameters that vary for each case are shown in table 7.1. A list of all other parameters, which are kept constant for each case, can be found in appendix E. The reasoning behind the four cases can be found in the next two subsections.

Table 7.1: Overview of parameters that are used in simulating the four different cases. Lowering cable: 1 = chains, 2 = polyester rope; Traction cable: A = steel wire rope, B = polyester cable.

Parameter	Case 1A	Case 1B	Case 2A	Case 2B
Lowering cable				
EA [MN]	22144.8	22144.8	1343	1343
m' [kg/m]	4800	4800	1092	1092
D [m]	0.51	0.51	1.11	1.11
MBL [kN]	630000	630000	210000	210000
SWL [kN]	180000	180000	60000	60000
Traction cable				
EA [MN]	1542	76	1542	76
m' [kg/m]	94	34	94	34
D [m]	0.133	0.229	0.133	0.229
MBL [kN]	14275	14715	14275	14715
SWL [kN]	4079	4204	4079	4204

Most of the literature on cables only mentions the minimum breaking load (MBL) value. However, by using DNV-OS-H205 [81] and an approximate value of $\gamma_{s,f} = 3.5$ the SWL can be estimated using:
 $SWL = MBL_{sling} / \gamma_{sf}$

7.3.1 Lowering cable

Chapter 6 described the method that is likely to be used for the installation of the SBGESS, which has many similarities with that of the BSR. For the BSR, four sets of four cables (attached to two AHTs) were used for the lowering [18]. The main part of these cables were chains. As the models only allow for one cable, this one cable should represent the whole lowering rigging configuration.

Therefore, the chain values of Chung et al. [82] are scaled such that the dimensions comply with the lowering chains for the BSR. It is then iteratively checked whether the SWL is approximately three times the static force calculated with equation 7.5. Hereafter, the polyester cable values of Neto et al. [65] are iteratively scaled such that the SWL also equals three times the static force. For both cables, the static force at the longest cable length (1000m) is used to calculate the static force. The resulting parameters and dimensions of both the cable and chains can be found in table 7.1.

7.3.2 Traction cables

The GES and BES elements described in chapter 3 are connected to the SBGESS by traction cables. Novogordcev JR. decided to use "Polyester fibre ropes or SSW to be defined in function of the total weight and dynamic behaviour" [22]. Therefore, in this dynamic simulation both type of cables should be considered. Only the GES elements are modelled as the static net vertical force of the BES elements is directed in the opposite direction of the payout direction and collisions and/or large vertical vibrations are thus less likely to occur.

With equation 7.5, using the dimensions of the GES elements as described in appendix D, the static net vertical force is found. The traction cable should have a vertical load capacity that can hold this static force, yet also the dynamic forces that will occur. Therefore, similar to the lowering cables, the SWL should equal approximately three times the obtained static force. Neto et al. [65] uses typical values for a steel wire rope and a polyester rope that meet this criteria. These values did therefore not need any scaling. The values are used in the cases and shown in the bottom half of table 7.1.

7.4 Installation: single unit or modular

One crucial choice in the installation procedure of the SBGESS is whether to lower the whole system as one unit or to have a modular installation. The latter meaning the main ballasting/buoyance element will be installed first, after which the GES and BES elements are lowered and connected. From a project management perspective the first option is preferred as it requires less time (and therefore a shorter weather window), reduces the need for special equipment (such as ROVs to connect the GES and BES elements) and any prevailing issues with the assembly will happen close to the surface, making it less challenging to fix.

However, three main risks can be associated with installing the SBGESS as a single unit:

1. Instabilities due to horizontal excursions of the GES/BES elements and/or overturning moments.
2. Collisions and/or interferences between the GES/BES elements and the SBGESS due to excessive vertical displacements.
3. Failing of components such as the traction cables due to high dynamic forces during installation

Regarding the first risk, the overturning moments are unlikely to cause issues as the symmetrical placement of the GES/BES elements and their equal vertical forces will not lead to an overturning moment. The horizontal excursions due to currents, but also during possible vortex formations behind the GES/BES elements could lead to local (and ultimately global) instabilities, but these effects are not modelled in this thesis.

The second and third risks can be assessed by simulations using the extended Tommasini model. The vertical displacement and resulting (dynamic) forces on the cable are modelled. It can therefore be checked whether the traction cable - GES/BES element system meets the same standards as the main system: No slack conditions and forces lower than the SWL. As stated above, only the GES elements are modelled as these are expected to be most critical, mostly due to the risk of slack conditions. The parameters for the two variants, with or without GES/BES elements, are shown in table 7.2. This also allows to check the influence of the variants on the main system, especially since the difference in mass will lead to a difference in natural period and could therefore lead to different resonance conditions.

Table 7.2: Overview of masses and volumes accounted for in the two variants.

Parameter	SBGESS (1x, incl. full ballasting)	GES (8x)	BES (8x)	Total
Variant 1				
Mass [t]	2800 + 9270	2717.6	96.65	14884.2
Volume [m^3]	10000	799.28	1932.96	12732.24
Submerged mass [t]	1770	1894.3	-1894.3	1770
Variant 2				
Mass [t]	2800 + 9270	0	0	12070
Volume [m^3]	10000	0	0	10000
Submerged mass [t]	1770	0	0	1770

As mentioned in chapter 3, the dimensions of the GES and BES elements were designed such that the combined net static vertical force is zero. This can also be seen in table 7.2 as the total submerged mass is equal for both variants. The lowering cables thus do not need to have their vertical load capacity increased.

In this thesis only variant 1 is modelled. However, if this leads to excessive motions or exceeding of the DNV criteria by either the SBGESS or the GES elements, future projects should look into variant 2.

8 | Results

In this chapter, the results of the simulations are presented. First a comparison between Gao and Tommasini is made and differences are highlighted and explained. Hereafter, the results of four scenarios for the extended Tommasini model are shown and discussed. It is also checked whether each of these scenarios would meet the criteria set by DNV. Finally, a sensitivity analysis is conducted for the parameters with the highest level of uncertainty: C_A , C_D and the ballasting fill percentage.

Regarding the nomenclature of the cases, two versions are used. If case 1 or case 2 is mentioned, only the type of lowering cable is implied, meaning chains (case 1) or polyester rope (case 2). The observations for these cases are therefore valid for both types of traction cables. If distinguishing between the types of traction cables is required, this is done by using the full case names as shown in table 7.1.

8.1 Comparison between Tommasini and Gao

Simulated: All combinations of $h_s = 0.3m, 1.0m$; $T_p = 9s, 13s$

Chapter 7 already mentioned the main differences between the two models, the discretizing in elements and the viscous cable drag for Gao and the acceleration term in Tommasini. Figures 8.1 and 8.2 show that these differences in the model do not lead to significant differences in the results for higher wave periods (13s). This suggests that for these conditions, the viscous cable drag and acceleration term are negligible. However, a difference in the model results can be observed when looking at the damping. In both figures, the damping for Tommasini for case 1 takes longer to restore the force to a small oscillation around the static force. As will be explained in the next section, this can be attributed to the fact that case 1 is more prone to slack conditions.

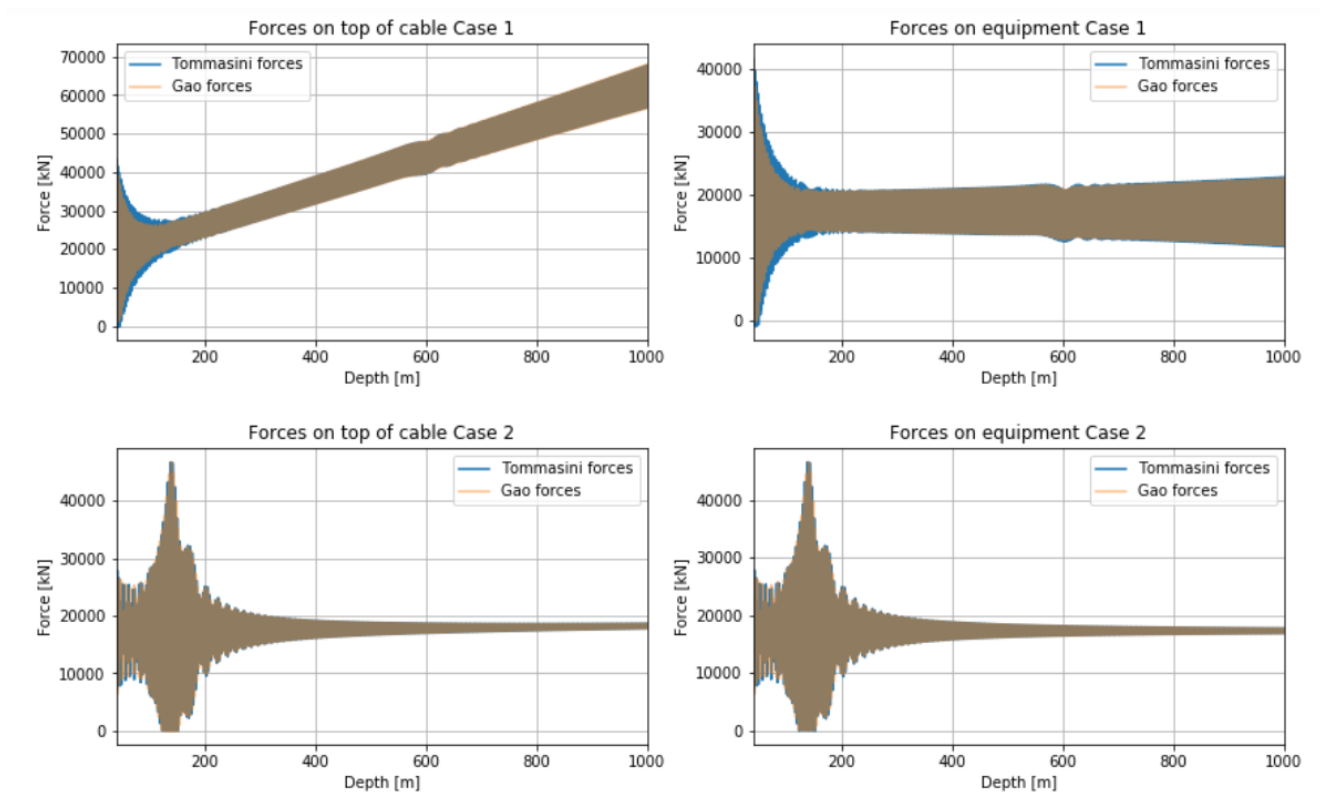


Figure 8.1: Forces comparison between Tommasini and Gao, for $h_s = 0.3m$ and $T_p = 13s$.

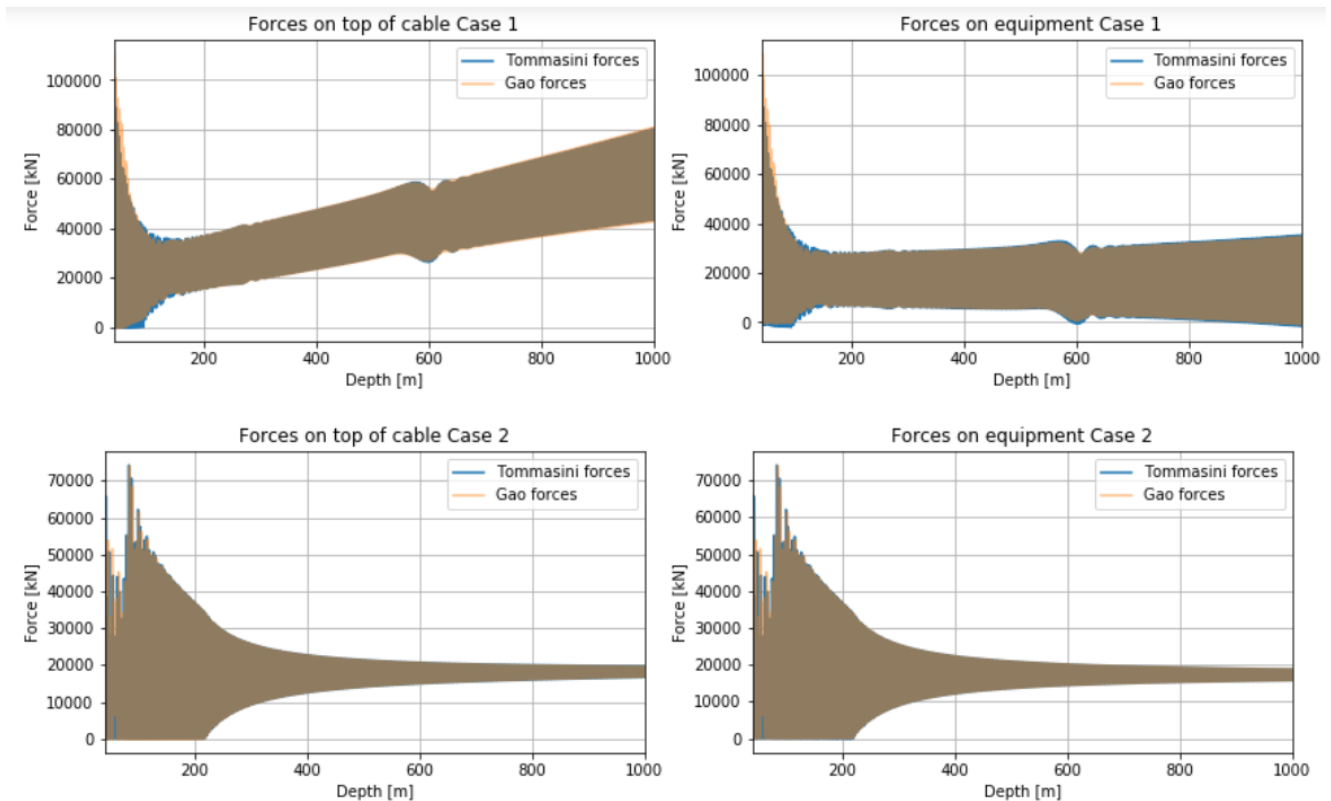


Figure 8.2: Forces comparison between Tommasini and Gao, for $h_s = 1.0\text{m}$ and $T_p = 13\text{s}$.

What can also be observed from figures 8.1 and 8.2 is that slack and resonance are not necessarily occurring at the same depth. Based on figure 8.1, it can be seen that resonance takes place around 120 - 150m of water depth (as does slack for these conditions). However, for higher amplitudes with the same period, slack occurs in the region of approximately 0 - 220m of water depth. As resonance will occur at the same water depth, the slack conditions are therefore only partially caused by the resonance. In the next session it is explained how the wave motions relative to the static elongation may be responsible for this effect.

Another general observation is that the difference between the forces at the top and at the equipment is large for case 1, yet almost non-existent for case 2. This can be clarified, as the linear mass of the polyester rope (case 2) is about the same as the water density, meaning the cable is basically neutrally buoyant. For case 1 the density of the cable exceeds the water density significantly. As the only difference in the equations for the force on the top and on the equipment is the submerged mass of the cables, the difference will only be visible for case 1.

Looking at the results of lower wave periods in figures 8.3 and 8.4 more significant differences between the two models can be observed, primarily for case 1. Two main observations are made: 1. The damping for Tommasini is less than for Gao and therefore experiences slack conditions more easily. 2. Gao enters the resonance region at a smaller depth than Tommasini. The latter observation can be explained by the discretizing of the cable into elements for the Gao model. Whereas for Tommasini the first natural frequency is computed using the cable mass, added mass and equipment mass, this is different for Gao. As Gao is discretized into elements, each element will have their own natural period. For the first $N-1$ elements this will be a rather small period (approx. 1s), yet the N th element will have a larger natural period due to the fact that the complete equipment and added mass is lumped on this element. Given that the cable mass that is used is still only $1/N$ of the cable mass that is included in the Tommasini natural period calculation, a difference between the two will occur and thus a difference in when resonance occurs.

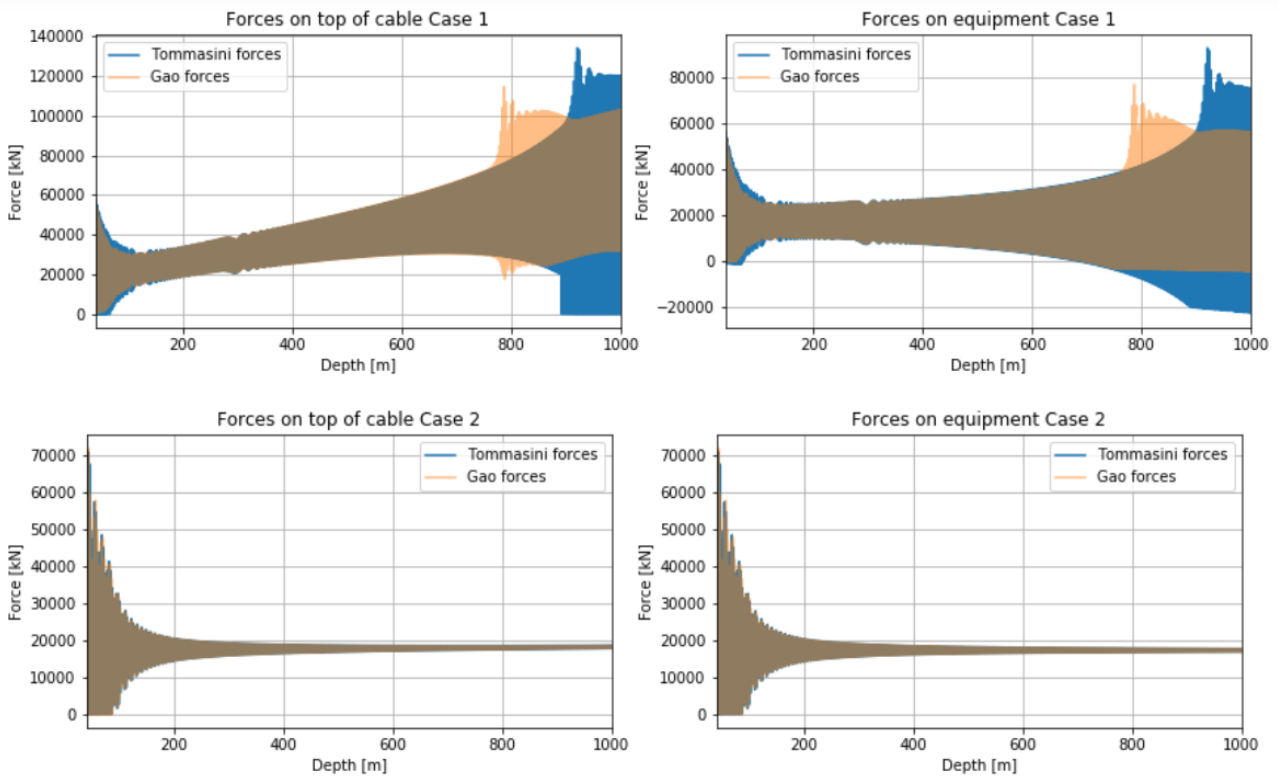


Figure 8.3: Forces comparison between Tommasini and Gao, for $h_s = 0.3\text{m}$ and $T_p = 9\text{s}$.

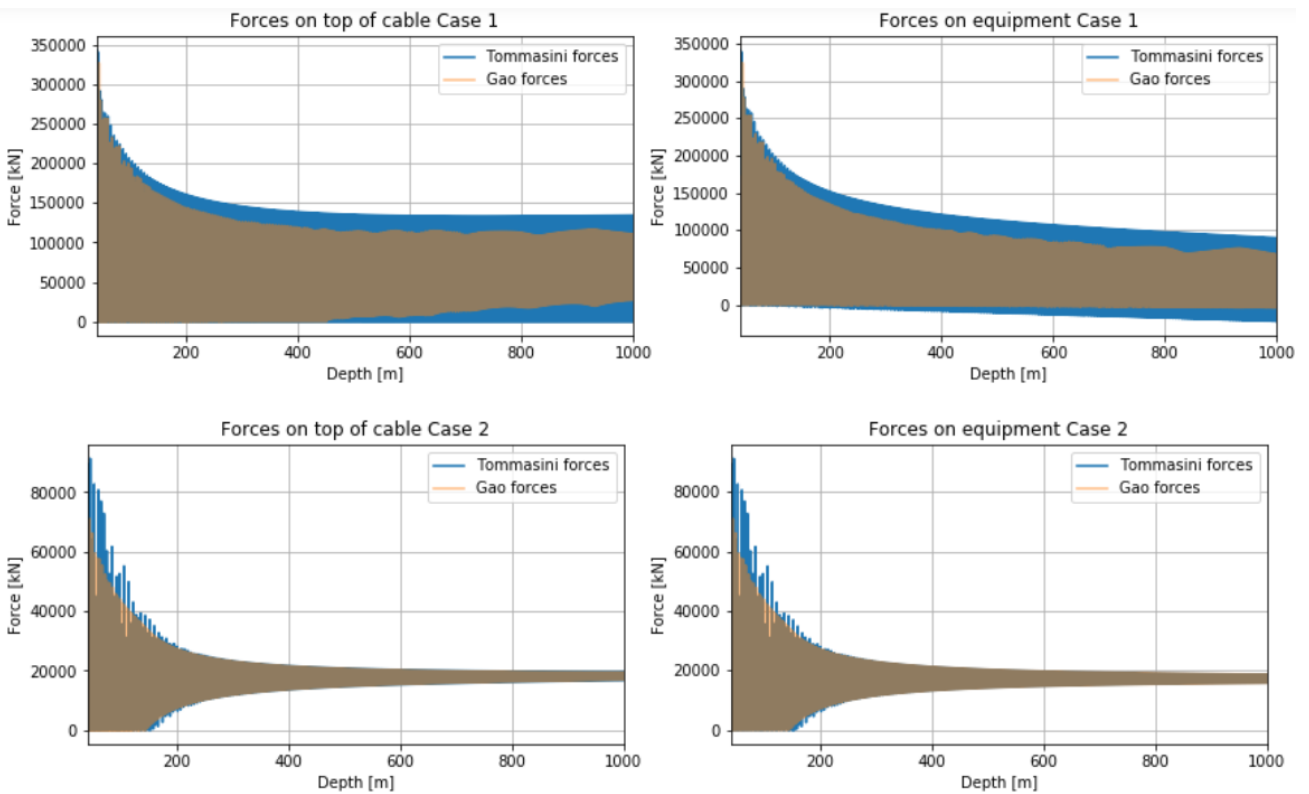


Figure 8.4: Forces comparison between Tommasini and Gao, for $h_s = 1.0\text{m}$ and $T_p = 9\text{s}$.

The difference in damping which is seen could be attributed to several potential causes. One being that the structural damping factor for Gao (ζ) does not equal the structural damping term in Tommasini. It could also be that the acceleration terms in Tommasini and the viscous drag term in Gao lead to relatively

higher oscillations for Tommasini, particularly in and near the resonance regions. What should also be noticed is that Tommasini, the cable being linearized, can either be in slack condition or not, while for Gao this may differ for each element. The fact that this is more pronounced for case 1 is explained in the next section.

Based on these results, one may argue that for larger wave periods the results of both models can be utilized for a simulation purpose. Yet for smaller wave periods (5 - 10s) the difference in forces and slack, and thus whether or not the DNV criteria are met, is too significant to only use one. The reason that these lower wave periods lead to different results should primarily be attributed to the fact that lower wave periods intersect with the natural period of heavier cables (case 1) and thus potentially lead to resonance and slack. It is here where the difference in slack and damping between the two models is most prominent. The damping factor for Gao could be scaled such that it leads to an equal size of damping as Tommasini, yet the discretization will remain to lead to different results for the lower wave periods for case 1.

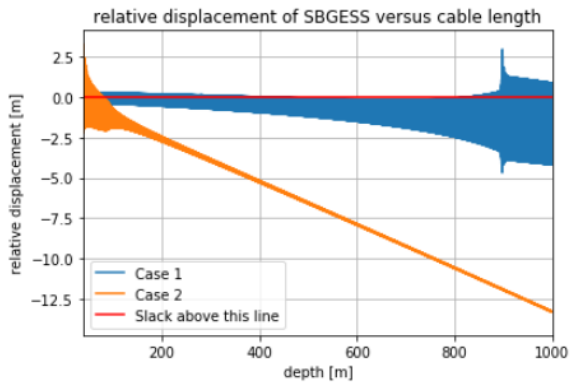
As the results for the two models are largely similar, the oscillations in resonance zones are larger for Tommasini, slack occurs more easily for Tommasini and Gao demands more computation time, the remainder of this thesis will use the (extended) Tommasini model to simulate several scenarios.

A final general observation that can be made from these simulations is that for case 1 the resonance occurs at larger depths, while for case it occurs in the shallower waters. This can be explained by the difference in natural periods, as a system with heavier cables (steel wire, chains, etc.) has a lower natural period than a similar system with lighter cables (e.g. polyester rope). The latter result is also supported by the observations of Neto et al. [65].

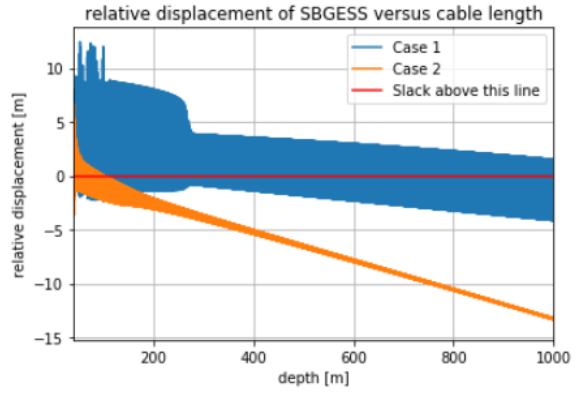
8.2 Simulations for different wave amplitudes and lowering velocities

Simulated: All combinations of $hs = 0.3m, 1.0m$; $Vc = 0.05m/s, 0.3m/s$; $Tp = 9s$

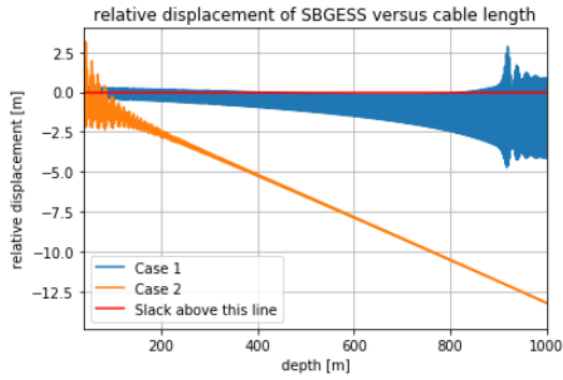
In this section the results from four scenarios are discussed. Two velocities and two wave amplitudes are used to assess their influence and the general behaviour of the two cases under these conditions. The vessel motion period is fixed at nine seconds, as this period allows to study possible resonance conditions for both cases. For all the scenarios, each case is checked whether it meets the two requirements: no slack and no forces higher than the SWL.



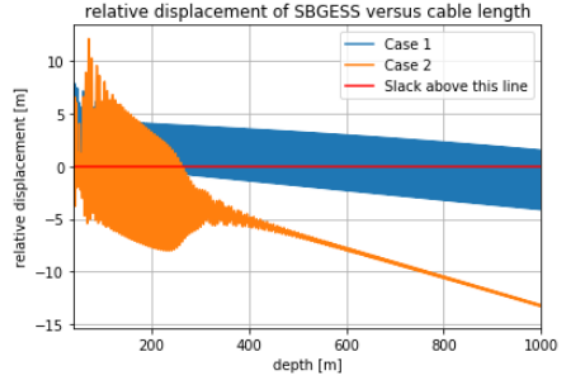
(a) $h_s = 0.3\text{m}; V_c = 0.05\text{m/s}$



(b) $h_s = 1.0\text{m}; V_c = 0.05\text{m/s}$

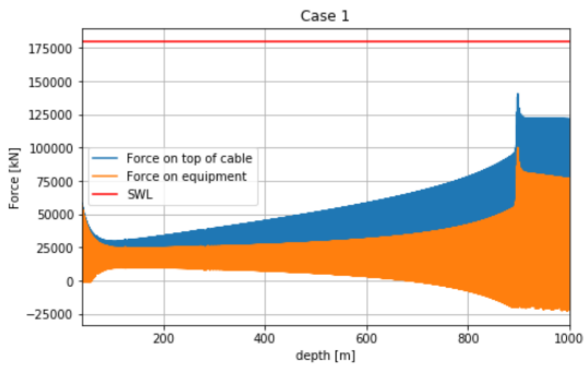


(c) $h_s = 0.3\text{m}; V_c = 0.3\text{m/s}$

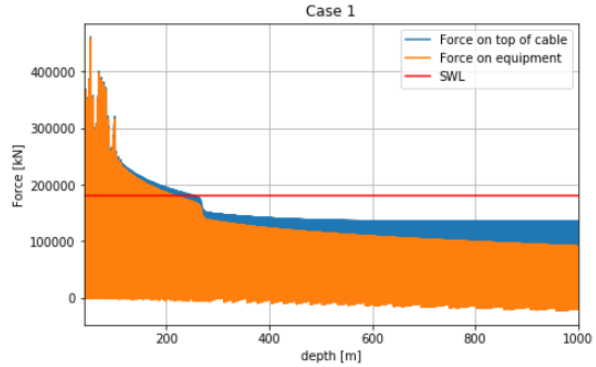


(d) $h_s = 1.0\text{m}; V_c = 0.3\text{m/s}$

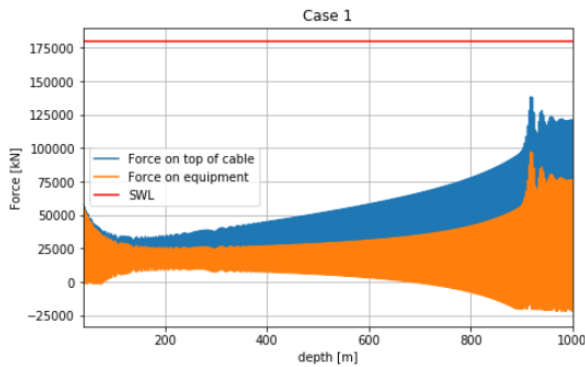
Figure 8.5: Relative displacement of SBGESS versus cable length. Simulation results for $T_p = 9\text{s}$.



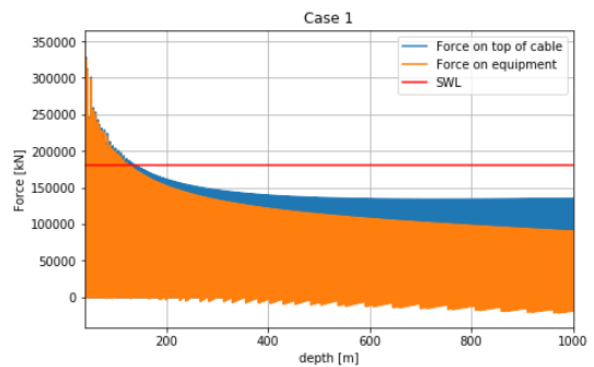
(a) $h_s = 0.3\text{m}; V_c = 0.05\text{m/s}$



(b) $h_s = 1.0\text{m}; V_c = 0.05\text{m/s}$



(c) $h_s = 0.3\text{m}; V_c = 0.3\text{m/s}$



(d) $h_s = 1.0\text{m}; V_c = 0.3\text{m/s}$

Figure 8.6: Forces on the lowering cable for cases 1A and 1B. Simulation results for $T_p = 9\text{s}$.

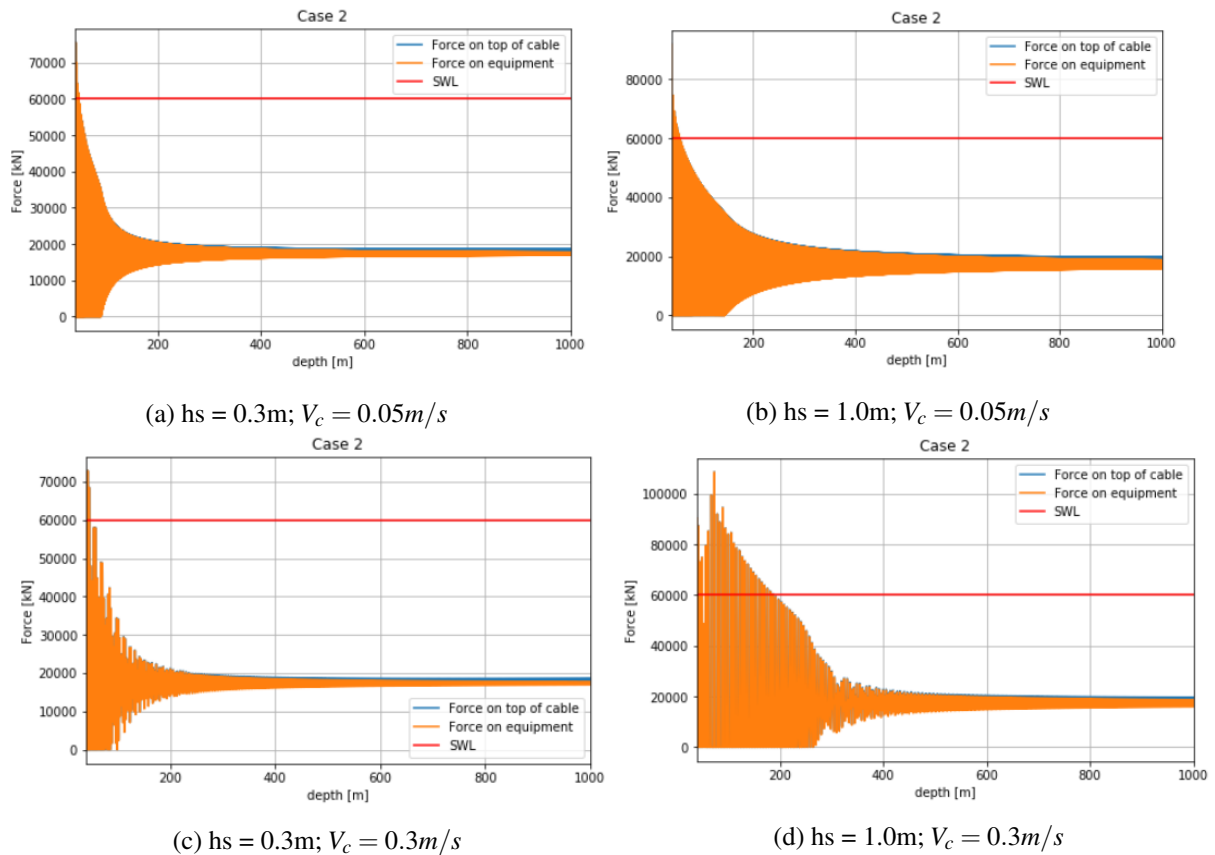


Figure 8.7: Forces on the lowering cable for cases 2A and 2B. Simulation results for $T_p = 9\text{s}$.

A general observation that can be made is that for the range of representative peak periods for JONSWAP wave spectra taken from the metocean data of Brazilian offshore locations normal wave periods (5 - 14s)[68][65], case 1 has resonance in the final part of the lowering operation and case 2 in the beginning (as expected by looking at figures a (natural periods) in appendix G). What also can be seen is that higher wave amplitudes lead to higher (dynamic) forces and more slack (figure 8.5, 8.6 and 8.7). This also goes for the GES elements. A lower payout velocity, although less visible for lower amplitudes, leads to lower forces. Contrary to what is expected, as going quicker through the resonance zone could lead to less dynamics[65], it can actually be explained as the influence of slack is governing here. A lower velocity allows for a quicker recovery from slack conditions and thus lower dynamic forces. Slack occurs more for higher amplitudes and thus is the reducing effect of the payout velocity more pronounced for higher amplitudes.

A more detailed look at figures 8.6 and 8.7 shows that for case one, the maximum total forces are approximately 2.5 times larger for the higher amplitudes. The payout velocity does not appear to have a reducing effect here on the maximum total forces, but does so on the slack recovery. For case 2 it is shown that the expected increase in maximum total force with an higher amplitude is countered by the decrease in payout velocity (see figures b,c,d).

Looking at figure 8.5, for both cases the slack is most pronounced in the early part of the lowering phase. For case 2, this can be partially explained by the resonance occurring in this phase. However, there is also another factor that is important here. As the cable length grows due to the payout, the stiffness term (EA/L) decreases and the mass term increases. This will lead to a higher absolute elongation of the cable due to the static downward force. If the elongation is larger, a larger oscillation is needed to reach slack, yet also important: the amplitude of the vessel is relatively smaller thus less likely leads to slack. Finally, what should also be considered is that the payout velocity is increased during approximately the first 100 meters, meaning there is an acceleration which may add to the oscillations via the acceleration term.

The SWL condition is met for all scenarios with $h_s = 0.3\text{m}$ (apart from very first part of lowering case 2). However, it is the slack condition that is more problematic as case 1 experiences severe slack for all scenarios and case 2 also experiences slack in the first part of lowering. The fact that this is more pronounced for case 1 is likely to be caused by the elongation of the cable, which is significantly less than for case 2, meaning only a small upward motion is needed for slack to occur. With an initial static elongation of only 0.03m (for case 1), one can imagine that higher wave amplitudes will rapidly lead to slack conditions. For case 2 the initial static elongation is 0.51m , meaning that slack may still occur for higher amplitudes but is less likely to occur for lower amplitudes (apart from resonance regions where oscillations will be significantly larger). These conclusions are supported by the results in figure 8.5.

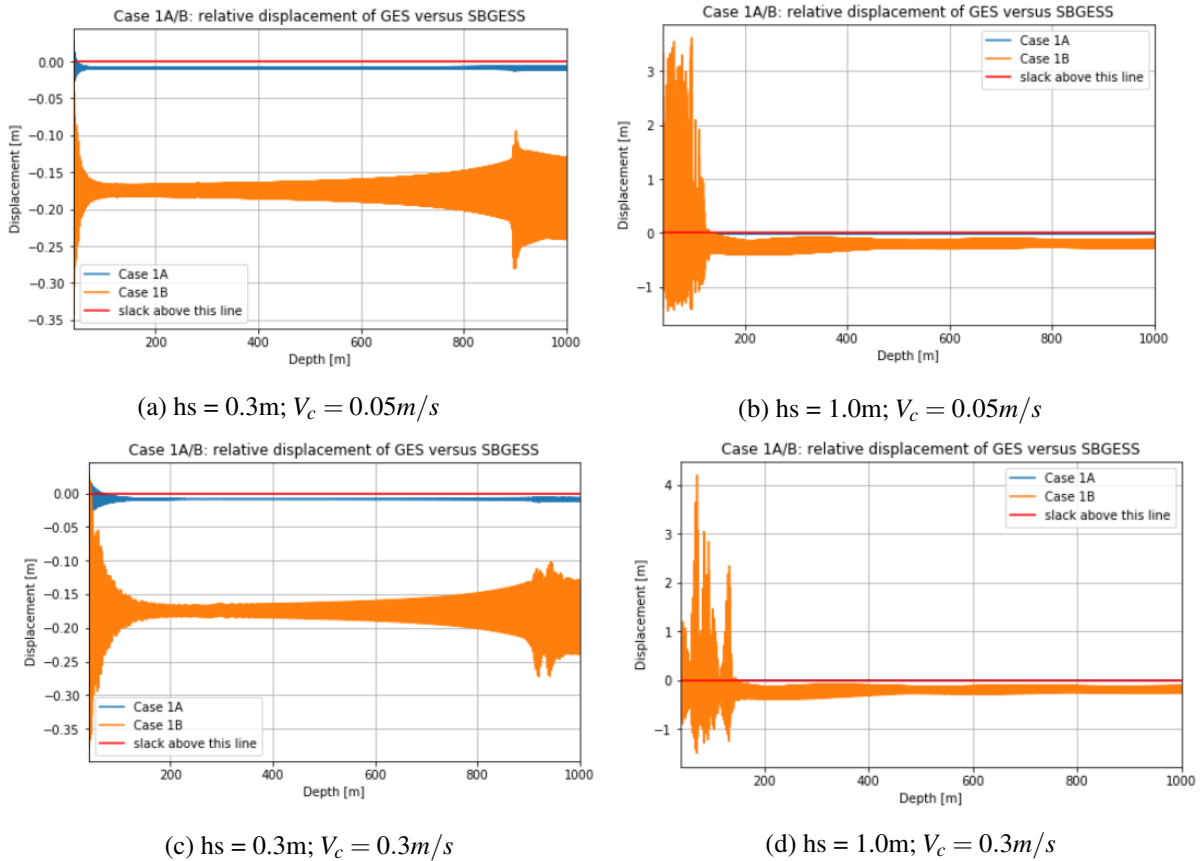


Figure 8.8: Relative displacement of GES versus SBGESS. Simulation results for $T_p = 9\text{s}$.

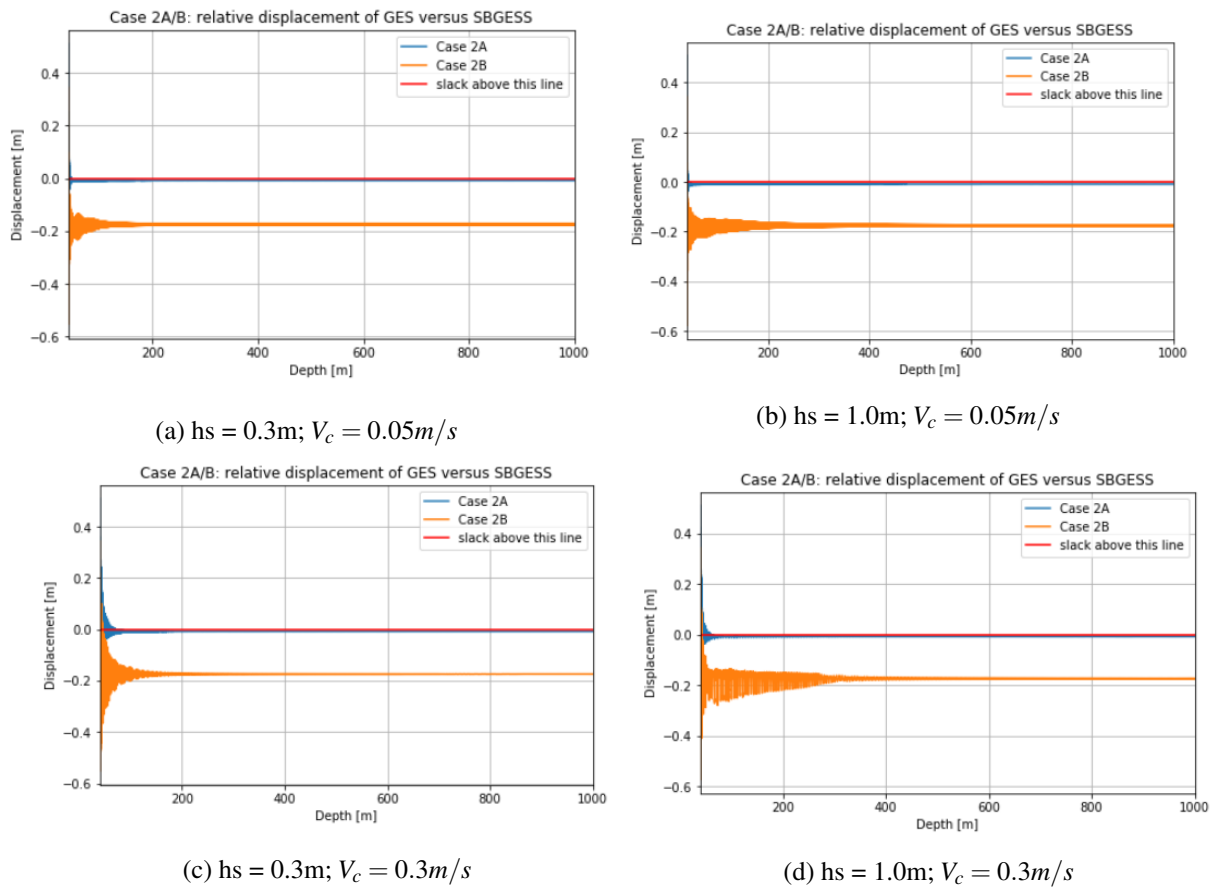


Figure 8.9: Relative displacement of GES versus SBGESS. Simulation results for $T_p = 9\text{s}$.

Case 1B is failing both criteria for larger wave amplitudes, for both velocities (figure 8.8, 8.9 and appendix G figures 8.4j and 8.2j). This is due to the intersecting of the natural periods of the polyester rope traction cables and the chains. Other than 1B, the GES elements meet the two conditions if the exceeding of the SWL in the first part can be eliminated by reducing the SBGESS motions in the initial part of the lowering operation.

8.3 Sensitivity analysis: Added mass coefficient, drag coefficient and ballasting fill percentage

Simulated: All combinations of $h_s = 0.3\text{m}, 1.0\text{m}; T_p = 9\text{s}, 13\text{s}$

As was stated in chapter 7, the uncertainty around the true values of the hydrodynamic coefficients is high. Particularly because they are Keulegan-Carpenter number dependent [67][68], and therefore are variable throughout the lowering phase as the magnitude of the oscillations will vary. These values were therefore subjected to a sensitivity analysis. A unique feature of the SBGESS is the ability to (de)ballast during the lowering phase without the need of an additional installation vehicle. To assess the influence of this parameters, the ballasting fill percentage (n) was also considered in this sensitivity analysis. All results can be found in appendix G.

8.3.1 Added mass coefficient

Figure G.1 shows that the dynamic force is relatively sensitive to the added mass coefficient, mostly so in and/or near resonance zones. From the figures two main observations can be made: 1. The location of the resonance region shifts to smaller depths for larger added mass coefficients 2. The dynamic force is higher for larger added mass coefficients.

The first observation is a direct consequence of the effect of C_A on the natural period. As C_A becomes larger, the natural period increases and thus will resonance occur at shallower depths. This can be best observed in figures c, j and l. The second observation is caused by the larger oscillations and thus elongations due to a larger added mass coefficient. By comparing figures c and j, one can observe that this effect is larger for shallower depths and/or lighter cables. This is due to the fact that with a larger cable length and/or cable density, the relative contribution of the added mass becomes smaller. For variant 2 (the modular installation, without GES/BES elements) the impact of the added mass coefficient is therefore expected to be even more significant.

8.3.2 Drag coefficient

Out of the three parameters that were subjected to a sensitivity analysis, the drag coefficient is the only parameter that does not alter the natural period of the system. It is therefore expected that only the magnitude of the oscillations (and therefore the dynamic force) will change as the drag coefficient changes. Looking at figure G.2, the influence of C_D can be observed to be relatively small compared to the other two parameters.

The mostly insignificant contribution of the drag coefficient can actually be quite well explained by studying the complete damping term in the equation of motion: $\left(\frac{m'\dot{L}}{3} + \frac{1}{2}\rho C_d A_p |\dot{w}|\dot{w}\right) \dot{w}$. Looking at the ratio $\frac{\frac{m'\dot{L}}{3}}{\frac{1}{2}\rho C_d A_p |\dot{w}|\dot{w}}$, for short cable lengths this ratio is small, but for larger cable lengths (e.g. 1000m) increases to 30 or more. Therefore, only for short cable lengths or for very high velocities would the drag term, and thus the drag coefficient, have a significant impact on the total damping. This is illustrated by the figures from case 1. In figure a, only during the resonance around 900m the influence of the drag coefficient becomes visible again as the velocities rise. In figures c,e and g a difference can only be observed in the beginning of the graph where the cable length is small and the velocities high.

This ratio of the damping term also explains the difference between case 1 and 2. As case 2 has a lower linear mass and has a resonance region that occurs at shorter cable lengths, C_D is expected to have a more significant impact for this case. This can be seen in all graphs, yet particularly where the oscillations are more severe, in figures d and h.

8.3.3 Ballasting fill percentage

A change in the ballasting fill percentage will lead to a change in the total mass and therefore the natural period of the system. This could lead to a shift in the depth at which resonance occurs, yet the contribution of the ballasting mass to the natural period is negligible as illustrated by figures G.3 a, b, g and h. Therefore, similar to the drag coefficient, only a difference in magnitude of the dynamic force is expected.

By studying figure G.3, the general observation can be made that outside of resonance regions the influence of the ballasting fill percentage on the dynamic force is negligible. The total force will increase with a higher mass, but as this is added to the static force, it will not impact the dynamic force. It should be noted that this can only be concluded for the range of ballasting percentages (>75%) for which the net vertical static force is downward. However, for figures e and f it can clearly be observed that there is a significant difference between the dynamic forces for the filling percentages, even outside the resonance zone. This can be explained by the occurrence of slack. For the lower ballasting fill percentages (75% and 80%), it takes longer to exit slack conditions as the static downward force is smaller. Based on earlier observations it was already concluded that cases 1A and 1B experience longer and more slack conditions, which complies with the figures e and f.

Besides the impact on slack duration and severity, there is one other visual effect of the ballasting fill percentage: higher dynamic forces during resonance. As can be best seen in figures c and j, the higher

the fill percentage, the higher the dynamic force. Adding this to the fact that the static force is higher for higher ballasting fill percentages, it can be concluded that (excluding slack regions) a higher ballasting fill percentage leads to higher forces in the cables.

9 | Conclusion & Recommendations

This thesis found that the SBGESS is able to supply power to a subsea system that does not require continuous power and allows for occasional shut-downs. A 10.32MWh SBGESS, with three power supply modes (including a power saving mode), is able to operate a 4.34MW water injection system with power being generated by two 12MW wind turbines. Based on historical wind data, this system is able to meet the reliability and performance criteria for such a system. To reach this 10.32MWh energy storage potential and supply the demanded power, 8 GES and 8 BES units are required.

The objective of this thesis was: *To assess the dynamic behaviour of the SBGESS system during installation and provide suggestions to increase workability by reducing the dynamic response.* First the possible methods of installation needed to be listed. For transportation, a wet tow was deemed most appropriate given the dimensions, installation method and avoidance of lifting through the splash zone. An installation method involving multiple AHTs with a tow configuration that decouples motions and potential additional heave compensation is deemed a viable option for installing the SBGESS.

The first research question was: *What is the dynamic response of the SBGESS during installation?* It was concluded that for the given set of parameters Gao's and Tommasini's models largely delivered the same results. However, in and/or near resonance zones and slack conditions, it is crucial to select an accurate and matching value for the damping terms for both models. It was observed that for heavier cables (chains, steel wire rope, etc.) resonance may occur for lower wave periods and in the last part of the lowering phase. For lighter lowering cables such as polyester rope, the opposite was observed.

As expected, higher wave amplitudes resulted in higher (dynamic) forces and more (severe) slack conditions. This is caused partially by the relative size of the vessel amplitudes compared to the static elongation of the cables. A larger payout velocity leads to larger dynamic forces, particularly for higher wave amplitudes which cause slack conditions. With a lower payout velocity the system is able to recover quicker and thus has a lower duration of slack. For case 2 it was observed that the lower payout velocity could fully counter the 50% increase in maximum force due to the higher vessel amplitude. For case 1 this effect was not visible for the simulated conditions.

The second research question was formulated as: *How can the selected installation method be improved for the proposed location?* Looking at the two conditions that needed to be met, 'no slack' is a more limiting factor than the SWL. Especially for case 1 as it failed to meet the slack criteria for all four scenarios discussed. Given that for case 1 the resonance occurs close to the final location and the fact that resonance with traction cables is more likely (see case 1B), a preliminary preference towards case 2 (polyester rope) can be suggested based on this model. However a solution must be found for the exceeding of the limitations during the first hundred meters. This may involve using heave compensation and implementing a lower payout velocity during the first part.

If the polyester rope is selected, the forces are likely to be below SWL and no slack occurs, especially with the precautions mentioned above. This means that, based on the vertical displacement model, variant 1 (a single-unit installation) would be preferable. However, stability issues should still be thoroughly checked. If a heavier lowering cable is selected, it may be better to select the SSW traction cable to avoid excessive slack and forces which will likely lead it to fail the criteria. If a SSW traction cable does turn out to be favorable for the operational phase, then variant 2 might be the best option to avoid having the traction cable fail the criteria during installation.

The added mass coefficient has a relatively large impact on the dynamic force and oscillations. A larger added mass coefficient will lead to larger dynamic forces and to a shift of the resonance region to

lower water depths. The ballasting fill percentage had a negligible influence on vertical oscillations and dynamic forces, therefore this parameter should be predominantly based on maintaining stability and/or increasing workable sea-states. Overall, The drag coefficient had a negligible influence on the damping and thus the total force in the cables, especially for longer cable lengths. However, for the polyester rope (case 2) the drag coefficient did have a significant influence during the early part of the lowering phase. As the polyester rope is the preliminary preferred choice and the early part of the lowering is most critical with regards to both the forces and the SWL, accurately modelling the C_D and its dependencies is essential.

As the SBGESS concept is being further developed and the design phase reaches a more detailed stage, further research into the installation procedure is required. First off, a more detailed layout, based on a structural design, of the SBGESS is needed in order to have more accurate parameters and therefore results. Once the dimensions are known, lab testing should be carried out to assess the hydrodynamic coefficients and their dependence on the KC number. Especially the added mass coefficient should be studied closely as the dynamics are highly sensitive to this parameter. This may be done by doing forced-oscillations tests which will result in a range of values for the added mass coefficient and its dependency on the KC number. The drag coefficient can be obtained by similar oscillation tests as well as tow tests. Once this is done, these values could be used as variable input in the model again to reassess the dynamics. By this time, a first selection of appropriate vessels can be made and (typical) RAOs can be used to convert the waves to vessel motions. To comply with DNV-RP-H103 [75], the waves should then be modelled as random time series and multiple simulations should be done to assess the likelihood of failing the criteria of no slack and forces lower than SWL. To limit the likelihood of slack conditions, a pre-tension in the cables could be implemented and studied as well. Finally, the more detailed model could also assess heave compensation, either passive through the tow configuration or active by implementing a device.

Parallel to the SDOF modelling, at some point a model should be developed in which also rotations are included as degrees of freedom. The most important issue to assess with this model is the stability during lowering, yet also during the transportation phase. This model may help to finalize the design of the SBGESS, especially the configuration and filling percentage of the ballasting tanks. To do so accurately, this model should then also consider the inclined surfaces in the ballasting tanks. A model which includes rotations can also look into the interaction of the GES/BES elements and the SBGESS as they may exercise a pendulum movement due to vortex formations behind the elements. Both for the SDOF as well as the multiple DOF model, it is important to verify the model. This can be done using software or using prototype testing on a lab scale. A final option before the actual installation is a field test.

The SBGESS is a promising concept that may lead to enabling the use of renewable energy resources at remote/isolated offshore locations. However, there are still many issues to be tackled. One of the most crucial perhaps is finding an economical solution to conduct maintenance at these depths.

Bibliography

- [1] Marta Torres Gunfaus and Henri Waisman. Assessing the adequacy of the global response to the paris agreement: Toward a full appraisal of climate ambition and action. *Earth System Governance*, page 100102, 2021. ISSN 2589-8116. doi: <https://doi.org/10.1016/j.esg.2021.100102>. URL <https://www.sciencedirect.com/science/article/pii/S2589811621000069>.
- [2] Sarah M. Watson. Greenhouse gas emissions from offshore oil and gas activities — relevance of the paris agreement, law of the sea, and regional seas programmes. *Ocean Coastal Management*, 185:104942, 2020. ISSN 0964-5691. doi: <https://doi.org/10.1016/j.ocecoaman.2019.104942>. URL <https://www.sciencedirect.com/science/article/pii/S0964569119301681>.
- [3] C Economics. The future of fossil fuels: how to steer fossil fuel use in a transition to a low-carbon energy system. *Energy transitions commission*, 2017.
- [4] W Mackenzie. Why powering oil and gas platforms with renewables makes sense. *Tech. rep*, 2019.
- [5] Sajjad Zereshkian and Dariush Mansoury. A study on the feasibility of using solar radiation energy and ocean thermal energy conversion to supply electricity for offshore oil and gas fields in the caspian sea. *Renewable Energy*, 163:66–77, 2021. ISSN 0960-1481. doi: <https://doi.org/10.1016/j.renene.2020.08.111>. URL <https://www.sciencedirect.com/science/article/pii/S0960148120313562>.
- [6] Sara Oliveira-Pinto, Paulo Rosa-Santos, and Francisco Taveira-Pinto. Electricity supply to offshore oil and gas platforms from renewable ocean wave energy: Overview and case study analysis. *Energy Conversion and Management*, 186:556–569, 2019. ISSN 0196-8904. doi: <https://doi.org/10.1016/j.enconman.2019.02.050>. URL <https://www.sciencedirect.com/science/article/pii/S0196890419302419>.
- [7] Atle Rygg Ardal, Kamran Sharifabadi, Oyvind Bergvoll, and Vidar Berge. Challenges with integration and operation of offshore oil gas platforms connected to an offshore wind power plant. Institute of Electrical and Electronics Engineers Inc., 2014. ISBN 9783952405932. doi: 10.1109/PCICEurope.2014.6900054.
- [8] Z Wang, R Carriveau, D.S.K Ting, W Xiong, and Z Wang. A review of marine renewable energy storage. *Wiley: International journal of energy research*, 43:6108–6150, January 2019.
- [9] Santiago Sanchez, Elisabetta Tedeschi, Jesus Silva, Muhammad Jafar, and Alexandra Marichalar. Smart load management of water injection systems in offshore oil and gas platforms integrating wind power. volume 11, pages 1153–1162. Institution of Engineering and Technology, 7 2017. doi: 10.1049/iet-rpg.2016.0989.
- [10] Yi Wang, Menglan Duan, Huaguo Liu, Runhong Tian, and Chao Peng. Advances in deepwater structure installation technologies. *Underwater Technology*, 34:83–91, 3 2017. ISSN 17560551. doi: 10.3723/ut.34.083.
- [11] Offshore Magazine. 2020 worldwide survey of subsea processing: status of complementary technologies and systems - march 2020, 2020. <https://www.offshore-mag.com/resources/maps-posters>.

- [12] et al F. M. Passarelli. Hisep: A game changer to boost the oil production of high gor and high co₂ content reservoirs. *Offshore technology conference*, October 2019.
- [13] Sara Oliveira-Pinto, Paulo Rosa-Santos, and Francisco Taveira-Pinto. Assessment of the potential of combining wave and solar energy resources to power supply worldwide offshore oil and gas platforms. *Energy Conversion and Management*, 223:113299, 2020. ISSN 0196-8904. doi: <https://doi.org/10.1016/j.enconman.2020.113299>. URL <https://www.sciencedirect.com/science/article/pii/S0196890420308384>.
- [14] Ernesto Santibanez-Borda, Anna Korre, Zhenggang Nie, and Sevket Durucan. A multi-objective optimisation model to reduce greenhouse gas emissions and costs in offshore natural gas upstream chains. *Journal of Cleaner Production*, 297:126625, 2021. ISSN 0959-6526. doi: <https://doi.org/10.1016/j.jclepro.2021.126625>. URL <https://www.sciencedirect.com/science/article/pii/S0959652621008453>.
- [15] Zahra Aghaeifar, Skule Strand, Tina Puntervold, Tor Austad, and Farasdaq Muchibbus Sajjad. Smart water injection strategies for optimized eor in a high temperature offshore oil reservoir. *Journal of Petroleum Science and Engineering*, 165:743–751, 2018. ISSN 0920-4105. doi: <https://doi.org/10.1016/j.petrol.2018.02.021>. URL <https://www.sciencedirect.com/science/article/pii/S0920410518301281>.
- [16] Johan Slätte, Dnv G1, Johan Sandberg, Todd Flach, Gerben Dekker, and Carl Sixtensson. Otc-25284-ms wind-powered subsea water injection pumping: Technical and economic feasibility, 2014. URL <http://onepetro.org/otconf/proceedings-pdf/14otc/4-14otc/d041s054r005/1505593/otc-25284-ms.pdf/1>.
- [17] Silvia Blajberg Schaffel, Fernanda Fortes Westin, Omar Mauricio Hernandez, and Emilio Lèbre La Rovere. Otc-29879-ms replacing fossil fuels by wind power in energy supply to offshore oilgas exploration and production activities-possibilities for brazil, 2019. URL <http://onepetro.org/otcbrasil/proceedings-pdf/19otcb/2-19otcb/d022s022r004/1136878/otc-29879-ms.pdf/1>.
- [18] Petrobras. Petrobras internal document, 2020.
- [19] Riccardo Giolo, Aurelie Berthelot, Pierre Pedenaud, and Graeme Skivington. Otc-29365-ms industrialisation of springs®, a qualified subsea sea water desulfation process, 2019. URL <http://onepetro.org/OTCONF/proceedings-pdf/190TC/1-190TC/D011S012R004/1135455/otc-29365-ms.pdf/1>.
- [20] Santeri Pöyhönen, Tero Ahonen, Jero Ahola, Pekka Punnonen, Simo Hammo, and Lauri Nygren. Specific speed-based pump flow rate estimator for large-scale and long-term energy efficiency auditing. *Energy Efficiency*, 12:1279–1291, 6 2019. ISSN 15706478. doi: 10.1007/s12053-018-9751-4.
- [21] Agência Nacional do Petróleo, Gás Natural e Biocombustíveis. Rodadas de licitações: Áreas de ep sob concessão, 2019. <http://www.anp.gov.br/exploracao-e-producao-de-oleo-e-gas/dados-tecnicos/padros-tecnicos-para-envio-de-dados-a-anp/rodadas-de-licitacoes-areas-de-e-p-sob-concessao>. Accessed on 07 January 2021.
- [22] André Reinaldo Novgorodcev Junior. Go/no go report: Offshore renewable energy production and storage for deep-water oil and gas production. Delft University of Technology, 9 2020.
- [23] A.R. JR. Novgorodcev and A. Jarquín-Laguna. Multi-criteria analysis to rank offshore renewable technologies to support deep-water oil and gas production. 2020.

- [24] K.P. Bassett, R Carriveau, and D.S.-K. Ting. Integration of buoyancy-based energy storage with utility scale wind energy generation. *Journal of Energy Storage*, 14:256–263, April 2017.
- [25] Serviço Geológico do Brasil - CPRM. Projeto batimetria, 2019. <http://www.cprm.gov.br/publique/Geologia/Geologia-Marinha/Projeto-Batimetria-3224.html>. Accessed on 23 November 2020.
- [26] I Cruz, C Claro, D Sahonero, L Otani, and J Pagot. The buoy supporting risers (bsr) system: A novel riser solution for ultra-deep water subsea developments in harsh environments. *Offshore Technology Conference*, October 2015.
- [27] J.G. van Diemen, J.F. Saint-Marcoux, L Otani, D Sahonero, and L Cerqueira Trovoado. Displacing 10,000t of water to install 2,500t of steel buoy at 250m below sea level. *Offshore Technology Conference*, May 2015.
- [28] H. Hersbach, B. Bell, P. Berrisford, G. Biavati, A. Horányi, J. Muñoz Sabater, J. Nicolas, C. Peubey, R. Radu, I. Rozum, D. Schepers, A. Simmons, C. Soci, D. Dee, and J-N. Thépaut. Era5 hourly data on single levels from 1979 to present. copernicus climate change service (c3s) climate data store (cds), 2018. accessed on 01-12-2020; 10.24381/cds.adbb2d47.
- [29] Copernicus. Era5 hourly data on single levels from 1979 to present, 2018. <https://cds.climate.copernicus.eu/cdsapp#!/dataset/reanalysis-era5-single-levels?tab=overview>. Accessed on 01 December 2020.
- [30] Stefan Emeis and Matthias Turk. Comparison of logarithmic wind profiles and power law wind profiles and their applicability for offshore wind profiles. In Joachim Peinke, Peter Schaumann, and Stephan Barth, editors, *Wind Energy*, pages 61–64, Berlin, Heidelberg, 2007. Springer Berlin Heidelberg. ISBN 978-3-540-33866-6.
- [31] Examining the trends of 35 years growth of key wind turbine components. *Energy for Sustainable Development*, 50:18–26, 6 2019. ISSN 23524669. doi: 10.1016/j.esd.2019.02.003.
- [32] General Electric. Haliade-x offshore wind turbine, 2021. <https://www.ge.com/renewableenergy/wind-energy/offshore-wind/haliade-x-offshore-turbine>. Accessed on 08 January 2021.
- [33] ASA BRANCA USINAEOLICA. Requerimento eb-2-2019; 48513.010255/2019-00, 2019.
- [34] Pierre Pedenaud, Luc Riviere, Raymond Hallot, Stéphane Anres, Graeme Skivington, and Veolia Water. Otc 24273 springs: Subsea seawater treatment-case study, 2013. URL <http://onepetro.org/OTCBRASIL/proceedings-pdf/130TCB/A11-130TCB/OTC-24273-MS/1572424/otc-24273-ms.pdf/1>.
- [35] et al Riviere. United states patent application publication - riviere et al - underwater water treatment unit and method for cleaning said unit, 2020. Pub. No.: US 2020/0269165 A1.
- [36] David L Stover. Otc-29473-ms barrier fluidless, sealless seawater canned motor pumps, 2019. URL <http://onepetro.org/OTCONF/proceedings-pdf/190TC/3-190TC/D031S030R006/1986325/otc-29473-ms.pdf/1>.
- [37] Jean François Toubeau, Chloé Ponsart, Christophe Stevens, Zacharie De Grève, and François Vallée. Sizing of underwater gravity storage with solid weights participating in electricity markets. *International Transactions on Electrical Energy Systems*, 30, 10 2020. ISSN 20507038. doi: 10.1002/2050-7038.12549.

- [38] J.P. Morgan. United states patent application publication - morgan - buoyancy energy storage and energy generation system, 2010. Pub. No.: US 2010/0107627 A1.
- [39] Chakib El Mokhi and Adnane Addaim. Optimization of wind turbine interconnections in an offshore wind farm using metaheuristic algorithms. *Sustainability (Switzerland)*, 12:1–24, 7 2020. ISSN 20711050. doi: 10.3390/su12145761.
- [40] Ander Madariaga, José Luis Martín, Inmaculada Zamora, Salvador Ceballos, and Olimpo Anaya-Lara. Effective assessment of electric power losses in three-core xlpe cables. *IEEE Transactions on Power Systems*, 28:4488–4495, 2013. ISSN 08858950. doi: 10.1109/TPWRS.2013.2263514.
- [41] Danielle K.S. Lima, Ruth P.S. Leão, Antônio C.S. dos Santos, Francisca D.C. de Melo, Vinícius M. Couto, Aurélio W.T. de Noronha, and Demercil S. Oliveira. Estimating the offshore wind resources of the state of ceará in brazil. *Renewable Energy*, 83:203–221, 11 2015. ISSN 18790682. doi: 10.1016/j.renene.2015.04.025.
- [42] Scott Greene, Mark Morrissey, and Sara E. Johnson. Wind climatology, climate change, and wind energy. *Geography Compass*, 4:1592–1605, 11 2010. ISSN 17498198. doi: 10.1111/j.1749-8198.2010.00396.x.
- [43] Abdul Hai Alami. Experimental assessment of compressed air energy storage (caes) system and buoyancy work energy storage (bwes) as cellular wind energy storage options. *Journal of Energy Storage*, 1:38–43, 2015. ISSN 2352152X. doi: 10.1016/j.est.2015.05.004.
- [44] Kai-Tung Ma, Yong Luo, Thomas Kwan, and Yongyan Wu. *Mooring system engineering for offshore structures*. Gulf professional publishing, 2019. ISBN 978-0-12-818551-3.
- [45] GICON-SOF. A technical response to the offshore wind industry’s challenges going forward, 2020. <http://www.gicon-sof.de/en/sof1.html>. Accessed on 23 December 2020.
- [46] Stylianos Chrisopoulos and Jakob Vogelsang. A finite element benchmark study based on experimental modeling of vibratory pile driving in saturated sand. *Soil Dynamics and Earthquake Engineering*, 122:248–260, 7 2019. ISSN 02677261. doi: 10.1016/j.soildyn.2019.01.001.
- [47] S. Bang, K. D. Jones, K. O. Kim, Y. S. Kim, and Y. Cho. Inclined loading capacity of suction piles in sand. *Ocean Engineering*, 38:915–924, 5 2011. ISSN 00298018. doi: 10.1016/j.oceaneng.2010.10.019.
- [48] Ju Hyung Lee, Nghiem Xuan Tran, and Sung Ryul Kim. Development and field application of gfrp suction pile. *Ocean Engineering*, 173:308–318, 2 2019. ISSN 00298018. doi: 10.1016/j.oceaneng.2018.12.070.
- [49] Yanbing Zhao and Haixiao Liu. Toward a quick evaluation of the performance of gravity installed anchors in clay: Penetration and keying. *Applied Ocean Research*, 69:148–159, 12 2017. ISSN 01411187. doi: 10.1016/j.apor.2017.10.009.
- [50] Jun Liu, Congcong Han, Yuqin Zhang, Yueyuan Ma, and Yuxia Hu. An innovative concept of booster for omni-max anchor. *Applied Ocean Research*, 76:184–198, 7 2018. ISSN 01411187. doi: 10.1016/j.apor.2018.05.007.
- [51] Jun Liu, Congcong Han, Yueyuan Ma, Zhongtao Wang, and Yuxia Hu. Experimental investigates on hydrodynamic characteristics of gravity installed anchors with a booster. *Ocean Engineering*, 158:38–53, 6 2018. ISSN 00298018. doi: 10.1016/j.oceaneng.2018.03.074.

- [52] Y. H. Kim, M. S. Hossain, and J. K. Lee. Loading performance of fish and omni-max anchors in crust-over-soft clays. *Applied Ocean Research*, 91, 10 2019. ISSN 01411187. doi: 10.1016/j.apor.2019.101904.
- [53] T Esteves Martins. Offshore anchoring systems with torpedo piles. *Proceedings of the 25th Offshore Symposium, February 27th 2020, Houston, Texas Texas Section of the Society of Naval Architects and Marine Engineers*, 2020.
- [54] M J Morrison. Otc 5106 generalized soil conditions encountered in the campos and sergipe basins, offshore brazil, 1986. URL <http://onepetro.org/otconf/proceedings-pdf/86otc/all-86otc/otc-5106-ms/2030955/otc-5106-ms.pdf/1>.
- [55] Y. H. Kim, M. S. Hossain, and D. Wang. Effect of strain rate and strain softening on embedment depth of a torpedo anchor in clay. *Ocean Engineering*, 108:704–715, 11 2015. ISSN 00298018. doi: 10.1016/j.oceaneng.2015.07.067.
- [56] Boram Kim and Tae wan Kim. Monte carlo simulation for offshore transportation. *Ocean Engineering*, 129:177–190, 1 2017. ISSN 00298018. doi: 10.1016/j.oceaneng.2016.11.007.
- [57] N Abdussamie, A Zaghwan, M Daboos, I Elferjani, and A Mehanna. Operational risk assessment of offshore transport barges. *Ocean Engineering*, 156:333–346, March 2018.
- [58] Hongyan Ding, Ruiqi Hu, Conghuan Le, and Puyang Zhang. Towing operation methods of offshore integrated meteorological mast for offshore wind farms. *Journal of Marine Science and Engineering*, 7, 4 2019. ISSN 20771312. doi: 10.3390/jmse7040100.
- [59] Boram Kim and Tae wan Kim. Scheduling and cost estimation simulation for transport and installation of floating hybrid generator platform. *Renewable Energy*, 111:131–146, 2017. ISSN 18790682. doi: 10.1016/j.renene.2017.03.098.
- [60] Yuguang Cao, Xueyang Hu, Shihua Zhang, Songsen Xu, Junglin Lee, and Jiancheng Yu. Design of a novel installation device for a subsea production system. *Applied Ocean Research*, 59:24–37, 9 2016. ISSN 01411187. doi: 10.1016/j.apor.2016.05.006.
- [61] A Joensen and D Paul. A low tech, low risk system for the installation of large structures in deep water. *SPE Offshore Europe Oil and Gas conference and exhibition, Aberdeen*, September 2011.
- [62] Tore Jacobsen and Bernt J. Leira. Numerical and experimental studies of submerged towing of a subsea template. *Ocean Engineering*, 42:147–154, 3 2012. ISSN 00298018. doi: 10.1016/j.oceaneng.2012.01.003.
- [63] J. L. Alamilla, D. Campos, C. Ortega, A. Soriano, and J. L. Morales. Optimum selection of design parameters for transportation of offshore structures. *Ocean Engineering*, 36:330–338, 4 2009. ISSN 00298018. doi: 10.1016/j.oceaneng.2008.12.008.
- [64] C. Guedes Soares. *Developments in renewable energies offshore : proceedings of the 4th International Conference on Renewable Energies Offshore (RENEW 2020), Lisbon, Portugal, 12-15 October 2020*. ISBN 9780367681319.
- [65] Elói Daniel de Araújo Neto, Bruno Martins Jacovazzo, Fabricio Nogueira Correa, and Breno Pinheiro Jacob. Numerical evaluation of a subsea equipment installation method designed to avoid resonant responses. *Applied Ocean Research*, 88:288–305, 7 2019. ISSN 01411187. doi: 10.1016/j.apor.2019.03.025.

- [66] Jun Ye, Milinko Godjevac, Simone Baldi, and Hans Hopman. Joint estimation of vessel position and mooring stiffness during offshore crane operations. *Automation in Construction*, 101:218–226, 2019. ISSN 0926-5805. doi: <https://doi.org/10.1016/j.autcon.2019.01.011>. URL <https://www.sciencedirect.com/science/article/pii/S0926580518306587>.
- [67] Rafael Guimarães Pestana, Daniel Fonseca de Carvalho e Silva, Camila do Nascimento Gomes, Leonardo de Oliveira Carvalho, Vinicius Vileti, Paulo de Tarso Themistocles Esperança, and Moohyun Kim. Subsea manifold installation: Operational windows estimation based on hydrodynamic model testing. *Ocean Engineering*, 219, 1 2021. ISSN 00298018. doi: 10.1016/j.oceaneng.2020.108364.
- [68] Rodrigo Batista Tommasini, Renato Pavanello, and Leonardo de Oliveira Carvalho. Prediction of design loads for deep water subsea lifting operations based on non-stationary time response. *Marine Structures*, 74, 11 2020. ISSN 09518339. doi: 10.1016/j.marstruc.2020.102818.
- [69] *Installation Challenges for Ultra-Deep Waters*, volume All Days of *Offshore Mediterranean Conference and Exhibition*, 03 2015. OMC-2015-441.
- [70] Antonio C Fernandes, José C L De Almeida, Jairo B Araújo, Marcos Rangel, Ricardo Franciss, Jorge Merino, and Joel S Sales. Proceedings of the marine operations specialty symposium 2008 - moss-60 parametric evaluations of the buoy supporting riser (bsr) installation, 2008.
- [71] Antonio C Fernandes, Jorge A Meriono Munoz, André R da Silva, Jairo B de Araújo, José C Lima de Almeida, and Ricardo Franciss. Dtec2008 - deepwater offshore technology symposium - shanghai - analysis of the installation of a buoy supporting risers (bsr) by numerical modeling and model testing, 2008.
- [72] WC Mahone, P van Luipen, and C Werenskiold. Otc5608 - offshore technology conference houston tx- installation of heavy subsea components using submerged motion compensator and multi-sheave block, 1987.
- [73] Pieter G Wybro, Shukai Wu, Johannes J Treu, and David E Chaplin. United states patent application publication - wybro et al - method of installation of a tension leg platform, 2003. Pub. No.: US7044685B2.
- [74] Aaron Larson Power mag. Clump weights in offshore mooring systems, 2019. url: <https://www.powermag.com/clump-weights-in-offshore-mooring-systems/>.
- [75] Det Norske Veritas. Recommended practice dnv-rp-h103 modelling and analysis of marine operations, 2011. <https://www.yumpu.com/en/document/view/11798016/dnv-rp-h103-modelling-and-analysis-of-marine-operations> Accessed on 23 July 2021.
- [76] Rodrigo Batista Tommasini, Leonardo de Oliveira Carvalho, and Renato Pavanello. A dynamic model to evaluate the influence of the laying or retrieval speed on the installation and recovery of subsea equipment. *Applied Ocean Research*, 77:34–44, 8 2018. ISSN 01411187. doi: 10.1016/j.apor.2018.05.001.
- [77] Pan Gao, Keliang Yan, Mingchen Ni, Xuehua Fu, and Zhihui Liu. A dynamic model for continuous lowering analysis of deep-sea equipment, based on the lumped-mass method. *Applied Sciences (Switzerland)*, 10, 5 2020. ISSN 20763417. doi: 10.3390/app10093177.
- [78] Chenling Tian, Mingyue Liu, Longfei Xiao, Rodolfo T. Goncalves, Wenhui Xie, and Shisheng Wang. Effects of the position of pipe-type appendages on the flow induced motions, energy transformation, and drag force of a tlp. *Applied Ocean Research*, 106, 1 2021. ISSN 01411187. doi: 10.1016/j.apor.2020.102464.

- [79] Murilo Augusto Vaz, Xiaotian Li, Junpeng Liu, and Xiuwei Ma. Analytical model for axial vibration of marine cables considering equivalent distributed viscous damping. *Applied Ocean Research*, 113, 8 2021. ISSN 01411187. doi: 10.1016/j.apor.2021.102733.
- [80] Wikipedia. Low-pass filter, 2021. https://en.wikipedia.org/wiki/Low-pass_filter Accessed on 26 July 2021.
- [81] Det Norske Veritas. Lifting operations (vmo standard - part 2-5), 2014. <https://rules.dnv.com/docs/pdf/DNVPM/codes/docs/2014-04/OS-H205.pdf> Accessed on 02 August 2021.
- [82] W. C. Chung, H. Y. Kang, and M. H. Kim. Multi-scale approach for chain-mooring opb-induced failure considering time-varying interlink bending stiffness and fairlead condition. *Applied Ocean Research*, 98, 5 2020. ISSN 01411187. doi: 10.1016/j.apor.2020.102128.
- [83] C.K.Y. Leung. Concrete as a building material. In K.H. Jürgen Buschow, Robert W. Cahn, Merton C. Flemings, Bernhard Ilchner, Edward J. Kramer, Subhash Mahajan, and Patrick Veysseyère, editors, *Encyclopedia of Materials: Science and Technology*, pages 1471–1479. Elsevier, Oxford, 2001. ISBN 978-0-08-043152-9. doi: <https://doi.org/10.1016/B0-08-043152-6/00267-9>. URL <https://www.sciencedirect.com/science/article/pii/B0080431526002679>.
- [84] Juan García-Abdeslem. On the seawater density in gravity calculations. *Journal of Applied Geophysics*, 183, 12 2020. ISSN 09269851. doi: 10.1016/j.jappgeo.2020.104200.
- [85] P.S. Liu and G.F. Chen. Chapter eight - applications of polymer foams. In P.S. Liu and G.F. Chen, editors, *Porous Materials*, pages 383–410. Butterworth-Heinemann, Boston, 2014. ISBN 978-0-12-407788-1. doi: <https://doi.org/10.1016/B978-0-12-407788-1.00008-3>. URL <https://www.sciencedirect.com/science/article/pii/B9780124077881000083>.

A | Additional wind speed data analysis

Table A.1: Statistics of wind speeds for 10 year ranges. Raw data obtained from [28]

Range	Mean [m/s]	Std [m/s]
1980 - 1989	8.29	3.64
1990 - 1999	8.36	3.65
2000 - 2009	8.38	3.65
2010 - 2019	8.48	3.70

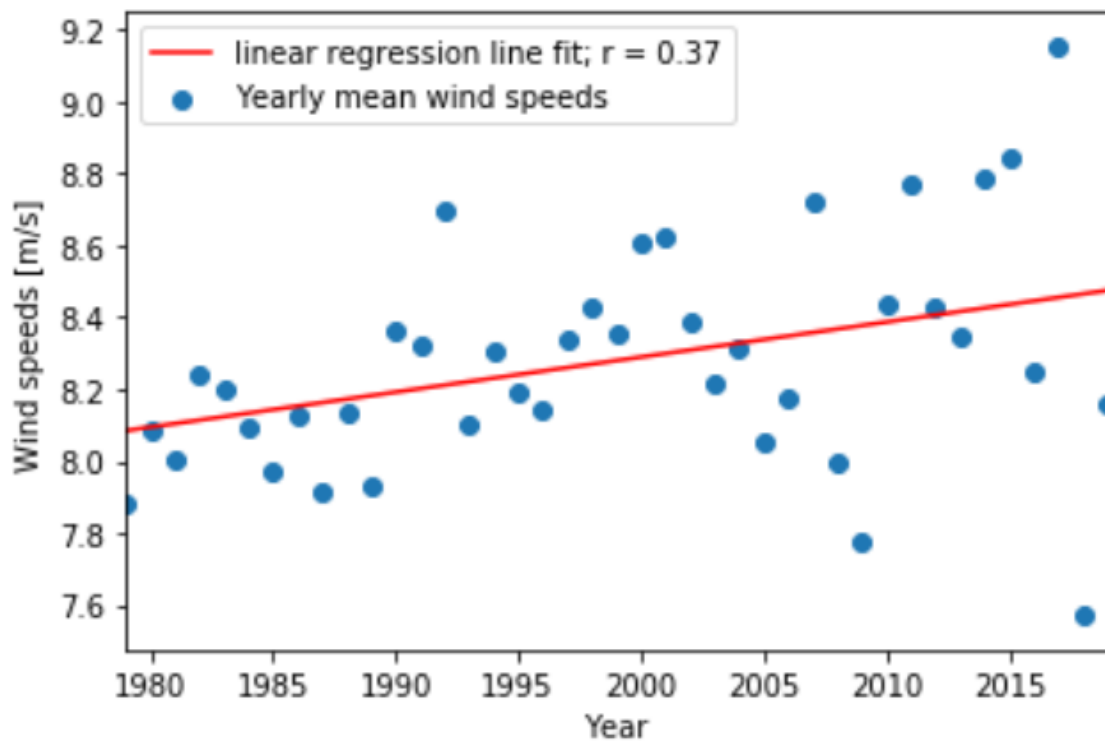


Figure A.1: Forty-one yearly average wind speeds including a fitted line (linear regression) that may suggest an upward trend.

B | Pump performance curve fit

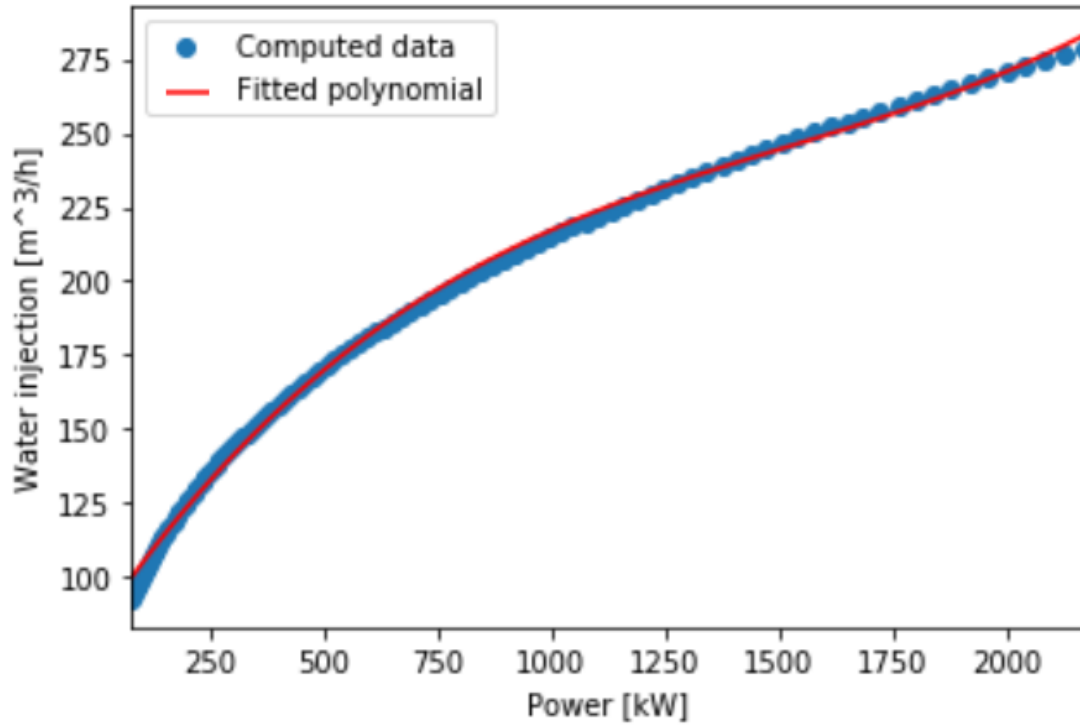


Figure B.1: Fitted third degree polynomial plotted over computed data by use of formulas 2.3 and 2.4

$$Q_{system} = \text{number of pumps} \cdot (aP^3 + bP^2 + cP + d) \quad (\text{B.1})$$

where:

Q_{System} = Water injection by the total system in m^3/h

P = Power input per pump in kW

$$a = 2.585 \cdot 10^{-8}$$

$$b = -1.181 \cdot 10^{-4}$$

$$c = 0.227$$

$$d = 82.581$$

The polynomial fit was conducted using an ordinary least squares method. This OLS resulted in an R^2 of 0.9981.

C | Sensitivity analysis - Energy storage

ES (MWh)	0 hours minimal power of		6 hours minimal power of		12 hours minimal power of		18 hours minimal power of	
	Mu_Flow 496.85	% of yrly stops above 70	Mu_Flow 496.85	% of yrly stops above 70	Mu_Flow 496.85	% of yrly stops above 70	Mu_Flow 496.85	% of yrly stops above 70
0	496,86	50	496,86	50	496,86	50	496,86	50
2	499,3	38,5	499,15	39,11	498,73	41	498,73	41
4	501	30,8	500,89	31,25	500,63	32,3	500,14	34,5
6	502,6	24,2	502,5	24,6	502,29	25,36	501,9	26,8
8	504,12	18,66	504,04	18,9	503,88	19,4	503,54	20,5
10	505,57	14,2	505,49	14,33	505,34	14,65	505,05	15,4
12	506,93	10,6	506,87	10,67	506,75	10,87	506,49	11,4
14	508,17	7,99	508,13	8	508,03	8,08	507,79	8,46
16	509,38	5,78	509,32	5,8	509,23	5,92	509,02	6,21
18	510,48	4,29	510,43	4,3	510,35	4,33	510,16	4,52

Figure C.1: Overview of simulations for different values of energy storage capacity and power saving mode

D | Detailed dimensioning parameters

Table D.1: Complete overview of input- and resulting parameters of the dimensioning of the SBGESS as described in chapter 3

Parameter	Value
Input values	
(dis)charging velocity	1m/s
Standard gravity	9.81m/s ²
(dis)charging distance	1000m
$\rho_{concrete}$	3400kg/m ³ [83]
$\rho_{Seawater}$	1030kg/m ³ [84]
$\rho_{styrofoam}$	50kg/m ³ [85]
Resulting dimensions	
Length of SBGESS	55m
Width of SBGESS	40m
Height of SBGESS	10m
Ballast tanks volume of SBGESS	8998m ³
radius of weights	2.5m
radius of floaters	2.5m
height of weights	5.02m
height of floaters	12.31m
nr. of weights	8
nr. of floaters	8
Total mass of weights	2681.6 tonnes
Total mass of floaters	96.65 tonnes
System properties	
Minimum charging time	16.67min
Energy storage capacity	10.32MWh
Maximum power supply (1 ESM)	4.65 MW

Table D.2: Segmented overview of ballasting volumes

Tank location	Ballasting volume
Left tank	3141.6m ³ ($\pi \cdot 10^2 \cdot 40$)
Right tank	3141.6m ³ ($\pi \cdot 10^2 \cdot 40$)
Sides	3714.6m ³ ($2(5 \cdot 10 \cdot (55 - 10) - \pi \cdot 10^2 \cdot 5)$)
Theoretical total ballasting volume	9997.8m ³
Practical total ballasting volume ¹	0.90 · 9997.8 = 8998 ≈ 9000m ³

¹Practical ballasting volume, meaning the theoretical ballasting volume reduced by volume losses due to wall thickness, partitions, equipment, etc.; Assumed to be roughly 90% of theoretical ballasting volume.

E | Detailed modelling parameters

Table E.1: Complete overview of input parameters of the modelling for both Tommasini and Gao

Parameter	Value
$\rho_{Seawater}$	$1030kg/m^3$
Drag coefficient SBGESS (C_D)	1.3
Added mass coefficient SBGESS (C_A)	2.0
Initial lowering cable length (L_0)	40m
Drag coefficient GES ($C_{D,w}$)	0.91
Added mass coefficient GES ($C_{A,w}$)	1.0
Traction cable length (l)	10m
Cable payout velocity target ($V_{c,target}$)	0.3 m/s
Standard gravity (g)	$9.81m/s^2$
Ballasting fill percentage	100%
Vessel motion frequency (ω_s)	0.698rad/s
Vessel motion amplitude (h_s)	0.3m/1.0m
Mass of SBGESS main structure	2800000kg
Total mass of GES elements	2681600kg
Total mass of BES elements	99902.6kg
Mass of ballasting	9270000kg
Volume of SBGESS	$10000m^3$
Acting surface of SBGESS	$1250m^2$
Damping coefficient (ζ)	0.1
Low-pass filter time constant (T)	25s
Number of discrete elements Gao (N)	20

F | Historical current and wave data

Wave period (T _p)	Significant wave height (h _s)																			Total				
	0.0 - 0.5	0.5 - 1.0	1.0 - 1.5	1.5 - 2.0	2.0 - 2.5	2.5 - 3.0	3.0 - 3.5	3.5 - 4.0	4.0 - 4.5	4.5 - 5.0	5.0 - 5.5	5.5 - 6.0	6.0 - 6.5	6.5 - 7.0	7.0 - 7.5	7.5 - 8.0	8.0 - 8.5	8.5 - 9.0	9.0 - 9.5		9.5 - 10.0			
0.0 - 2.0	0	0	0	0	0	0	0	0	0	0	0	0	0	0	0	0	0	0	0	0	0	0	0	0
2.0 - 4.0	0	0	0,000272	0	0	0	0	0	0	0	0	0	0	0	0	0	0	0	0	0	0	0	0	0,000272
4.0 - 6.0	0	0,023358	0,966908	1,980803	0,224073	0,004889	0,000272	0	0	0	0	0	0	0	0	0	0	0	0	0	0	0	0	0,000272
6.0 - 8.0	0	0,382417	7,21134	11,08712	8,108174	2,685614	0,437553	0,02879	0,001086	0	0	0	0	0	0	0	0	0	0	0	0	0	0	0,000272
8.0 - 10.0	0	0,119777	6,443789	10,80492	4,528986	1,712187	0,584219	0,180616	0,043728	0,013037	0,002173	0	0	0	0	0	0	0	0	0	0	0	0	0,000272
10.0 - 12.0	0	0,048889	2,483269	9,546314	7,82788	2,367566	0,670317	0,24906	0,076592	0,021728	0,017111	0,000272	0	0	0	0	0	0	0	0	0	0	0	0,000272
12.0 - 14.0	0	0,020913	0,886785	3,385807	4,992612	3,790768	1,449004	0,442442	0,154814	0,046716	0,011679	0,004617	0,001086	0	0	0	0	0	0	0	0	0	0	0,000272
14.0 - 16.0	0	0,006679	0,300393	0,664613	0,711601	0,610564	0,547281	0,333257	0,09832	0,019284	0,003802	0,000815	0,000272	0	0	0	0	0	0	0	0	0	0	0,000272
16.0 - 18.0	0	0,001086	0,060024	0,105925	0,076049	0,051876	0,038568	0,018197	0,009778	0,001358	0	0	0	0	0	0	0	0	0	0	0	0	0	0,000272
18.0 - 20.0	0	0,000815	0,003259	0,006679	0,007333	0,002716	0,001358	0	0	0	0	0	0	0	0	0	0	0	0	0	0	0	0	0,000272
20.0 - 22.0	0	0	0	0,006518	0,001901	0	0	0	0	0	0	0	0	0	0	0	0	0	0	0	0	0	0	0,000272
Total	0	0,604046	18,35604	37,58881	26,47861	11,22618	3,72857	1,252363	0,384319	0,102123	0,034765	0,005704	0,001358	0	0	0	0	0	0	0	0	0	0	0,00842
																								99,76289

Figure F.1: Wave scatter diagram, significant wave height versus wave period for the Santos Basin. Values in percentages.

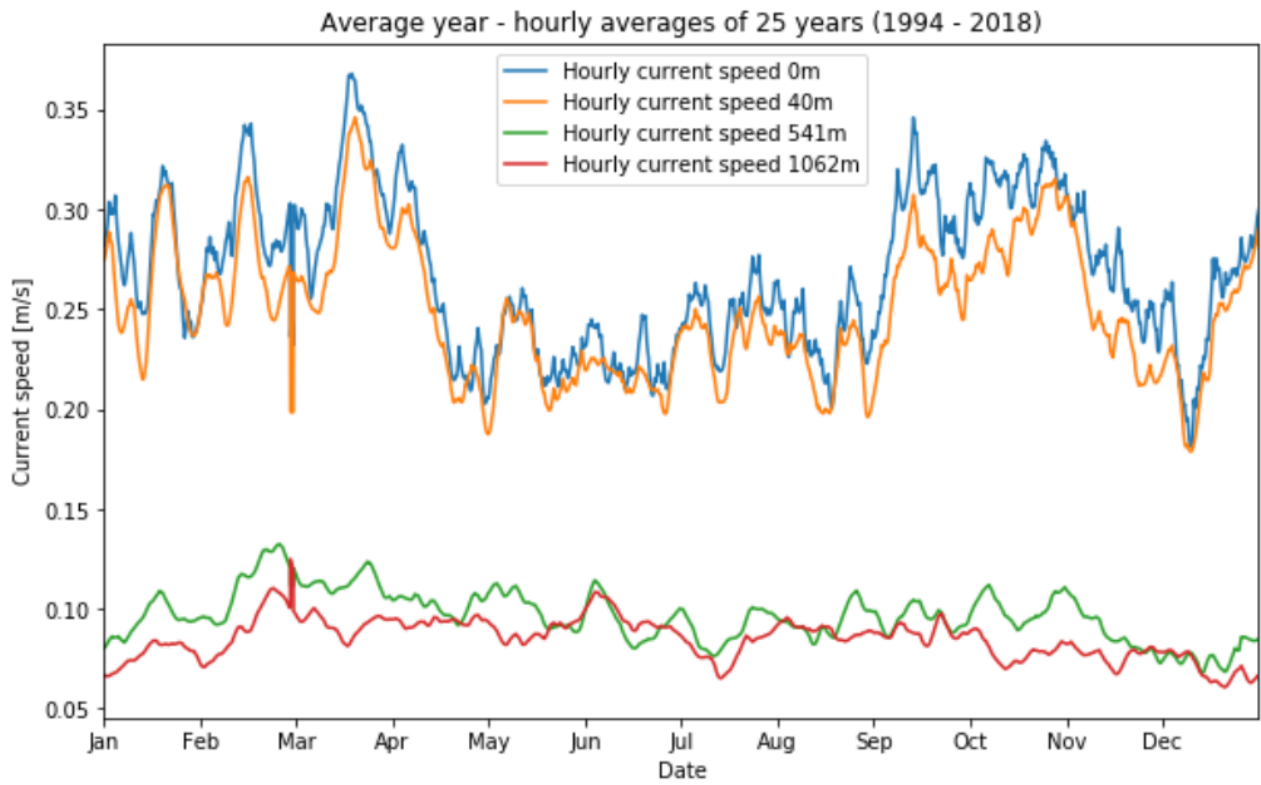
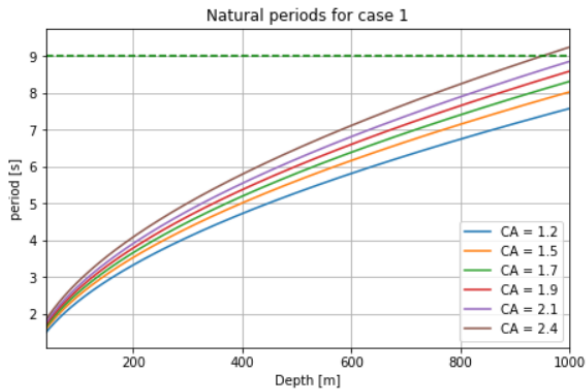


Figure F.2: Hourly current speeds for the average year at four different depths.

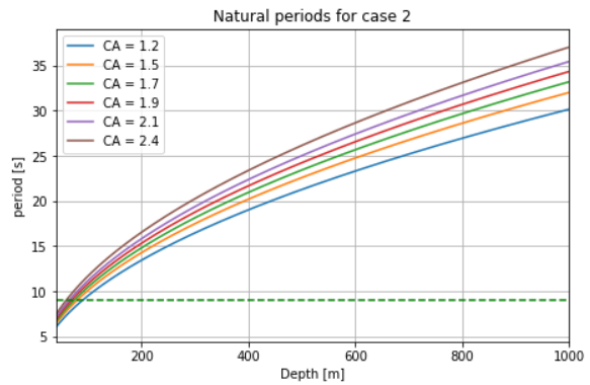
G | Detailed results and figures

G.1 Sensitivity analysis

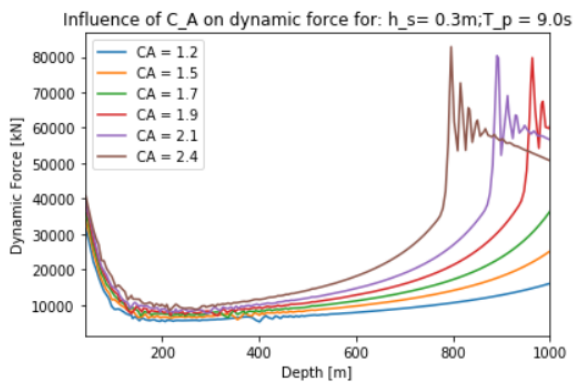
G.1.1 Sensitivity of dynamic force to added mass coefficient



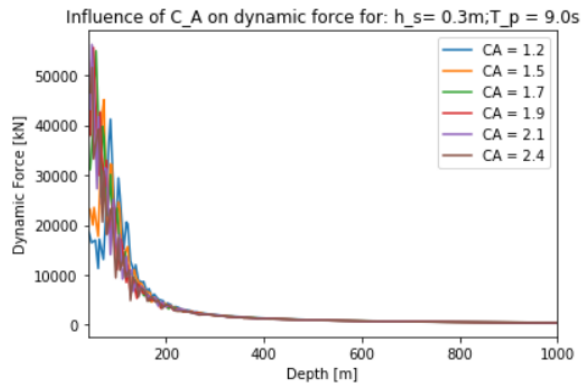
(a)



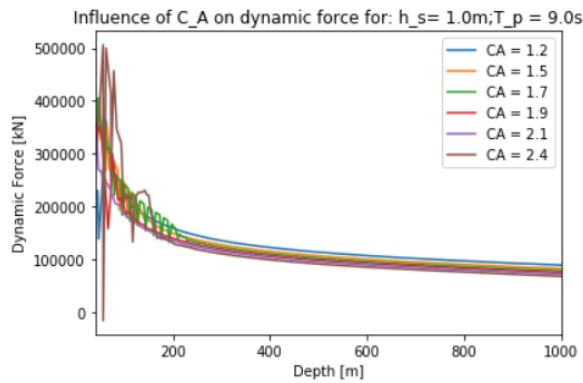
(b)



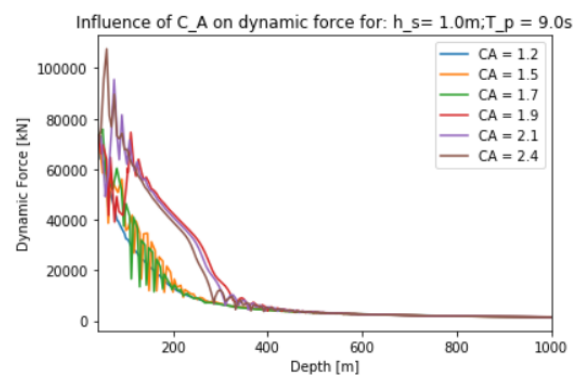
(c)



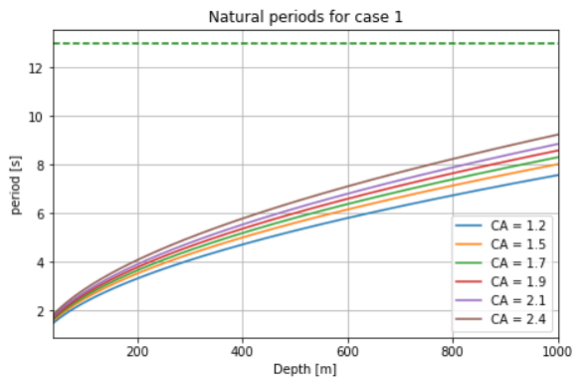
(d)



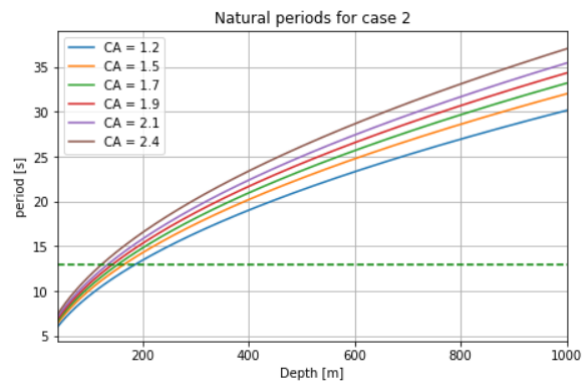
(e)



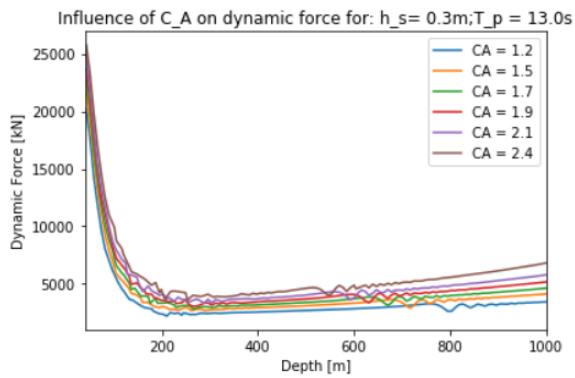
(f)



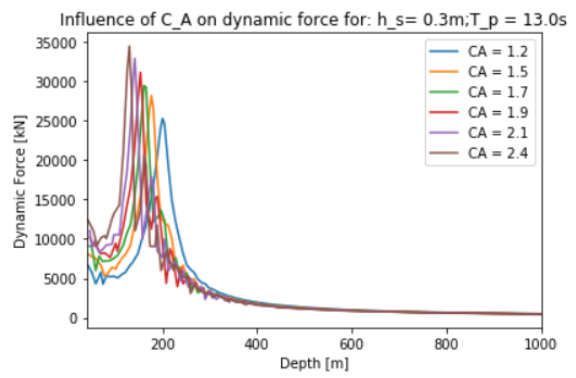
(g)



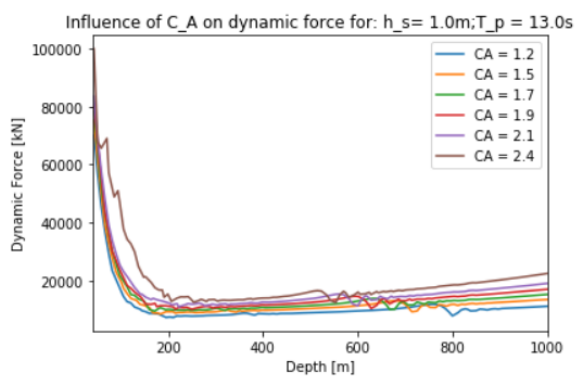
(h)



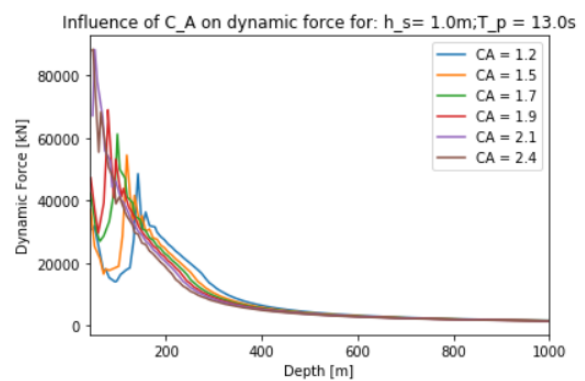
(i)



(j)



(k)



(l)

Figure G.1b: Simulation results for added mass coefficient (C_A) ranging from 1.5 to 2.4. Left is case 1, right is case 2.

G.1.2 Sensitivity of dynamic force to drag coefficient

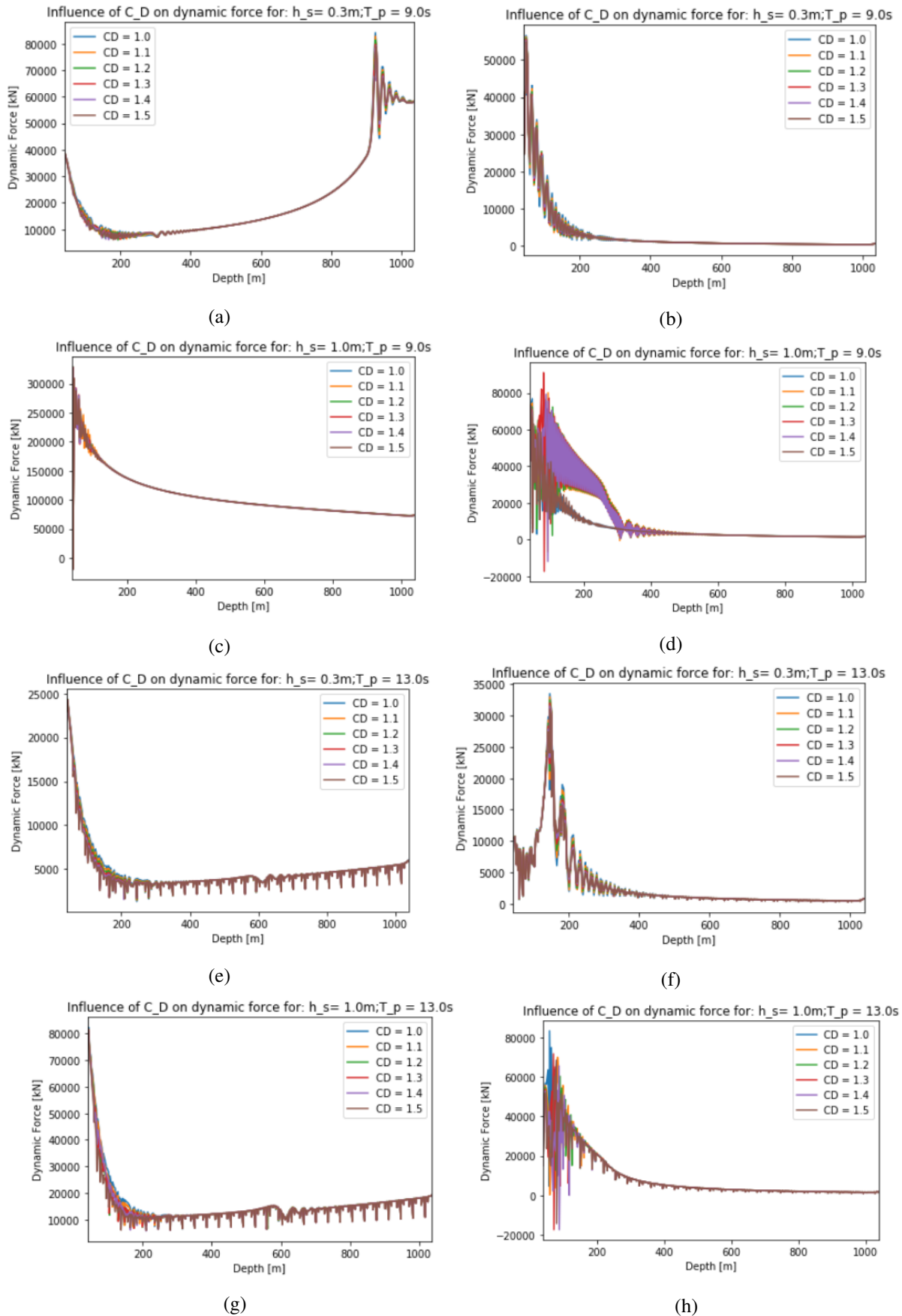
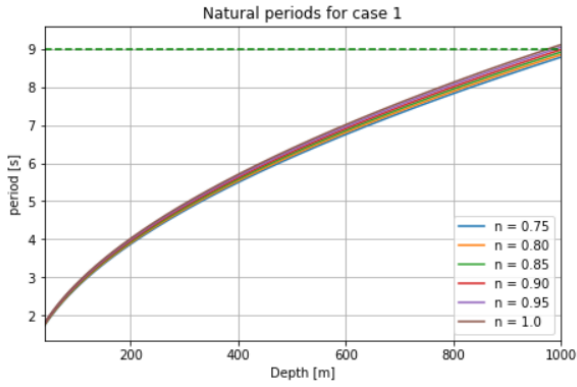
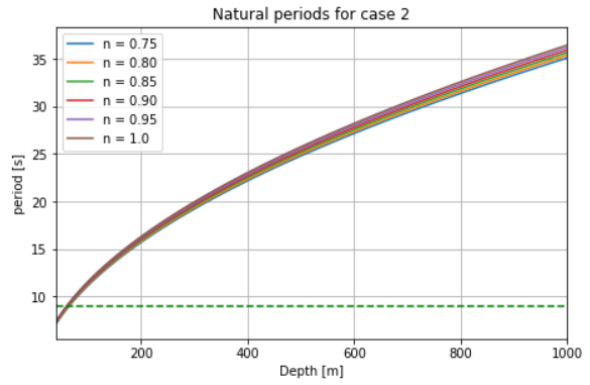


Figure G.2: Simulation results for drag coefficient (C_D) ranging from 1.0 to 1.5. Left is case 1, right is case 2.

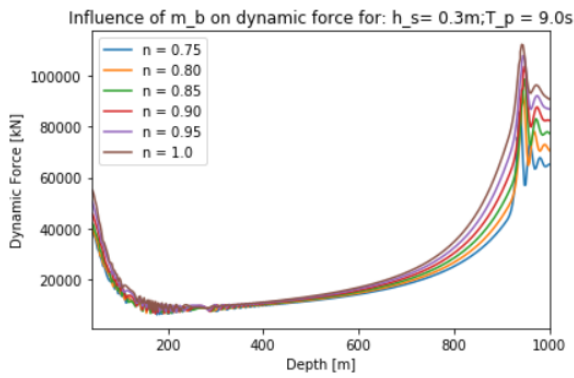
G.1.3 Sensitivity of dynamic force to ballasting fill percentage



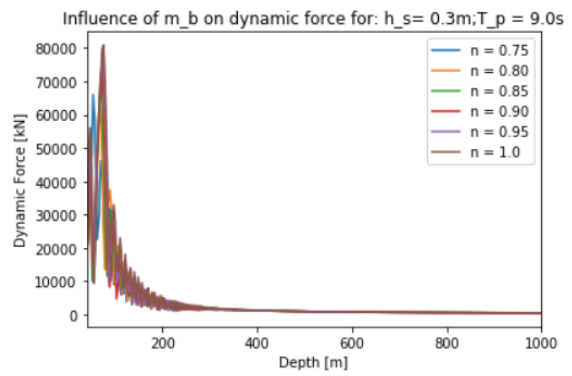
(a)



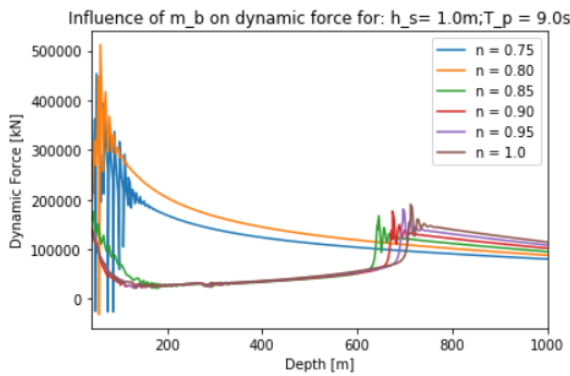
(b)



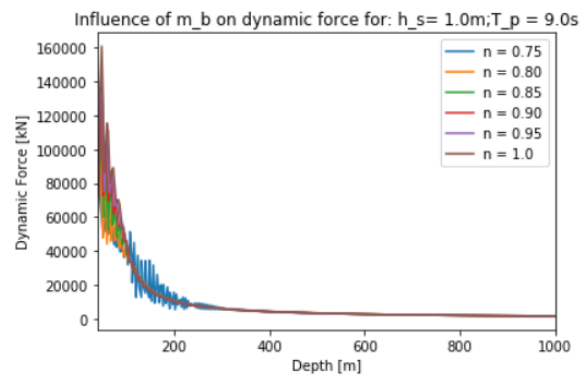
(c)



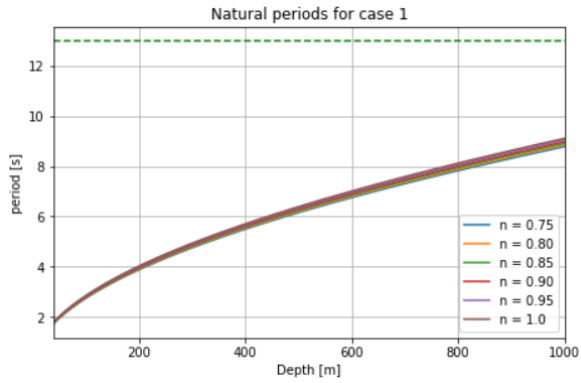
(d)



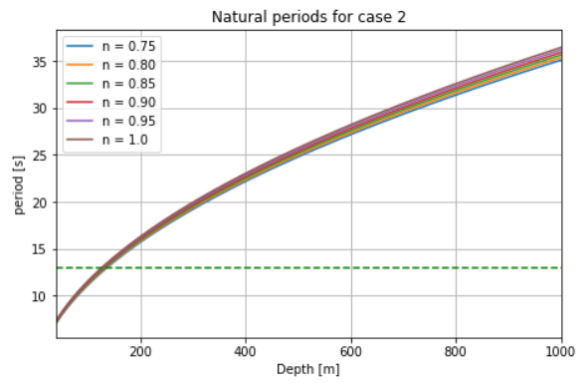
(e)



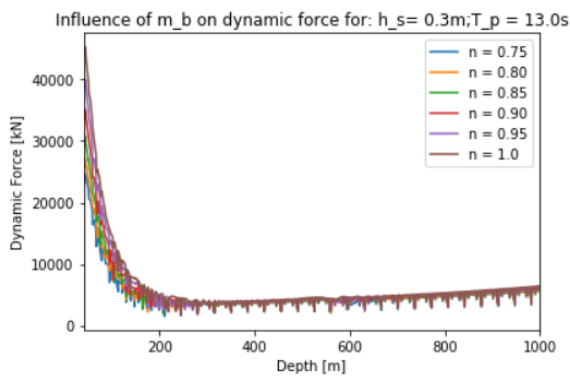
(f)



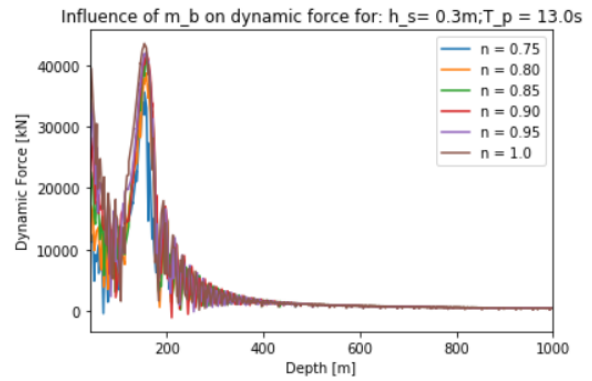
(g)



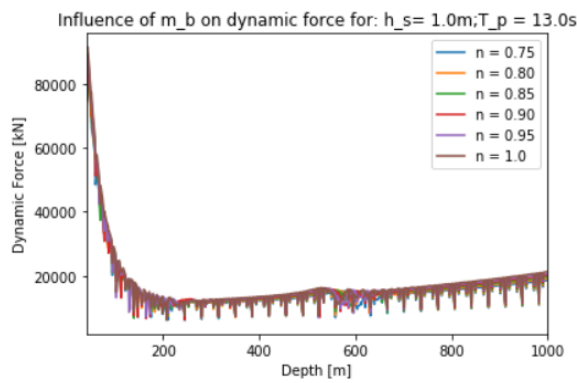
(h)



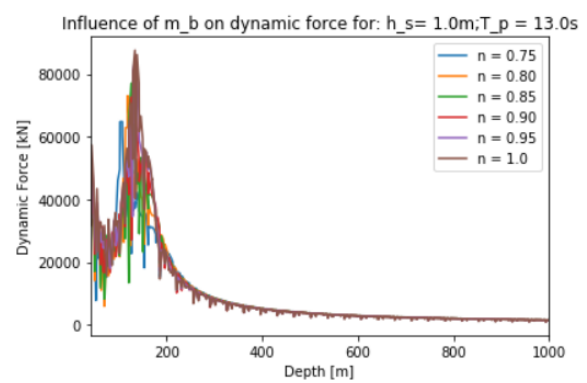
(i)



(j)



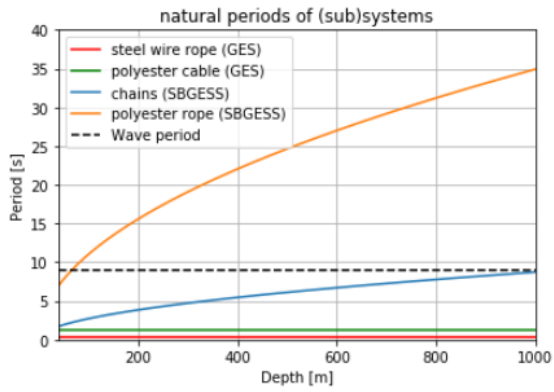
(k)



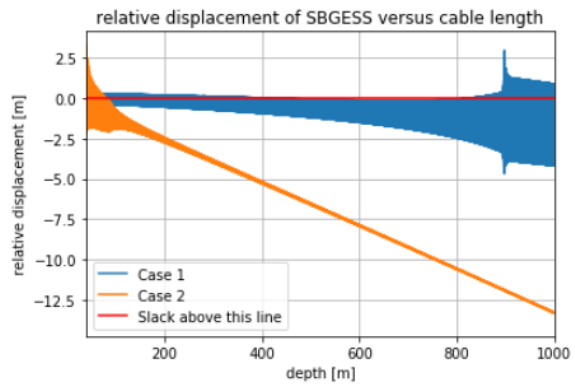
(l)

Figure G.3b: Simulation results for ballasting fill percentage (n) ranging from 0.75 to 1.0. Left is case 1, right is case 2.

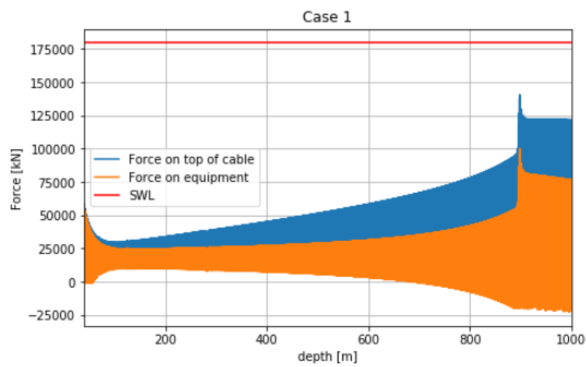
G.2 Complete overview of results for scenarios and cases mentioned in chapter 7



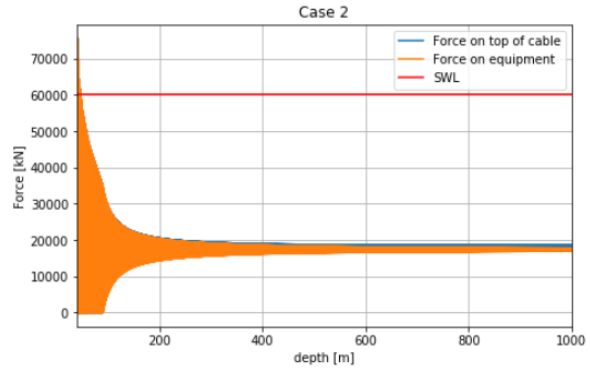
(a)



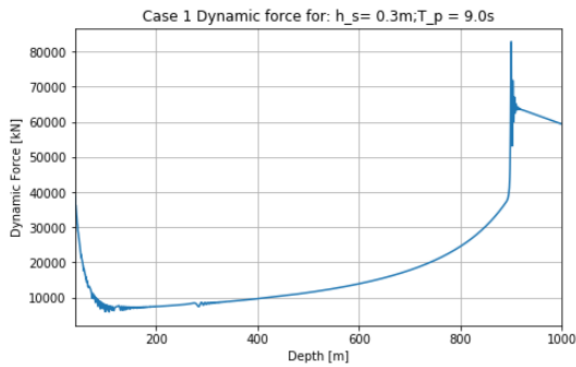
(b)



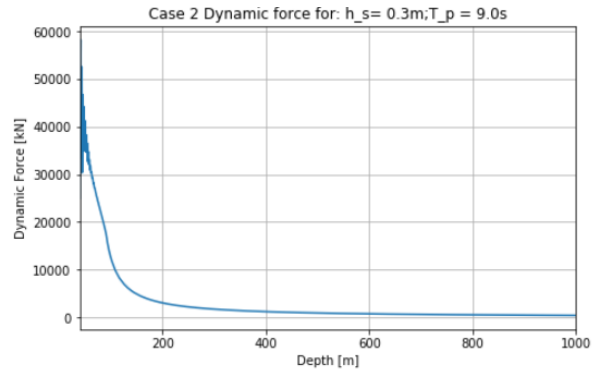
(c)



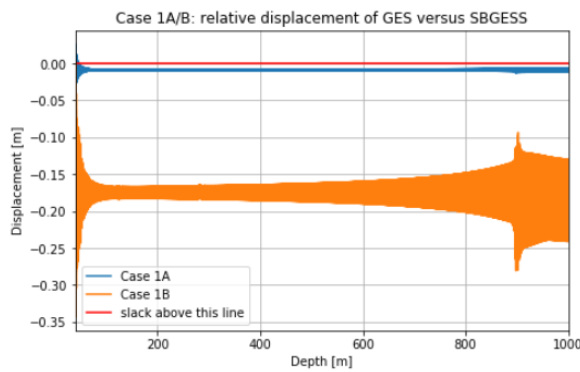
(d)



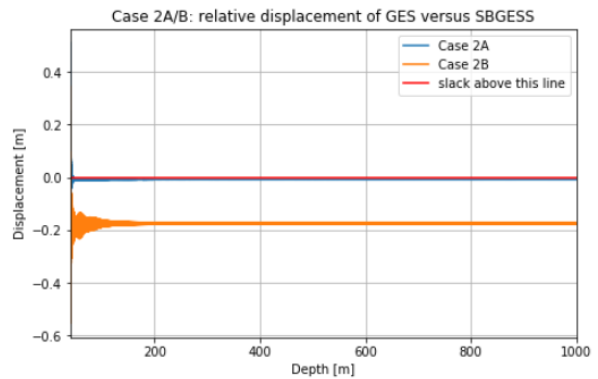
(e)



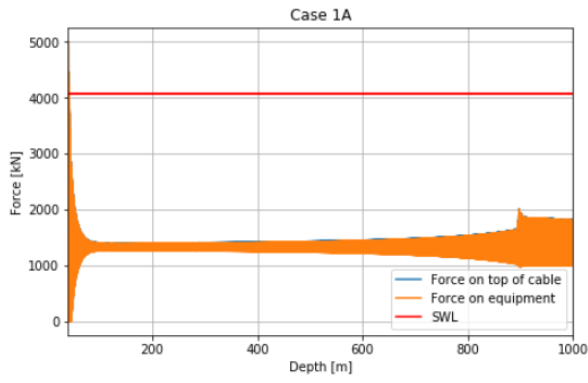
(f)



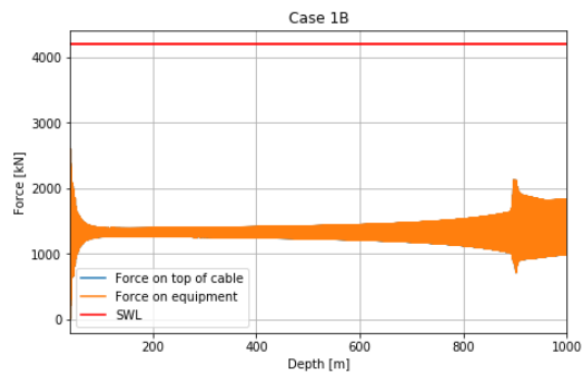
(g)



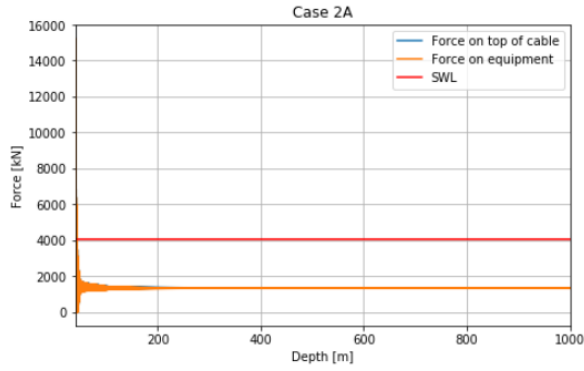
(h)



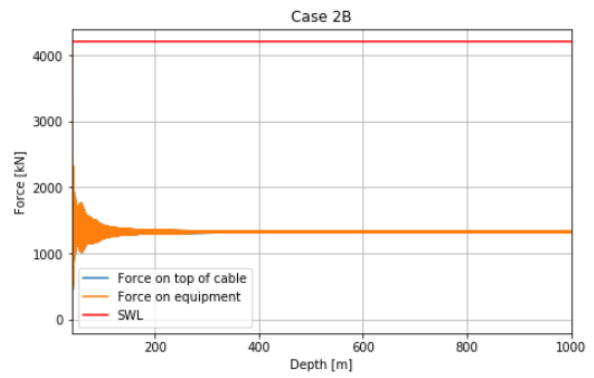
(i)



(j)

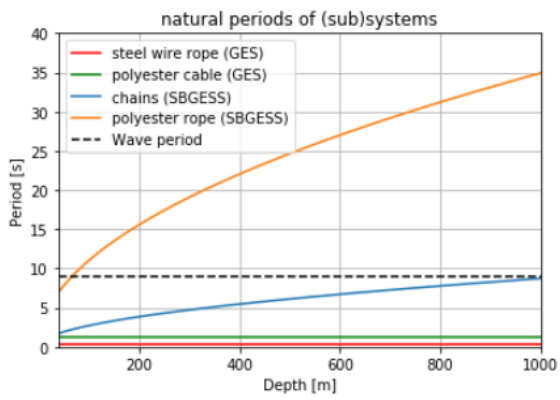


(k)

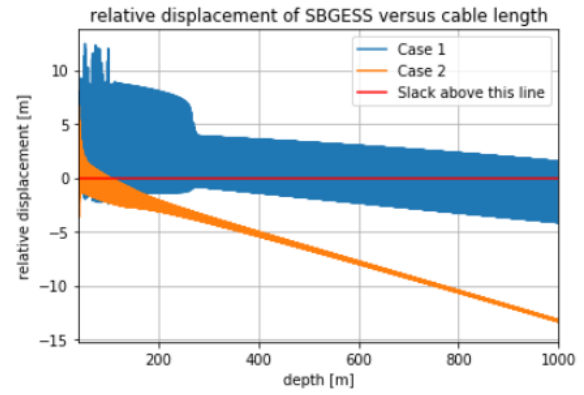


(l)

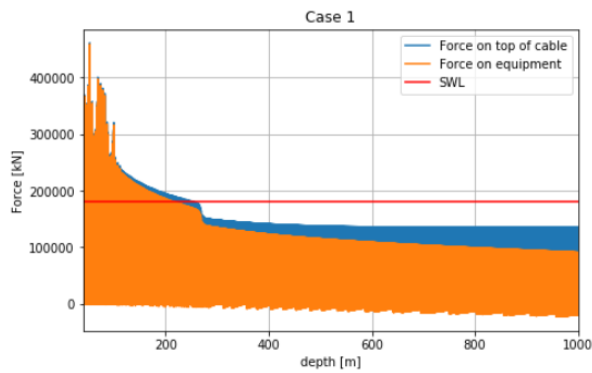
Figure G.4b: Simulation results for $V_c = 0.05m/s$, $h_s = 0.3m$ and $T_p = 9s$.



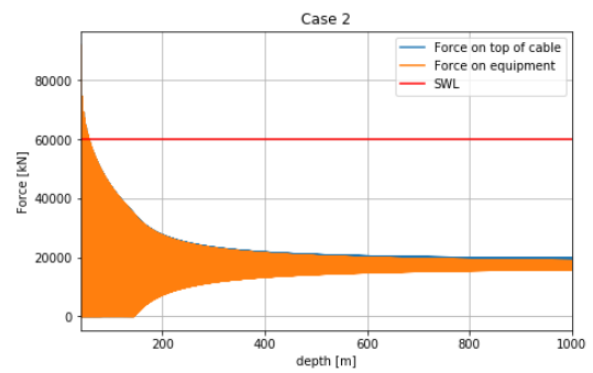
(a)



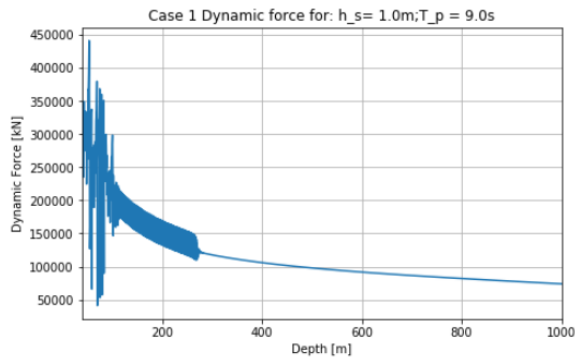
(b)



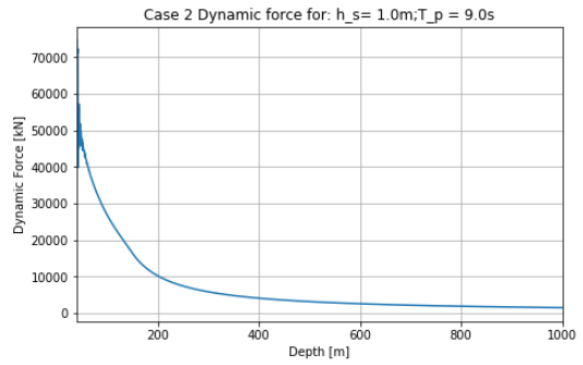
(c)



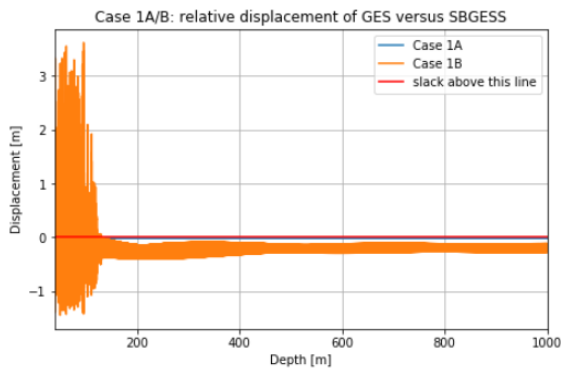
(d)



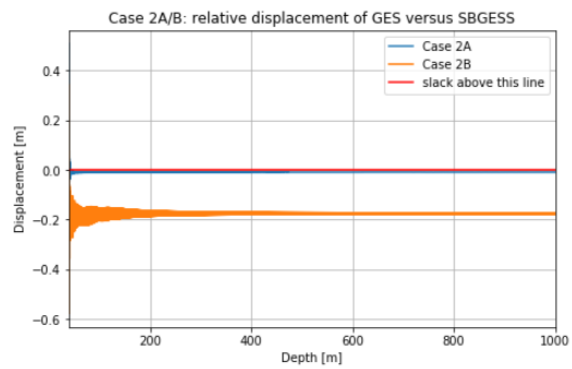
(e)



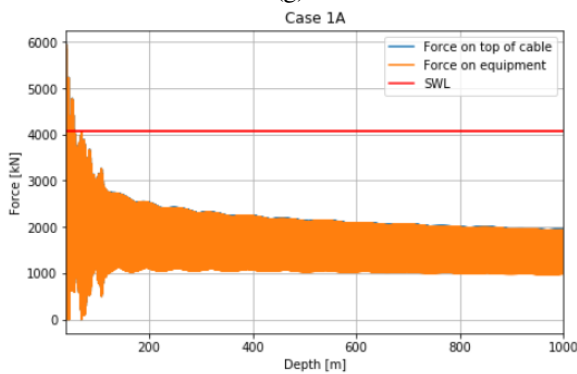
(f)



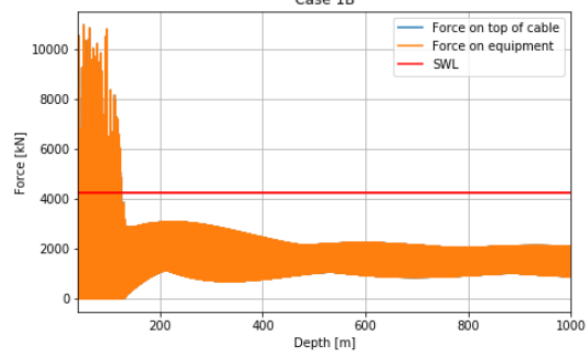
(g)



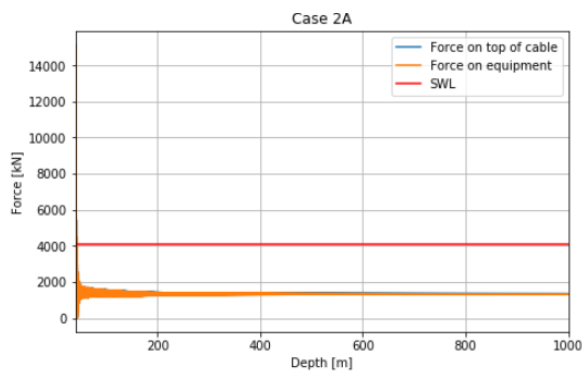
(h)



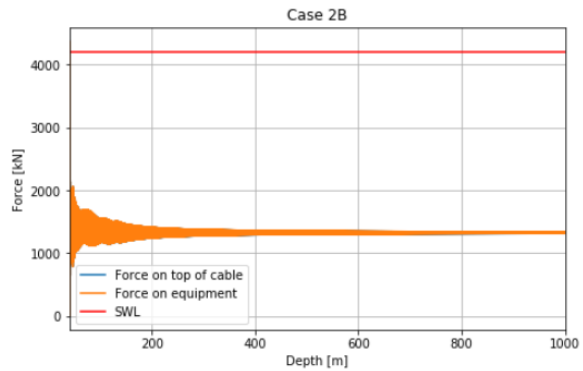
(i)



(j)

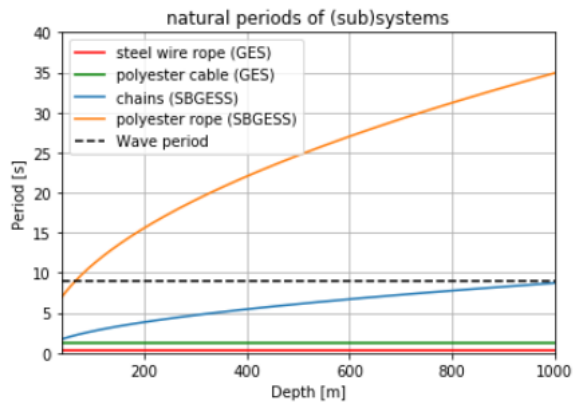


(k)

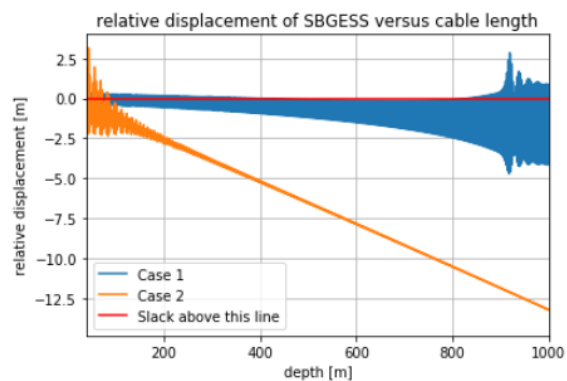


(l)

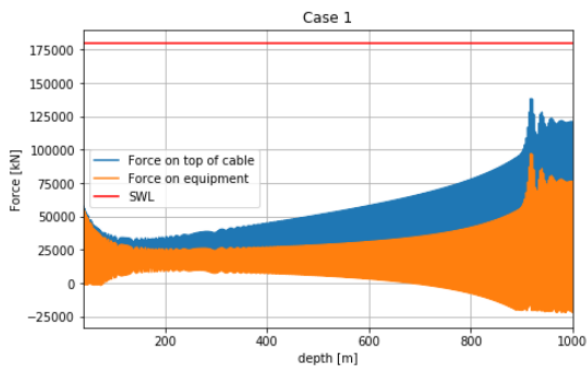
Figure G.5b: Simulation results for $V_c = 0.05\text{m/s}$, $h_s = 1.0\text{m}$ and $T_p = 9\text{s}$.



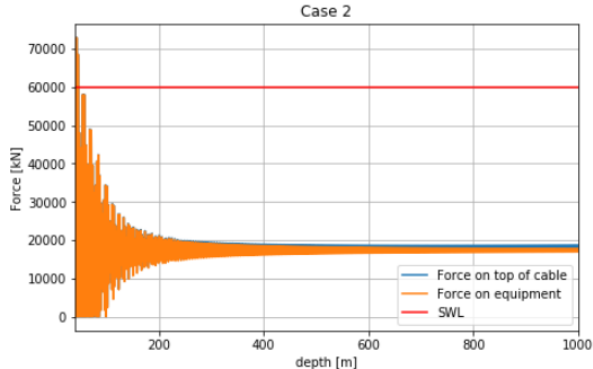
(a)



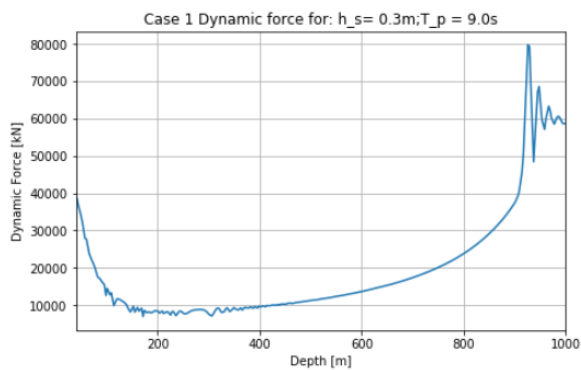
(b)



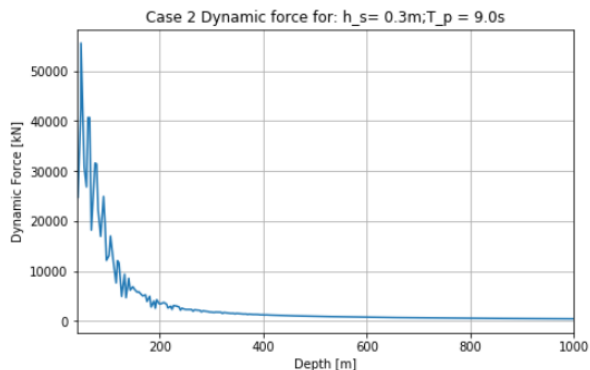
(c)



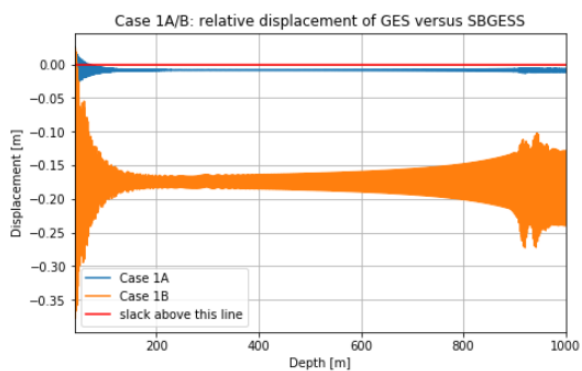
(d)



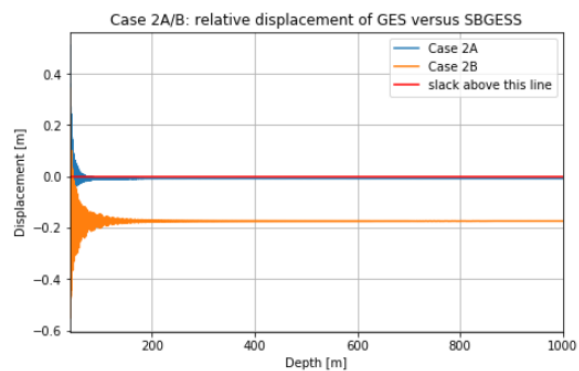
(e)



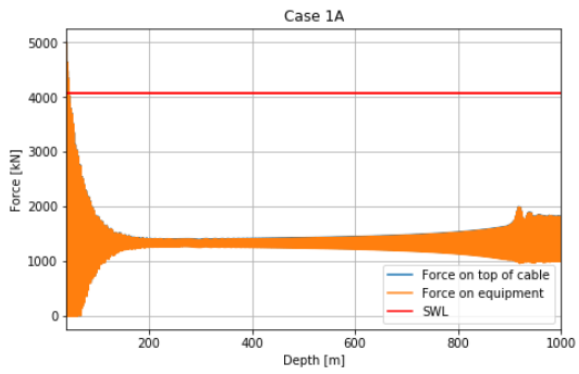
(f)



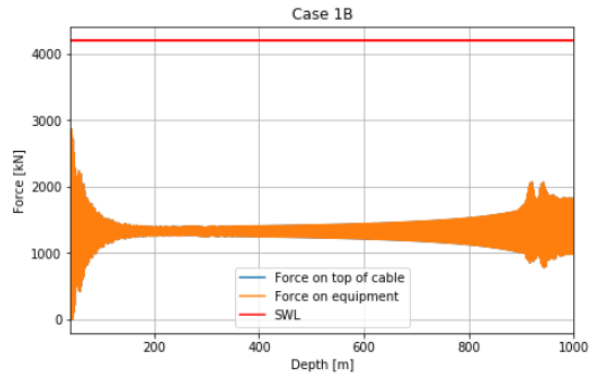
(g)



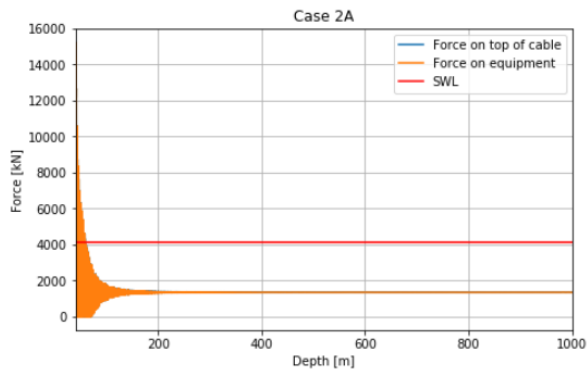
(h)



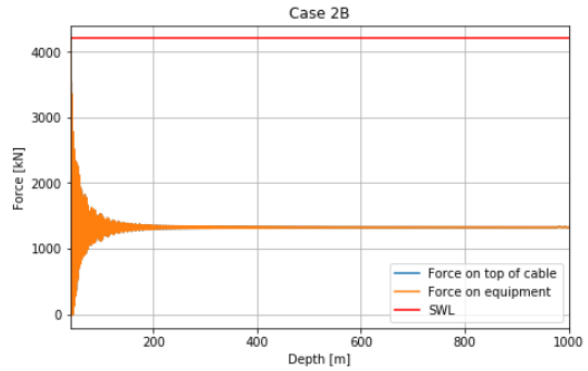
(i)



(j)

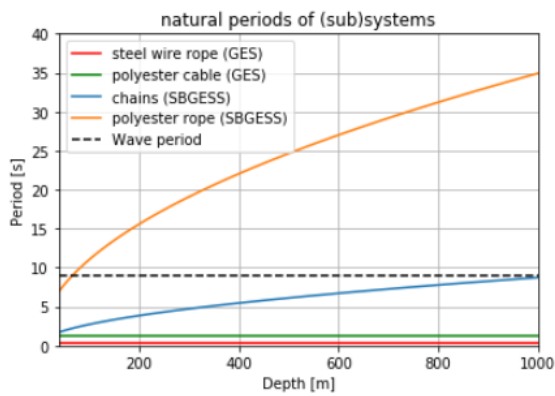


(k)

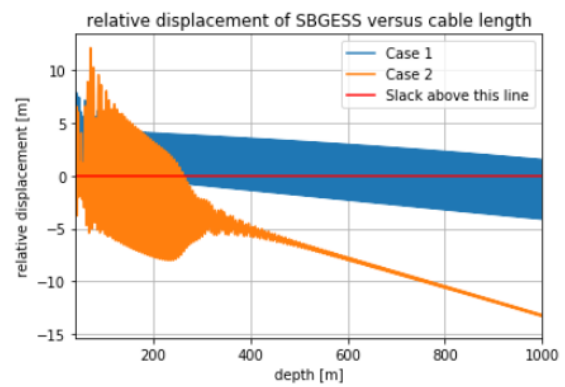


(l)

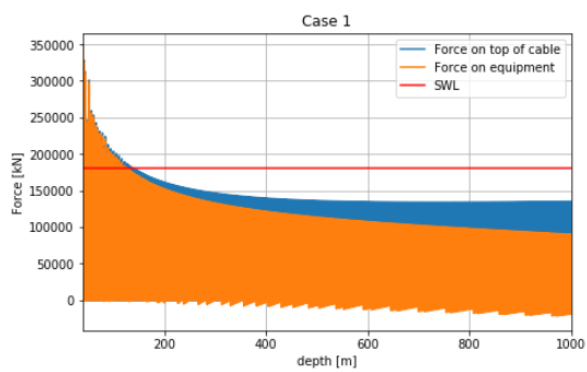
Figure G.6b: Simulation results for $V_c = 0.3m/s$, $h_s = 0.3m$ and $T_p = 9s$.



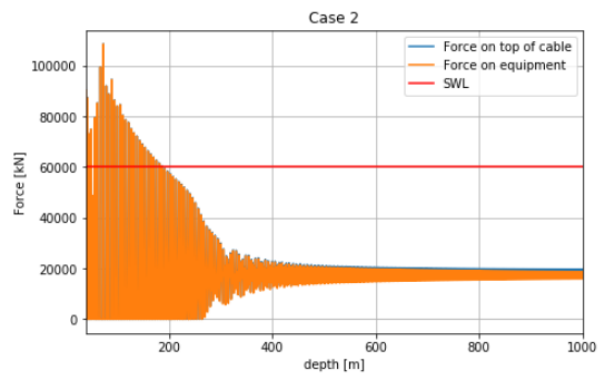
(a)



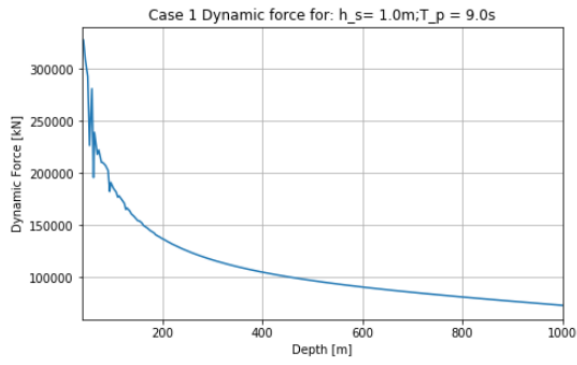
(b)



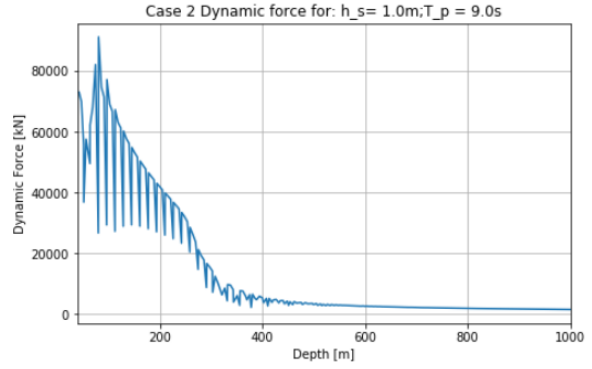
(c)



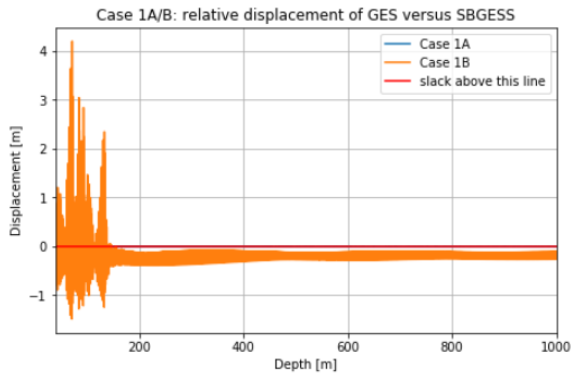
(d)



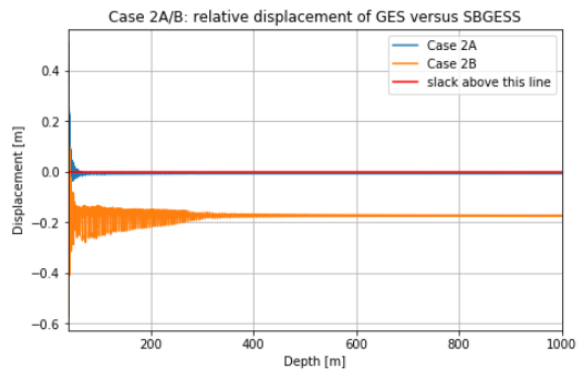
(e)



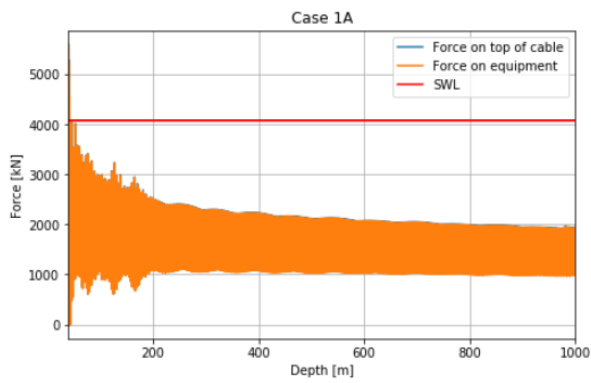
(f)



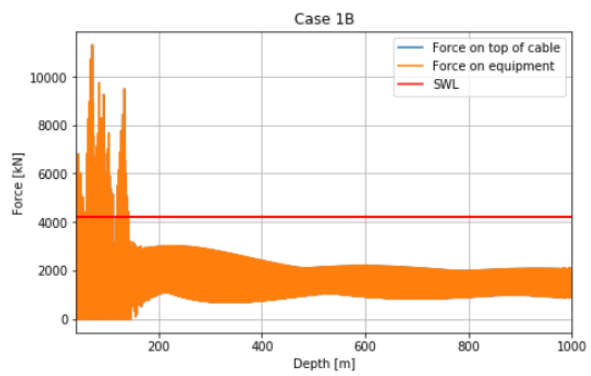
(g)



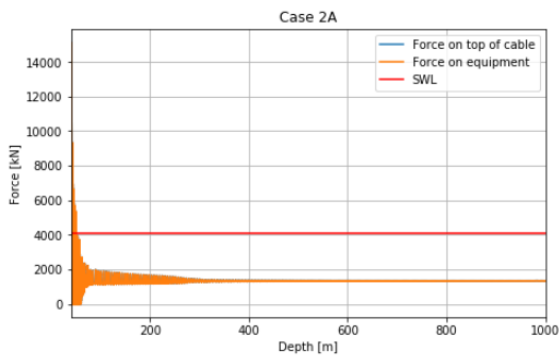
(h)



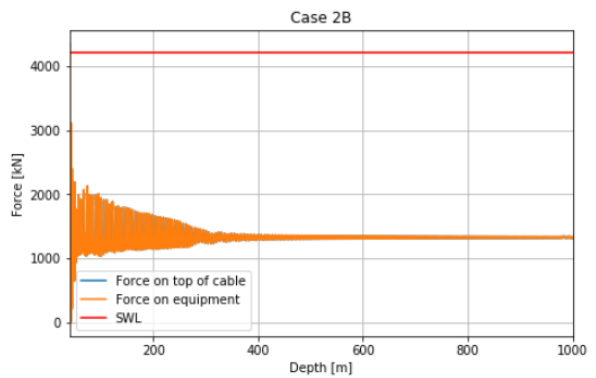
(i)



(j)



(k)



(l)

Figure G.7b: Simulation results for $V_c = 0.3m/s$, $h_s = 1.0m$ and $T_p = 9s$.